THERMAL EFFECTS OF MICROSTRIP SILICON IMPATT OSCILLATORS

BY

R.W. MCKILLICAN

CARLETON UNIVERSITY
FACULTY OF ENGINEERING

TECHNICAL REPORT

MARCH 1973

THERMAL EFFECTS OF MICROSTRIP SILICON IMPATT OSCILLATORS

by

R.W. McKillican

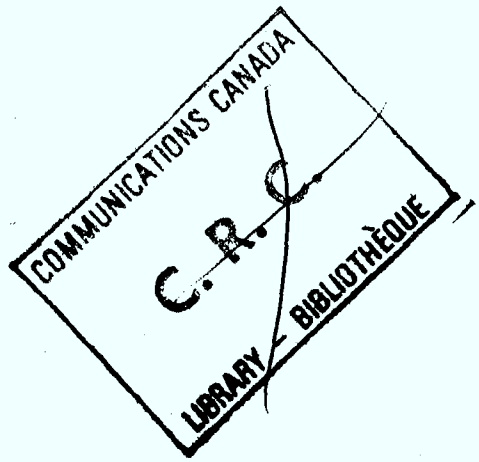

This report was prepared for the Department of Communications Communications Research Center under Contract No. OGR2-0073

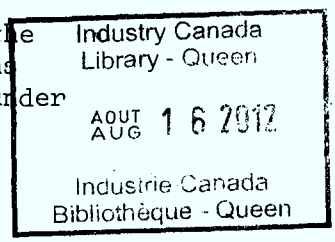

Carleton University
Ottawa, Ontario

March 1973

ABSTRACT

The variation of the frequency of a microstrip silicon IMPATT oscillator with temperature is studied experimentally and analytically. Results of a temperature-sensitive small-signal analysis show that the IMPATT diode may be adequately modelled to predict the temperature characteristics of an oscillator.

Experimental results on the shift of frequency with pulse width in pulse mode operation are compared to a theoretical analysis. It is shown that rapid rise in diode-junction temperature plus an electronic tuning effect are responsible for the frequency shift.

Heat flow resistance measurements are performed to determine the diode-junction temperature rise during operation and to also obtain a value for the thermal time constant of the diode junction.

ACKNOWLEDGEMENTS

The author acknowledges the support and encouragement of his supervisor, Dr. V. Makios.

The author is grateful to Dr. W.J. Chudobiak of Communications Research Center, Ottawa, who provided many useful suggestions during the course of this study.

The Department of Communications provided the financial support (Contract Numbers OGRO-222 and OGR2-0073) and the facilities for this work and the author thanks the staff whose assistance was invaluable.

TABLE OF CONTENTS

TABLE OF CONTENTS (cont'd)

LIST OF FIGURES

LIST OF FIGURES (Cont'd)

LIST OF FIGURES (Cont'd)

LIST OF SYMBOLS

A	Area of diode junction
a	Thermal time constant of diode junction
α	Ionization coefficient of electrons in silicon
α'	Ionization coefficient derivative of electrons in silicon
B	Reverse breakdown voltage temperature coefficient
β	Ionization coefficient of holes in silicon
β'	Ionization coefficient derivative of holes in silicon
C	Capacitance of packaged diode under reverse voltage (low frequency)
C_j	Capacitance of diode chip
C^*	Thermal capacitance of diode
c	Specific heat of silicon
D	Slew rate of current pulse
E_m	Maximum value of electric field in the diode
E_I	3/2 of the band gap energy of silicon
$\langle E_p \rangle$	Average optical phonon energy

LIST OF SYMBOLS (Cont'd)

ε_r	Relative dielectric constant of microstrip substrate
ε_{ro}	Relative dielectric constant of microstrip substrate at room temperature
ε_s	Relative dielectric constant of silicon
f_o	Frequency of oscillator
Δf	Change in frequency of oscillator
f_{av}	Average frequency of oscillator
f_{-3dB}	Frequency at which small-signal resistance of diode is reduced by 3dB (for frequencies less than the avalanche frequency)
$\Delta f/\Delta T$	Frequency-temperature coefficient of an oscillator
I	Bias current flowing in diode
I_o	Maximum value of bias current
J_o	Current density in diode
ℓ	Ionization layer width
ℓ_d	Length of diode
ℓ_o	Drift length of electrons in diode
$\ell(f)$	Length of oscillator tuning stub

LIST OF SYMBOLS (Cont'd)

N_B	Background impurity concentration of silicon substrate
N_{N+}	Impurity concentration of silicon in donor region
N_P	Impurity concentration of silicon in acceptor region
η	Efficiency of DC to RF power conversion
P_{DIS}	Power dissipated in diode
P_{IN}	Power input to diode
P_o	Power output from diode
PW	Pulse width of bias current
q	Electronic charge
R^*	Resistance of electrical analog circuit of heat flow network
R_D	Negative resistance of packaged diode
R_{D_C}	Negative resistance of diode chip
R_{DC}	DC resistance of avalanching diode
R_L	Resistance of microwave circuit at diode terminals
R_{SC}	Space-charge resistance of diode

LIST OF SYMBOLS (Cont'd)

R_{TH}	Thermal resistance of diode
R_{TOT}	Total small-signal resistance of diode (for frequencies less than the avalanche frequency)
T	Temperature
T_o	Room temperature
T_j	Temperature of diode junction
ΔT	Change in temperature
ΔT_{max}	Maximum change of temperature in diode junction
t	Time
V	Voltage
V_b	Breakdown voltage of reverse-biased diode
V_{b_o}	Breakdown voltage of reverse-biased diode at room temperature
ΔV_b	Change in breakdown voltage of reverse-biased diode
V_p	Punch-through voltage of reverse-biased diode
v_n	Scattering limited velocity of electrons in silicon
v_p	Scattering limited velocity of holes in silicon

LIST OF SYMBOLS (Cont'd)

W	Total depletion width of reverse-biased diode
W_n	Depletion width of n region of diode
W_p	Depletion width of p region of diode
ω	Angular frequency in radians
ω_o	Avalanche frequency of diode
X_D	Reactance of packaged diode
X_{D_C}	Reactance of diode chip
X_L	Reactance of microwave circuit at diode terminals
Z_{j_c}	Impedance of diode chip
θ_j	Heat flow resistance of diode
θ_n	Transit angle for electrons in the depleted n region
θ_p	Transit angle for holes in the depleted p region
λ_n	Optical phonon mean free path for electrons
λ_p	Optical phonon mean free path for holes
Φ	Effective ionization coefficient derived from the ionization coefficients and their derivatives[15]

$\bar{\tau}$	Average transit time for holes and electrons in the ionization layer[15]
ρ	Density of silicon substrate

CHAPTER 1

INTRODUCTION

1.1 Introduction

A characteristic feature of the development of modern radio is the rapid introduction of semiconductor devices for microwave frequencies. In recent years, the discovery of two-terminal negative-resistance devices has led to a broad class of microwave oscillators and amplifiers. Among these devices are included tunnel, IMPATT, TRAPATT, Gunn and BARRIT diodes. A basic problem associated with all of these microwave sources is the temperature stability of the frequency when these devices are used as fundamental oscillators. The techniques available for reducing the temperature drift of these oscillators usually involves the use of a high-Q waveguide cavity and/or a temperature controlled varactor tuning diode. The recent interest in microstrip transmission lines and circuit elements has stimulated workers to develop microwave integrated circuits. Unfortunately, these new circuits possess a lower Q than waveguide circuits, with the result that the frequency of oscillation of the microwave source is controlled largely by the device rather than the circuit. Consequently, the study of the thermal characteristics of silicon IMPATT microstrip oscillators is the subject of this thesis.

1.2 Background

In 1954, Shockley[1] suggested several variants of p-n diodes, in which the negative dynamic resistance is the result of transit effects accompanying the diffusion and drift of the majority carriers in a thin layer of n-type semiconductor under the influence of an electric field.

Later, in 1958, Read[2] proposed a high frequency negative-resistance diode based on the principle of the impact ionization effect in an inversely biased p-n junction. Read's theory was substantiated shortly after by Johnson et al[3] who fabricated the first impact avalanche transit time (IMPATT) oscillator in a waveguide circuit. In the ensuing years, a large body of knowledge has accumulated on the phenomenon of negative resistance resulting from the impact avalanche transit time effect. The small-signal theory developed by Read[2] was soon expanded by a number of authors. Large-signal analyses, which more accurately define the diode operating characteristics, were also developed. As a result of both the large- and small-signal descriptions of the IMPATT diode, practical devices have emerged and are finding increased use in communication systems as fundamental power sources.

Although the power output of an oscillator is important, the effects of temperature on the oscillator characteristics are of equal importance. In 1968, Allamando et al[4] considered the effect of ambient temperature on CW IMPATT oscillators and showed that the power output first increases and then decreases with temperature. The increase in power output with temperature was confirmed later by Chudobiak[5] experimentally. The variation of oscillator frequency with temperature was explored both experimentally and theoretically by Schroeder and Haddad[6] in 1971. The downward shift in frequency with temperature for a waveguide circuit was found to be primarily due to the IMPATT diode. To explain this effect, they utilized Gilden and Hines[7] small-signal analysis of a Read diode and employed temperature-sensitive parameters. The results showed an increasing device susceptance with temperature which caused a downward shift in frequency. Recently, Grierson[8] has

obtained similar results using the small-signal analysis of Misawa[9] which is more accurate than the simpler model of Gilden and Hines.

IMPATT oscillators have been constructed which exhibit good frequency-temperature characteristics. In 1970, Nagano and Kondo[10] designed and built a highly stabilized half-watt IMPATT oscillator with a frequency-temperature coefficient of 28.6KHz/°C. Their oscillator was a cavity type constructed of invar and brass. The invar cavity has an extremely low thermal coefficient of expansion and further, the unloaded Q of the cavity was approximately 20,000. This ensured that the frequency-temperature coefficient of the oscillator was controlled by the circuit rather than a combination of the circuit and the diode.

To date, the frequency-temperature characteristics of IMPATT diode oscillators have been explored only lightly, and in all cases, the oscillator circuits have been either coaxial or waveguide. Very little attention, if any, has been given to the frequency-temperature characteristics of IMPATT microstrip oscillators.

1.3 Thesis Objectives and Format

The objective of this thesis is to explore the effect of temperature on the frequency and output-power characteristics of silicon IMPATT low-Q microstrip oscillators when they are operated in continuous wave and pulsed conditions.

In Chapter 2, a small-signal model for the IMPATT diode chip is modified such that the parameters may be varied with diode junction temperature. The diode chip is mounted in a microwave package, mathematically speaking, and the terminal characteristics of the packaged diode are examined with respect to frequency and temperature. The

temperature characteristics of the microstrip circuit are determined and the frequency-temperature coefficients of two similar CW oscillators, separated in frequency, are found. The results are compared to experimental measurements, and it is shown that a close correspondence exists between the measured and predicted results.

In Chapter 3, the effect of temperature on the operation of a pulsed IMPATT diode is examined. It is shown experimentally that the oscillator frequency reduces as the pulse width is increased. Various reasons for this downward shift are investigated and it is shown that the increase in diode temperature may account partially for this phenomenon.

Chapter 4 discusses the measurement of the heat flow resistance of an IMPATT diode in order to estimate the diode junction temperature-rise during operation. An experimental value for the thermal time constant of the diode junction is obtained.

The concluding remarks of this thesis are presented in Chapter 5 and areas requiring further work are isolated.

CHAPTER 2

FREQUENCY-TEMPERATURE CHARACTERISTICS OF C.W. SILICON IMPATT MICROSCTRIP OSCILLATORS

2.1 Introduction

In this Chapter, the frequency-temperature characteristic of a silicon IMPATT microstrip oscillator is considered from an experimental and theoretical viewpoint. For the theoretical analysis, a small-signal model is modified appropriately to reflect the effect of temperature on the diode properties. A microwave package is chosen to enclose the diode chip and the predicted packaged diode characteristics are examined. The theoretical resonant frequency of oscillation is determined by a computer program which considers the temperature-sensitive diode and the microstrip circuit. It is shown that the measured and predicted results agree qualitatively.

2.2 Frequency-Temperature Coefficient Derivation

The frequency-temperature coefficient ($\Delta f_{OSC}/\Delta T$) for an IMPATT oscillator may be determined from the fundamental equation for oscillation. Oscillation will occur when the diode and load impedances satisfy the following equation:

$$R_D + jX_D + R_L + jX_L = 0 \qquad (2.1)$$

and the frequency of oscillation is determined by the reactances. At resonance, the reactive terms are equal in magnitude and they may be described by a derivative expansion.

$$X_L = \frac{\partial X_L}{\partial T} \cdot \Delta T + \frac{\partial X_L}{\partial f} \cdot \Delta f + C_1$$

$$= - X_D$$

$$= - \frac{\partial X_D}{\partial T} \cdot \Delta T - \frac{\partial X_D}{\partial f} \cdot \Delta f - C_2 \qquad (2.2)$$

where

X_L = the reactance presented to the IMPATT diode (packaged chip) by the circuit

X_D = the output reactance of the IMPATT diode (packaged chip)

$C_1 = -C_2$ = constant (for $\Delta T = \Delta f = 0$, the constants C_1 and C_2 are the conjugate reactances and define the steady state values)

In Equation (2.2), it is assumed (and will be justified later) that $\partial X/\partial T$ and $\partial X/\partial f$ are relatively insensitive functions of frequency and temperature respectively. Solving Equation (2.2) for $\Delta f/\Delta T$, we obtain:

$$\frac{\Delta f}{\Delta T} = - \frac{\frac{\partial X_D}{\partial T} + \frac{\partial X_L}{\partial T}}{\frac{\partial X_D}{\partial f} + \frac{\partial X_L}{\partial f}} \qquad (2.3)$$

The terms $\partial X_L/\partial T$ and $\partial X_L/\partial f$ in Equation (2.3) may be readily calculated for most circuits (particularly microstrip and coaxial circuits). The term $\partial X_D/\partial f$ may be either measured or calculated if a valid packaged diode model is available. The term $\partial X_D/\partial T$ cannot be readily measured and so must be determined with the aid of a packaged diode model.

The numerator of Equation (2.3) indicates that the oscillator frequency-temperature coefficient, $\Delta f/\Delta T$, can be reduced to zero provided the temperature sensitive diode and load reactance derivatives have opposite signs and equal magnitudes. In a later section, it will

be demonstrated that a zero temperature coefficient can, in fact, be obtained.

The denominator of Equation (2.3) shows clearly the effect of the external circuit on the magnitude of the frequency-temperature coefficient. In waveguide circuits, for example, the unloaded Q may be quite large, which implies that the term $\partial X_L/\partial f$ in Equation (2.3) is also large. Since $\partial X_D/\partial f$ is a slowly varying function (demonstrated later) over the diode's range of operation, its magnitude is negligibly small compared to $\partial X_L/\partial f$. This implies that for waveguide circuits the denominator of Equation (2.3) and hence the frequency temperature coefficient is largely controlled by the circuit. However, for the case of microstrip, where the unloaded circuit Q is small in comparison with waveguide, the terms of the denominator of Equation (2.3) are similar in magnitude and hence the frequency-temperature coefficient will be determined by both the circuit and the diode.

In the following section, a temperature and frequency sensitive packaged-diode model is described.

2.3 Packaged-Diode Model

Large-signal IMPATT diode models with varying degrees of complexity have been developed by a number of authors[11,12,13,14]. However, the large-signal models do not have closed-form solutions and therefore require lengthy computation times in comparison to closed-form small-signal models. A number of small-signal models with closed-form solutions are available[2,7,15,16]. However, the model suggested by Fisher[15] is of particular interest in that it includes the effects of

unequal hole and electron ionization rates and saturation velocities and ionization layer width variations. Further, Fisher has shown that it compares favourably with the computer analysis of Misawa[9].

In this thesis, Fisher's[15] small-signal model will be used to compute the impedance of an IMPATT diode chip and special attention will be given to those parameters which are temperature-sensitive.

Fisher's equation for the small-signal impedance of an IMPATT diode chip (Equation [57] in Ref. 15) can be rewritten as:

$$Zj_c = \frac{1}{\omega C_j}\left[\frac{\frac{W_p}{W}\cdot\frac{1-\cos\theta_p}{\theta_p}+\frac{W_n}{W}\cdot\frac{1-\cos\theta_n}{\theta_n}}{1-\frac{\omega^2}{\omega_o^2}}\right]$$

$$-\frac{j}{\omega C_j}\left[1-\frac{\frac{W_p}{W}\cdot\frac{\sin\theta_p}{\theta_p}+\frac{W_n}{W}\cdot\frac{\sin\theta_n}{\theta_n}}{1-\frac{\omega^2}{\omega_o^2}}\right] \qquad (2.4)$$

$$= R_{D_C} + jX_{D_C} \qquad (2.5)$$

and it is noted that for frequencies greater than the avalanche frequency, ω_o, the real part of the diode chip impedance, R_{D_C}, is negative.

The diode variables in Equation (2.4) are all temperature-sensitive to varying degrees, but three simplifying assumptions are made. First, it is assumed that the diode is punched-through as shown in Figure 1 and so the temperature dependence of the depletion width, W, may be

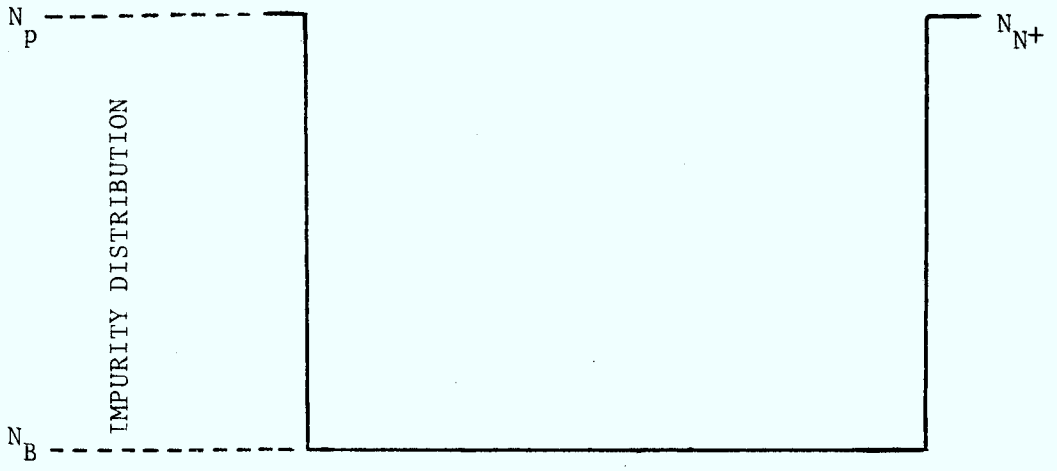

FIG. 1a. IDEALIZED IMPURITY CONCENTRATION PROFILE OF AN IMPATT DIODE

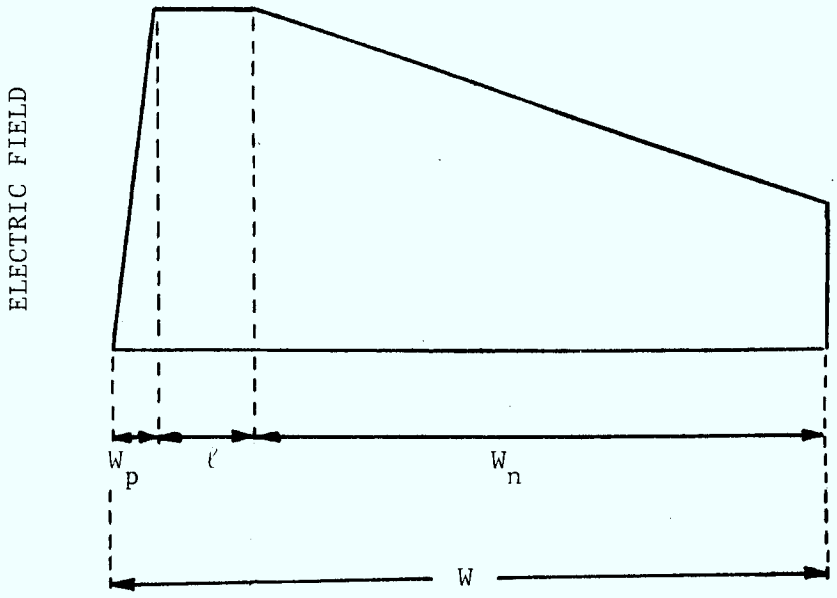

FIG. 1b. IDEALIZED ELECTRIC FIELD DISTRIBUTION OF AN IMPATT DIODE WITH p AND n DEPLETION REGIONS AND AVALANCHE LAYER

neglected. Second, it is assumed that the thermal coefficient of expansion of silicon is negligibly small. Thirdly, it is assumed that the relative dielectric constant of silicon is relatively temperature-insensitive. These assumptions allow the temperature dependence of the diode cross-sectional area, A, and the depletion capacitance, C_j, to be neglected.

The diode variables in Equation (2.4) may be determined by electrical and mechanical measurements and assigned a temperature dependence. The depletion widths, W_p and W_n, are dependent on the total depletion width W and the ionization layer width[15]. As noted above, W was assumed to be fixed and so the depletion widths, W_p and W_n, are dependent on the ionization layer width alone. The ionization layer width is derived from a knowledge of the ionization coefficients for the electrons and holes. In turn, the ionization coefficients are proportional to the magnitude of the electric field distribution. The electric field distribution is related to the reverse breakdown voltage which is temperature dependent, hence the temperature dependence of the depletion widths may be determined starting from the variation of the reverse breakdown voltage with temperature. In Sections 2.3.1, 2.3.2, and 2.3.3, the temperature dependencies of the electric field distribution, the ionization coefficients and their derivatives, and the ionization layer widths are developed respectively and in Section 2.3.4, these dependencies are collected together to arrive at the temperature variation of the depletion regions, W_p and W_n.

The avalanche frequency, ω_o, is a temperature sensitive function which is dependent on the ionization coefficients, the ionization layer width and the scattering limited velocities of the holes and the electrons in silicon. As stated above, the ionization coefficients and the ionization layer width are temperature dependent. In Section 2.3.5, the temperature dependence of the scattering limited velocities of the electrons and the holes are described and in Section 2.3.6, the temperature variation of the avalanche frequency is discussed.

The transit angles in the n and p depletion zones, θ_p and θ_n, are a function of the depletion layer widths, W_p and W_n, the frequency of operation, ω, and the scattering limited velocities of the holes and the electrons in the depleted p and n regions respectively. In Section 2.3.7, the temperature dependencies of the transit angles are formulated, and finally, in Section 2.3.8, the small-signal diode junction impedance is computed for various frequencies and temperatures.

2.3.1 The Electric Field Distribution

A model describing the temperature dependence of the electric field distribution of a punched-through diode may be derived from a knowledge of the breakdown voltage-temperature characteristic which may be easily measured.

In Figure 2, a theoretical field distribution is shown from which the breakdown voltage can be obtained as;

$$V_b = \frac{q N_B W^2}{2 \varepsilon_s} + E_o W \qquad (2.6)$$

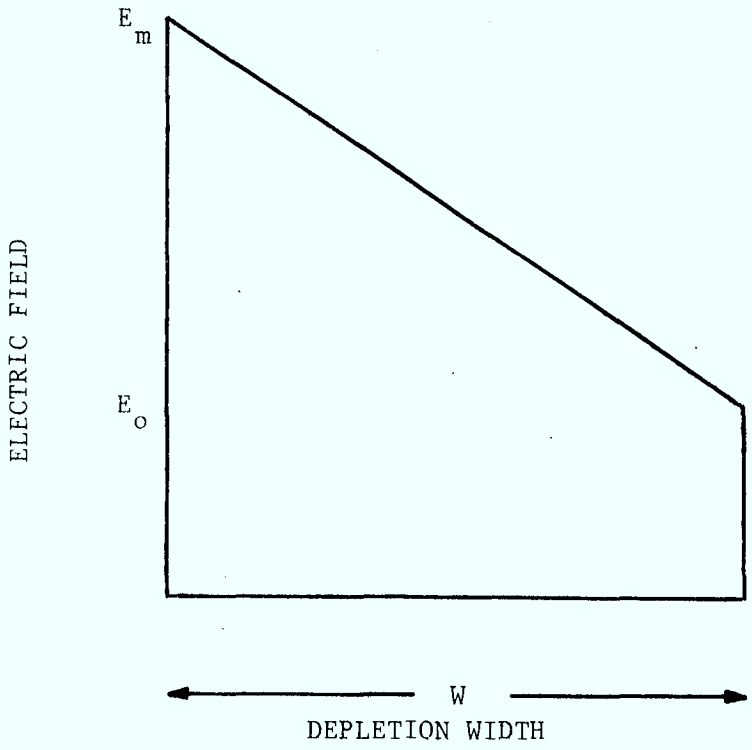

FIG. 2. IDEALIZED ELECTRIC FIELD DISTRIBUTION OF PUNCHED-THROUGH IMPATT DIODE FOR COMPUTATION OF ELECTRIC FIELD

and the maximum value of the field is given by:

$$E_m = E_o + \frac{q\ N_B\ W}{\varepsilon_s} \tag{2.7}$$

Solving the above equation for E_o, we get:

$$E_o = E_m - \frac{q\ N_B\ W}{\varepsilon_s} \tag{2.8}$$

and substituting into the voltage equation (2.6):

$$V_b = E_m W - \frac{q\ N_B\ W^2}{2\varepsilon_s} \tag{2.9}$$

The breakdown voltage, V_b, is temperature sensitive and therefore we obtain an expression for the temperature dependence of the electric field distribution:

$$E_m(T) = \frac{V_b(T)}{W} + \frac{q\ N_B\ W}{2\varepsilon_s} \tag{2.10}$$

$V_b(T)$ can be easily measured for a particular diode and expressed in the form:

$$V_b(T) = V_{b_o}\left[1 + B(T-T_o)\right] \tag{2.11}$$

where

$$B = \frac{1}{V_{b_o}} \cdot \frac{\Delta V_b}{\Delta T}$$

Equation (2.10) may then be rewritten as:

$$E_m(T) = \frac{V_{b_o}\left[1 + B(T-T_o)\right]}{W} + \frac{q\, N_B\, W}{2\varepsilon_s} \qquad (2.12)$$

The magnitude of the electric field at room temperature may be readily estimated as follows.

i) Measure the depletion capacitance as a function of reverse voltage at a low frequency (eg. 1MHz) and plot the result on log-log co-ordinates. For the diodes considered here, a typical plot is shown in Figure 3. At a reverse voltage of 40 volts, the slope of the curve reduces indicating that punch-through occurs at this voltage. Applying abrupt-junction theory, the depletion width is given by:

$$W = \frac{\varepsilon_s A}{C} \qquad (2.13)$$

ii) Measure the diode junction area of wasted devices. Typical areas were found to be $1.25\times10^{-4}\text{cm}^2$. Therefore, the depletion width is, from Equation (2.13):

$$W = 1.9\times10^{-4}\text{cm}.$$

iii) The background doping density, N_B, is obtained utilizing the field profile at punch-through and the punch-through voltage, V_p. At punch-through,

$$E = \frac{q\, N_B\, W}{\varepsilon_s} = \frac{2V_p}{W} \qquad (2.14)$$

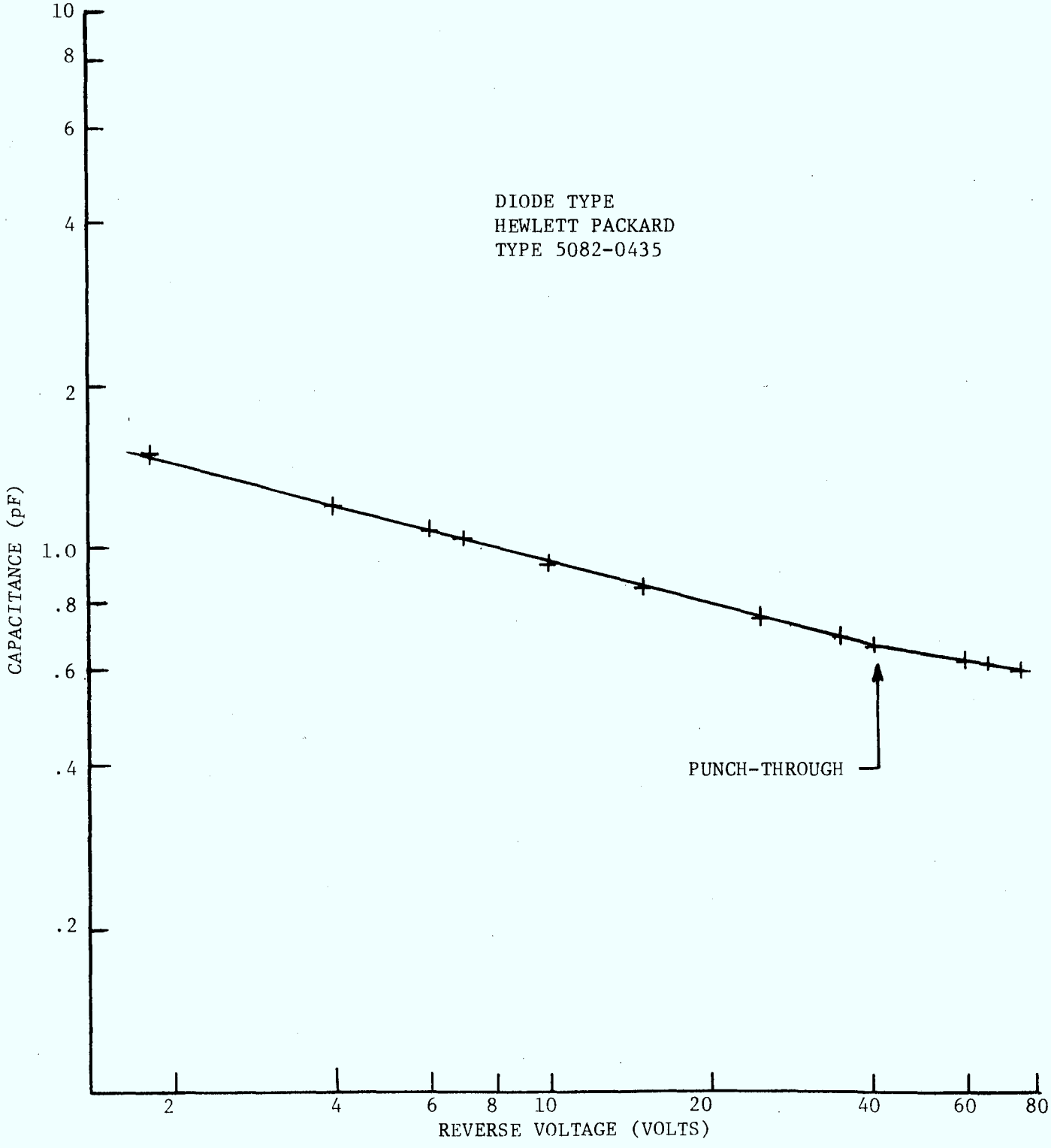

FIG. 3. PACKAGED DIODE CAPACITANCE VERSUS REVERSE VOLTAGE

and

$$N_B = \frac{2V_{p}\epsilon_s}{W^2 q} = 1.44\times10^{16}\text{cm}^{-3}$$

iv) Measure the breakdown voltage of the diode at room temperature. Typical values are:

$$V_{b_o} = 75 \text{ volts}$$

v) Insert the above values into Equation (2.12).

$$E_m(T_o) = \frac{V_{b_o}}{W} + 4.0\times10^5\text{volts/cm} \qquad (2.15)$$

At room temperature, T_o, the maximum value of the electric field becomes:

$$E_m(T_o) = 7.94\times10^5\text{volts/cm.}$$

For variations in diode junction temperature, the electric field may be described using Equations (2.13) and (2.15):

$$E_m(T) = \frac{75\left[1 + B(T-T_o)\right]}{1.9\times10^{-4}} + 4.0\times10^5\text{volts/cm} \qquad (2.16)$$

The breakdown voltage-temperature coefficient, B, was measured with low reverse current and found to be typically $1.18\times10^{-3}K^{-1}$.

The ionization coefficients for electrons and holes and their derivatives may now be computed for various diode junction temperatures and electric field values.

2.3.2 Ionization Coefficients (α,β) and Coefficient Derivatives (α',β')

Cromwell and Sze[17] have derived the following empirical equation which describes the ionization coefficient for electrons using data reported by Baraff[18]:

$$\alpha(E_m,T) = \frac{1}{\lambda_n} \exp\left[\frac{au^2}{E_m^2} + \frac{bu}{E_m} + C\right] \qquad (2.17)$$

where

$$u = \frac{E_I}{q\lambda}$$

$$a = 11.5\Omega^2 - 1.17\Omega + 3.9\times10^{-4}$$

$$b = 46\Omega^2 - 11.9\Omega + 1.75\times10^{-2}$$

$$c = -757\Omega^2 + 75.5\Omega - 1.92$$

$$\Omega = \frac{<E_p>}{E_I}$$

The ionization coefficient for holes, $\beta(E_m,T)$ is of the same form as Equation (2.17). Equation (2.17) may be differentiated with respect to E_m to obtain the ionization coefficient derivative

$$\alpha'(E_m,T) = \frac{d\alpha(E_m,T)}{dE_m} \qquad \text{(for electrons)}$$

and

$$\beta'(E_m,T) = \frac{d\beta(E_m,T)}{dE_m} \qquad \text{(for holes)}$$

Performing the differentiation, Equation (2.17) becomes:

$$\alpha' = \frac{d\alpha(E_m, T)}{dE_m} = \frac{1}{\lambda_n}\left[-\frac{2au^2}{E_m^3} - \frac{bu}{E_m^2}\right] \exp\left[\frac{au^2}{E_m^2} + \frac{bu}{E_m} + C\right] \qquad (2.18)$$

The ionization coefficients for electrons and holes, α and β respectively and their derivatives, α' and β', can be used to determine the width of the ionization layer ℓ, the depletion widths in the n- and p-regions W_n and W_p respectively, and the avalanche frequency, ω_o.

2.3.3 The Ionization Layer Width Temperature Dependence (ℓ)

In Figure 1, an idealized field distribution for a step junction punched-through IMPATT diode with p and n depletion areas is shown. The ionization layer width, ℓ, is given by[15]:

$$\ell = \frac{\log\left(\frac{\alpha}{\beta}\right)}{\alpha - \beta} \qquad (2.19)$$

For a range of diode junction temperatures, the variation of the width of the ionization layer is shown in Figure 4 and it is noted that for low temperatures the ionization layer width becomes quite large. This suggests that IMPATT diodes, constructed for high frequency operation where the total depletion width, W, is of the order of 10^{-4}cm, may behave as PIN diodes if the junction is at a low temperature (eg: in pulse mode operation the junction temperature will be nearly equal to the ambient if a low duty cycle is employed).

The depletion widths in the p- and n-regions may now be determined.

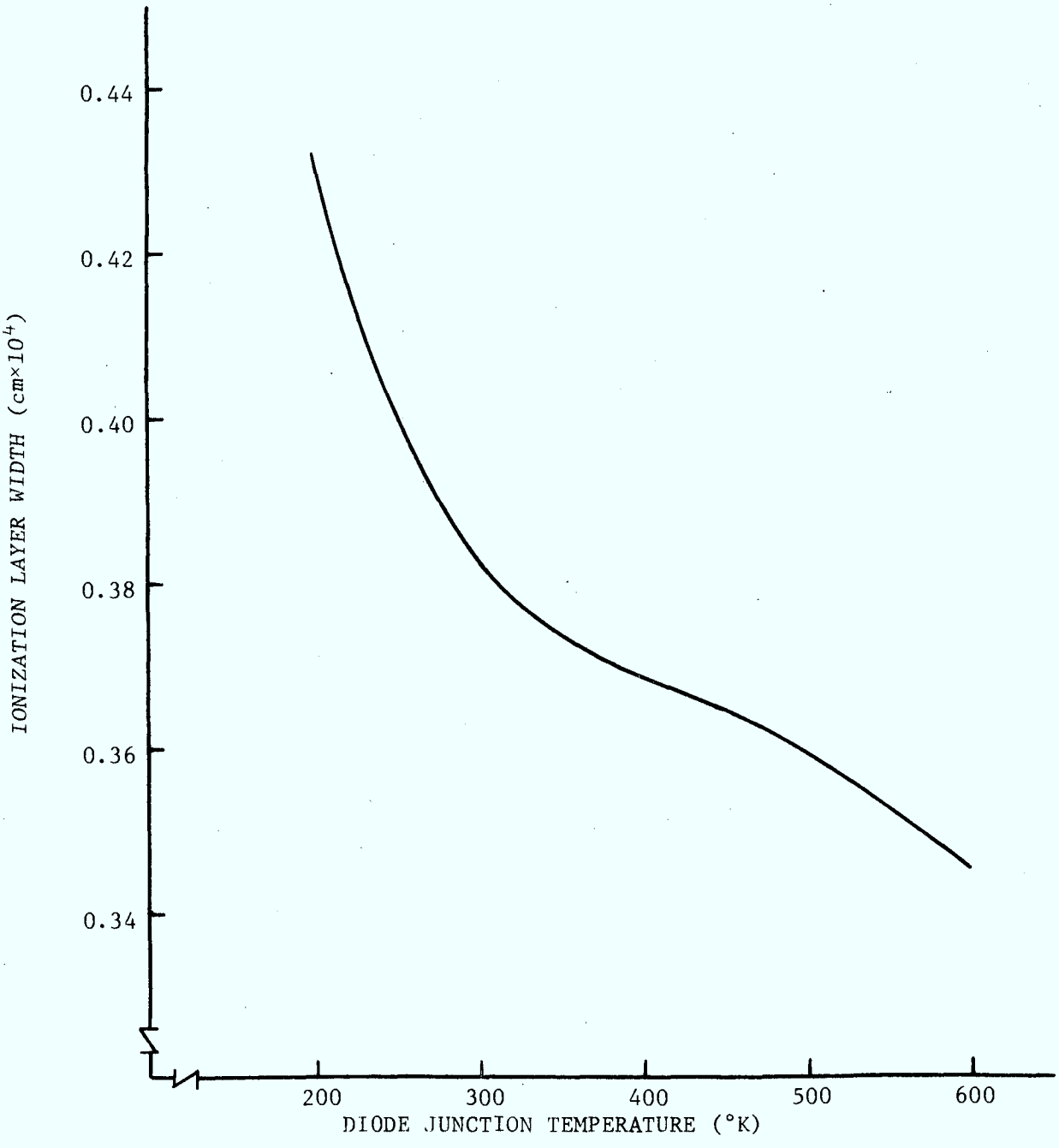

FIG. 4. VARIATION OF IONIZATION LAYER WIDTH WITH DIODE-JUNCTION TEMPERATURE

2.3.4 p and n Region Depletion Width Temperature Dependence (W_p and W_n)

The p-region depletion width, W_p, is small, compared to either the total depletion width, W, or the ionization layer width, ℓ, for normal values of p-region impurity doping densities (see Fig. 1). To justify this claim, the following calculation is performed using parameter values which are common for commercially available diodes for X-band use.

$E_m = 4\times10^5$ volts/cm (maximum value of electric field in a non-punched-through diode)

$W = 2\times10^{-4}$ cm (total depletion width)

$\ell = 0.37\times10^{-4}$ cm (ionization layer width)

$N_p = 10^{18}$ cm^{-3} (p-region doping density)

The p-region depletion width, W_p, can then be calculated as:

$$W_p = \frac{\varepsilon_s E_m}{q N_p} = 0.025\times10^{-4}\text{ cm}$$

Hence

$$W_p << \ell < W$$

Therefore, the temperature dependence of the p-region depletion width will be neglected and the n-region depletion width variation with temperature may be described as:

$$W_n(T) = W - W_p - \ell(T)$$

where W_p is assigned a constant value as found in the above calculation.

In the above discussion and previously in Section 2.3, it was assumed that the total depletion width, W, is invariant. However, silicon does have a linear coefficient of thermal expansion given by:

$$\frac{\Delta x}{x\Delta T} = 2.6\times10^{-6}\,^{\circ}C^{-1} \quad (19) \qquad (2.20)$$

That is, for a change in temperature of $\Delta T^{\circ}C$, the resulting change in length will be:

$$\Delta x = 2.6\times10^{-6} x.\Delta T \qquad (2.21)$$

For the depletion widths considered in this study, $W \approx 2\times10^{-4}$cm. Therefore, the depletion width temperature coefficient is given by:

$$\frac{\Delta W}{\Delta T} \approx 5.2\times10^{-10}\,\text{cm}/^{\circ}C$$

Comparing this result with the variation of the ionization layer width, ℓ, with temperature (Figure 4) we obtain:

$$\frac{\Delta \ell}{\Delta T} \approx 2.2\times10^{-8}\,\text{cm}/^{\circ}C \quad (300^{\circ} - 500^{\circ}K)$$

which is two orders of magnitude larger than the $\Delta W/\Delta T$ coefficient found above. This justifies the assumption that the depletion width is temperature invariant for computational purposes.

In the next section, the temperature dependence of the scattering limited velocities are discussed.

2.3.5 The Scattering Limited Velocities of Holes and Electrons Temperature Dependence (v_p and v_n)

The following empirical equation was developed using a 3-point interpolation formula from the experimental data reported by Duh and Moll[20].

$$v_n(T) = 1.05\times10^7 f(t) \tag{2.22}$$

where

$$f(T) = 1.11 - 0.0011(T-200) + 5\times10^{-6}(T-200)(T-300) \tag{2.23}$$

Equation (2.22) describes the temperature dependence of the scattering limited drift velocity of electrons in silicon for electric field strengths greater than 2×10^5volts/cm.

In obtaining an empirical equation describing the temperature dependence of the scattering limited drift velocity of holes in silicon, the measurement obtained by Rodriguez et al[21] was used. However, Rodriguez et al performed their measurements only at one temperature (300°K) and results for other temperatures are not available. The value for the velocity of holes obtained by Rodriguez et al at 300°K is:

$$v_p = 7.5\times10^6 \text{cm/sec}$$

In this study, the temperature dependence of the velocity of holes is assumed to be of the same form as for the electrons. Incorporating the value obtained by Rodriguez et al[21], we can write:

$$v_p(T) = 7.5\times10^6 f(T) \tag{2.24}$$

With the aid of Section 2.3.2 and this section, the temperature dependence of the avalanche frequency is formulated in the next section.

2.3.6 The Avalanche Frequency Temperature Dependence (ω_o)

Fisher[15] has defined the avalanche frequency as:

$$\omega_o = \left[\frac{J_o \Phi}{\varepsilon_s \bar{\tau}}\right]^{\frac{1}{2}} \tag{2.25}$$

and for a constant current density Φ and $\bar{\tau}$ are temperature sensitive functions. In this study, all experiments on the IMPATT oscillator were conducted under constant current conditions.

Φ is defined by Fisher as:

$$\Phi = \frac{\alpha'}{\alpha} f\left(\frac{\alpha}{\beta}\right) + \frac{\beta'}{\beta} g\left(\frac{\alpha}{\beta}\right) \tag{2.26}$$

where

$$f\left(\frac{\alpha}{\beta}\right) = \frac{\ell n\left(\frac{\alpha}{\beta}\right)}{\left[\frac{\frac{\alpha}{\beta}+1}{\frac{\alpha}{\beta}-1} \cdot \ell n\left(\frac{\alpha}{\beta}\right) - 2\right]} \cdot \left[\frac{\left(\frac{\alpha}{\beta}\right) \ell n\left(\frac{\alpha}{\beta}\right)}{\frac{\alpha}{\beta}-1} - 1\right] \tag{2.27}$$

and

$$g\left(\frac{\alpha}{\beta}\right) = \frac{\ell n\left(\frac{\alpha}{\beta}\right)}{2\left[\frac{\frac{\alpha}{\beta}+1}{\frac{\alpha}{\beta}-1} \ell n\left(\frac{\alpha}{\beta}\right) - 2\right]} \cdot \left[1 - \frac{\ell n\left(\frac{\alpha}{\beta}\right)}{\frac{\alpha}{\beta}-1}\right] \tag{2.28}$$

The temperature dependencies of the ionization coefficients and their derivatives were described in Section 2.3.2 and may be used for computing the temperature dependence of Φ in Equation (2.26).

$\bar{\tau}$, the average transit time for holes and electrons in the ionization layer, is given by[15]

$$\bar{\tau} = \frac{1}{2}\left(\frac{\ell}{v_n} + \frac{\ell}{v_p}\right) \tag{2.29}$$

and since the ionization layer width and the scattering limited velocities are temperature dependent (see Sections 2.3.3 and 2.3.5 respectively) we obtain for $\bar{\tau}$:

$$\bar{\tau} = \frac{1}{2}\left(\frac{\ell(T)}{v_n(T)} + \frac{\ell(T)}{v_p(T)}\right) \tag{2.30}$$

The avalanche frequency as a function of diode-junction temperature may be computed by specifying the current density. The predicted variation of the avalanche frequency with diode-junction temperature is shown in Figure 5 and it is noted that the avalanche frequency decreases as the diode-junction temperature is increased. A swept-frequency reflection measurement was performed on the packaged diode to determine the actual avalanche frequency. The diode was placed at the end of a 50 ohm microstrip transmission line which was mounted on the same heat sink as the oscillator circuit. For various bias current values, the avalanche frequency was measured and the value corresponding to the current used in computing Figure 5 is plotted as a single point. Thermal resistance measurements indicated that the diode-junction temperature underwent a 150°K temperature rise for this bias current value.

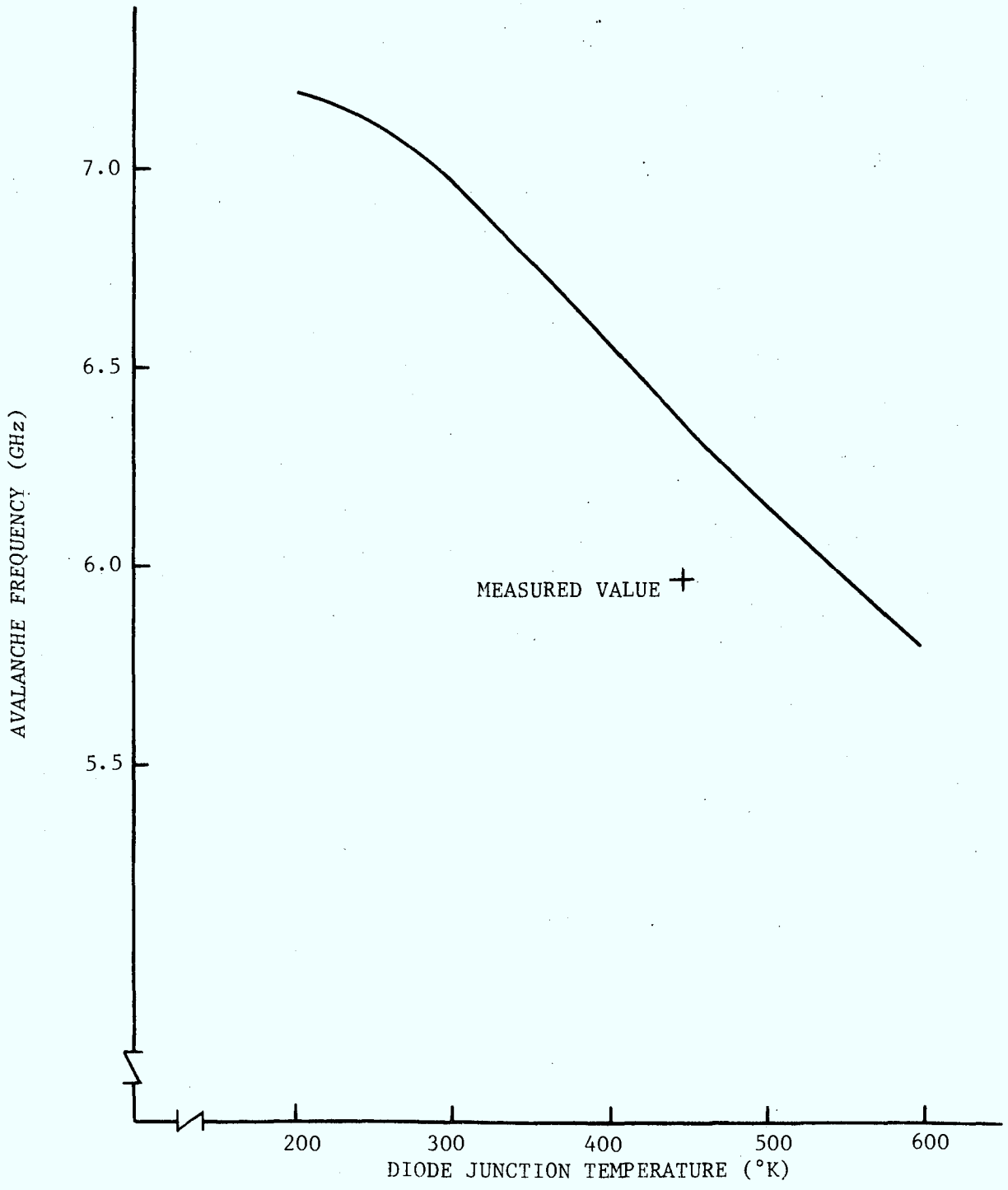

FIG. 5. VARIATION OF AVALANCHE FREQUENCY WITH DIODE-JUNCTION TEMPERATURE

The 10% error between the measured and computed value of the avalanche frequency is not unexpected. For example, the current density term in Equation (2.25) has the diode junction area as a factor. Measurements of the cross-sectional area are probably no better than 10% accurate. The ionization coefficients of the holes and electrons, and their derivatives, have been computed subject to a number of assumptions concerning the electric field distribution. Above all, the calculation of the avalanche frequency is based on a small-signal theory, thus the 10% error between the measured and the computed frequency is acceptable.

2.3.7 The Transit Angles Temperature Dependence (θ_p and θ_n)

The transit angles in the p- and n-depletion regions are defined as[22]:

$$\theta_p = \frac{\omega W_p}{v_p} \tag{2.31}$$

and

$$\theta_n = \frac{\omega W_n}{v_n} \tag{2.32}$$

In Sections 2.3.4 and 2.3.5, the temperature dependencies of the depletion layer widths and the scattering limited velocities were developed and may be employed in the above equations to give the temperature variation of the transit angles:

$$\theta_p(T) = \frac{\omega W_p}{v_p(T)} \tag{2.33}$$

and

$$\theta_n(T) = \frac{\omega W_n(T)}{v_n(T)} \qquad (2.34)$$

As outlined in Section 2.3.4, we have assumed that W_p is insensitive to temperature and so $\theta_p(T)$ is only affected by the temperature variation of the holes, $v_p(T)$. However, $\theta_n(T)$ is dependent on both the variation of $W_n(T)$ and $v_n(T)$.

2.3.8 IMPATT Diode Junction Impedance

The temperature sensitive relationships for the various parameters of Equation (2.4) allows us to compute the small-signal IMPATT diode impedance for various operating frequencies and diode-junction temperatures. Figure 6 shows an impedance plot over a large range of frequencies for two widely different diode-junction temperatures (300°K and 500°K) and it is noted that for all frequencies the device capacitance increases with temperature while the magnitude of the negative resistance reduces. A more common representation is shown in Figure 7 where the device admittance is plotted for various frequencies and diode-junction temperatures. Schroeder and Haddad[6] computed a similar curve for a non-punched-through Read type diode, using the small-signal analysis of Gilden and Hines[7]. They found that the maximum negative conductance increases with temperature and the frequency for maximum negative conductance decreases. Further, the computed results showed an increase in the device capacitive susceptance at a constant frequency for increased diode junction temperature. The

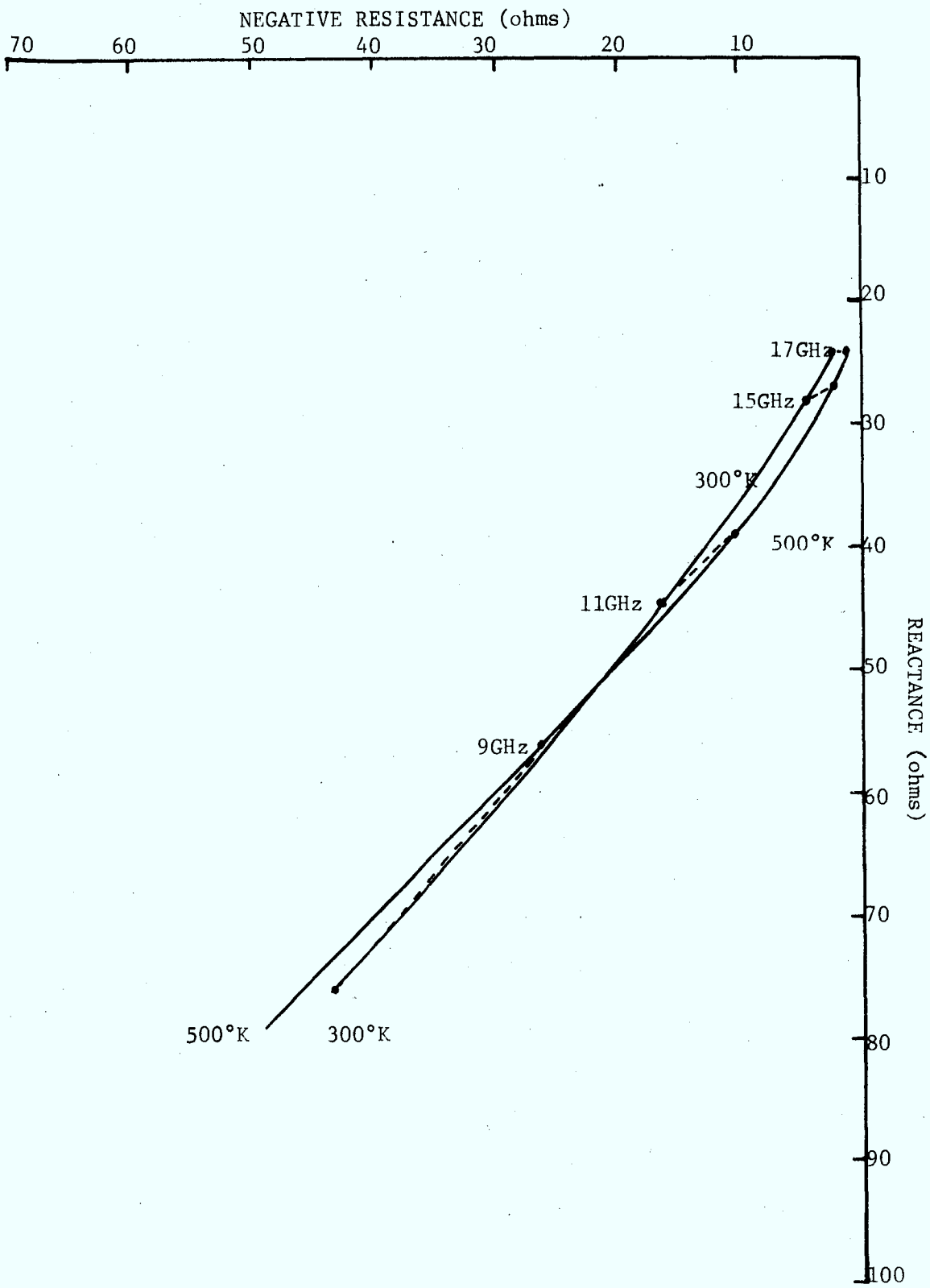

FIG. 6. IMPATT DIODE SMALL-SIGNAL IMPEDANCE FOR DIODE-JUNCTION TEMPERATURES OF 300°K AND 500°K

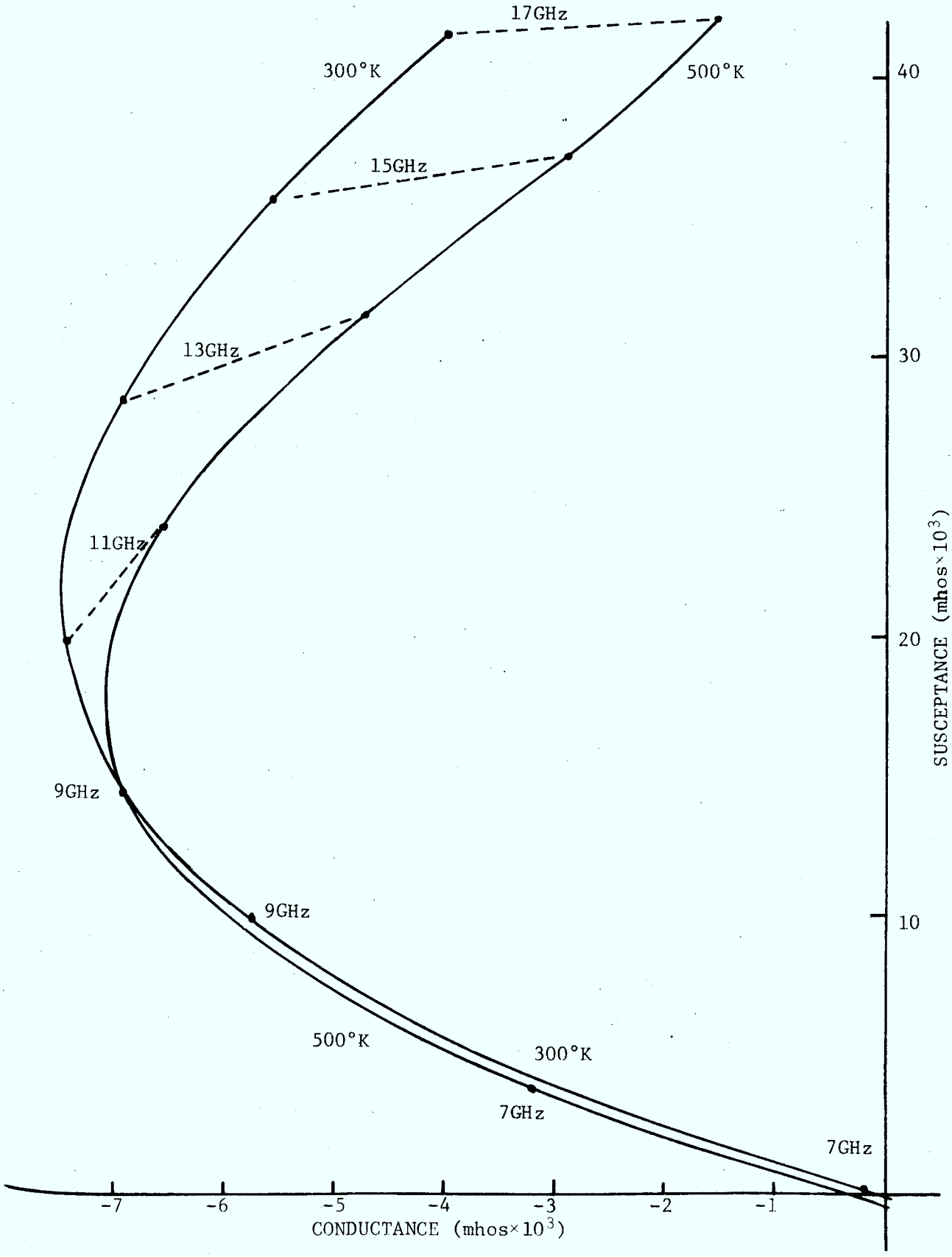

FIG. 7. IMPATT DIODE SMALL-SIGNAL ADMITTANCE FOR DIODE-JUNCTION TEMPERATURES OF 300°K AND 500°K

analysis presented here, however, shows that the magnitude of the negative conductance decreases with temperature rather than the increase as predicted by Schroeder and Haddad.

Grierson[8] also used the analysis of Gilden and Hines[7] in his study on the effect of temperature on the operation of an IMPATT diode and his results substantiated those of Schroeder and Haddad[6]. However, Gilden and Hines analysis has several limitations with no account of hole velocity, arbitrary avalanche/drift region distinction and arbitrary avalanche frequency. Recognizing this fact, Grierson[8] employed the computer analysis of Misawa[9] and computed an admittance curve for the same device for a range of frequencies and diode-junction temperatures. The more exact small-signal analysis of Misawa showed that the magnitude of the negative conductance decreases with temperature rather than increases, as the Gilden and Hines model predicts. These results are in agreement with the results presented here and displayed in Figure 7.

Although the above results provide a great deal of information on the frequency-temperature characteristics of the IMPATT diode junction, the circuit designer must work with an encapsulated device. The next section considers a microwave package for encapsulating the IMPATT diode and the frequency-temperature characteristics of the diode and package combination are examined.

2.3.9 Microwave Diode Package and Overall Frequency-Temperature Characteristics of the Diode

Thus far, the temperature sensitive IMPATT diode chip has been described and it remains only to assign a suitable microwave package for the chip. Figure 8 indicates a package layout commonly used[23,24,25] and the parameter values of the components. It is assumed that the package components are temperature insensitive. The component values initially used were obtained from Reference (23) and were subsequently adjusted so as to give a packaged diode output reactance similar to that of the diodes used for this study. The output impedance of the diodes used was measured using a coaxial jig with an accessible diode reference point.

A computer program was developed which first evaluated the diode chip impedance [Equation (2.4)] then transformed this impedance through the microwave diode package to the terminals (see Figure 8). An impedance plot is shown in Figure 9 indicating the results of this computation.

A number of observations are worth noting on Figure 9. First, the microwave diode package strongly affects the shape of the impedance plot. While Figure 6, which shows the impedance plot of the diode chip, is monotonic in nature, the transformed impedance is highly irregular. However, this is not surprising when one considers that the frequency range covered is more than one octave and the microwave package has three discrete elements. Second, for frequencies below approximately 9GHz (the cross-over point), the magnitude of the negative resistance increases with diode-junction temperature for constant frequency, while

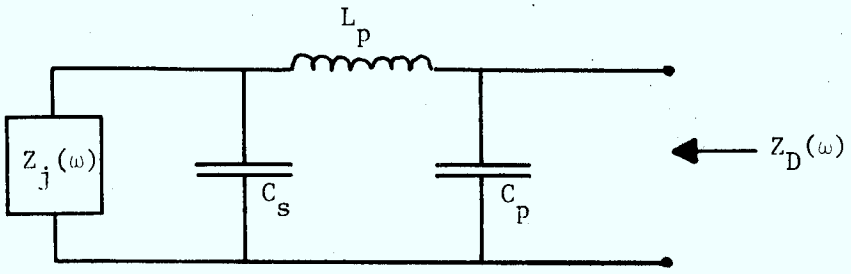

$L_p = 0.4nH$

$C_s = 0.1pF$

$C_p = 0.25pF$

FIG. 8. MICROWAVE DIODE PACKAGE LUMPED ELEMENT MODEL

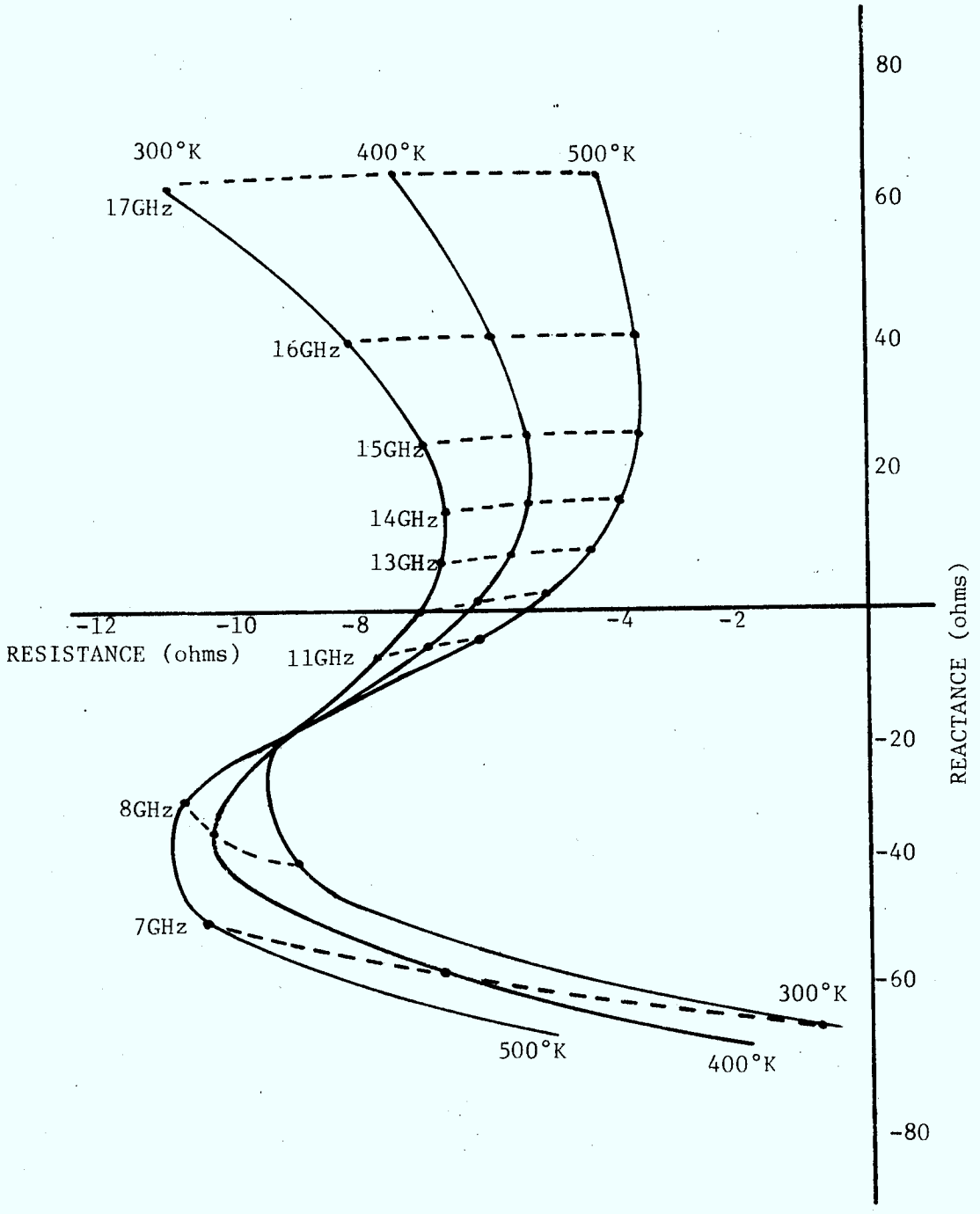

FIG. 9. PACKAGED DIODE IMPEDANCE FOR THREE DIFFERENT DIODE-JUNCTION TEMPERATURES: 300°K, 400°K AND 500°K

above the cross-over point, the magnitude of the negative resistance decreases with diode-junction temperature. Third, the packaged diode reactance increases with temperature for constant frequency. This fact alone indicates that the oscillator frequency would shift downward if the oscillator circuit was temperature insensitive and a diode having the characteristics of Figure 9 was used. Schroeder and Haddad[6] have observed this effect in a controlled experiment.

Earlier in Section 2.2, Equation (2.3) was developed for the frequency-temperature coefficient of an oscillator. Two terms of that equation are $\partial X_D/\partial f$ and $\partial X_D/\partial T$. These terms are plotted in Figures 10 and 11 as the predicted variations of the packaged diode output reactance with frequency and temperature respectively. In Figure 10, the measured large-signal reactance is shown and it is noted that there is general agreement between the shape of the measured large-signal curve and the shape of the small-signal predicted curve. As noted earlier in Section 2.2, the assumption that $\partial X_D/\partial f$ is relatively insensitive to temperature is effectively demonstrated in Figure 10. The plot of the packaged diode output reactance against diode-junction temperature, Figure 11, shows that the slope of the curves, $\partial X_D/\partial T$, may vary significantly over very wide frequency ranges and it is shown later that this variation may be used to advantage when designing temperature stable oscillators.

In the following section, the temperature sensitive packaged diode model will be coupled with a microwave circuit so that the frequency-temperature characteristic of an IMPATT oscillator may be examined and compared to measured results.

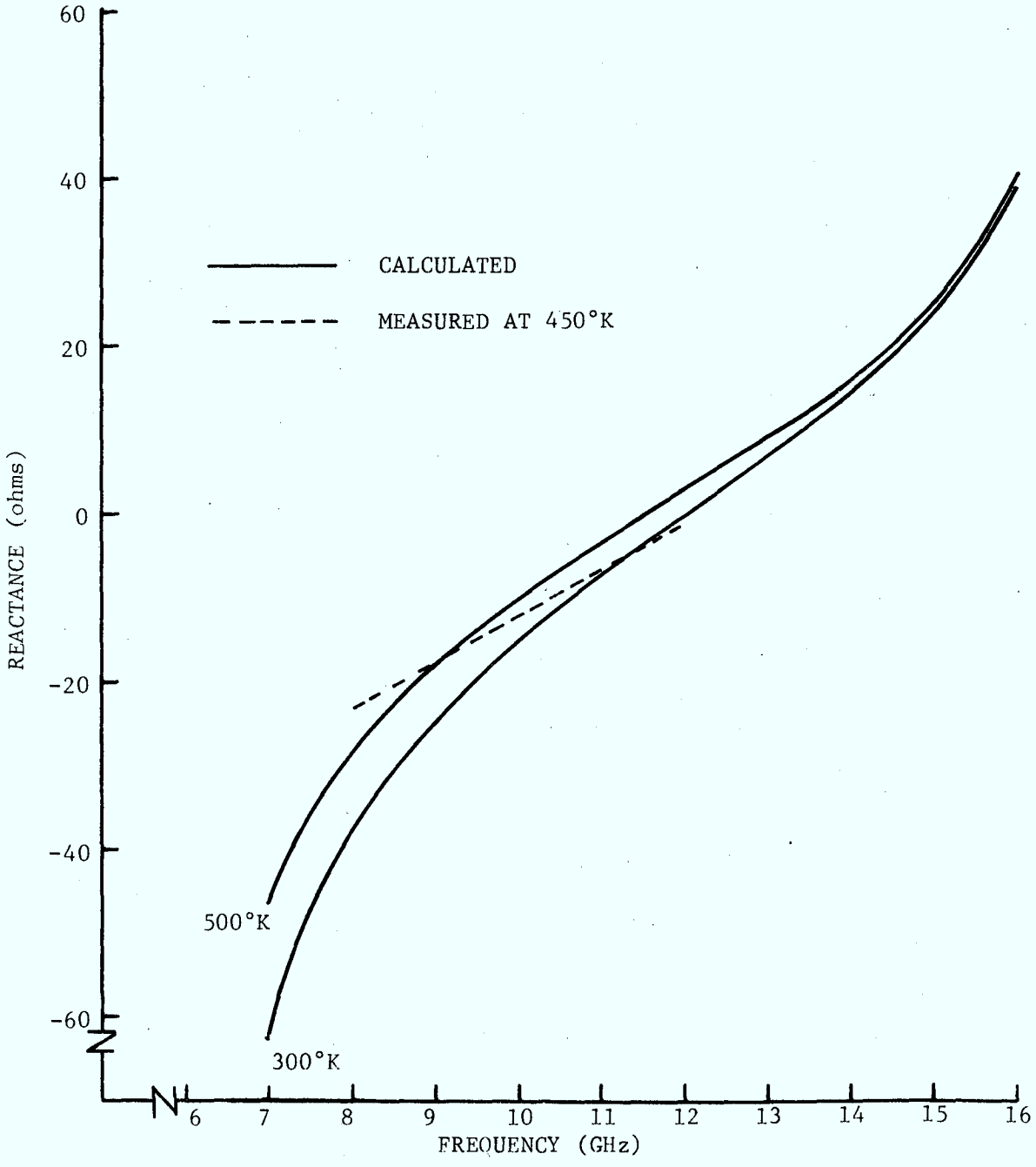

FIG. 10. PACKAGED DIODE REACTANCE VERSUS FREQUENCY FOR DIODE-JUNCTION TEMPERATURES OF 300°K AND 500°K

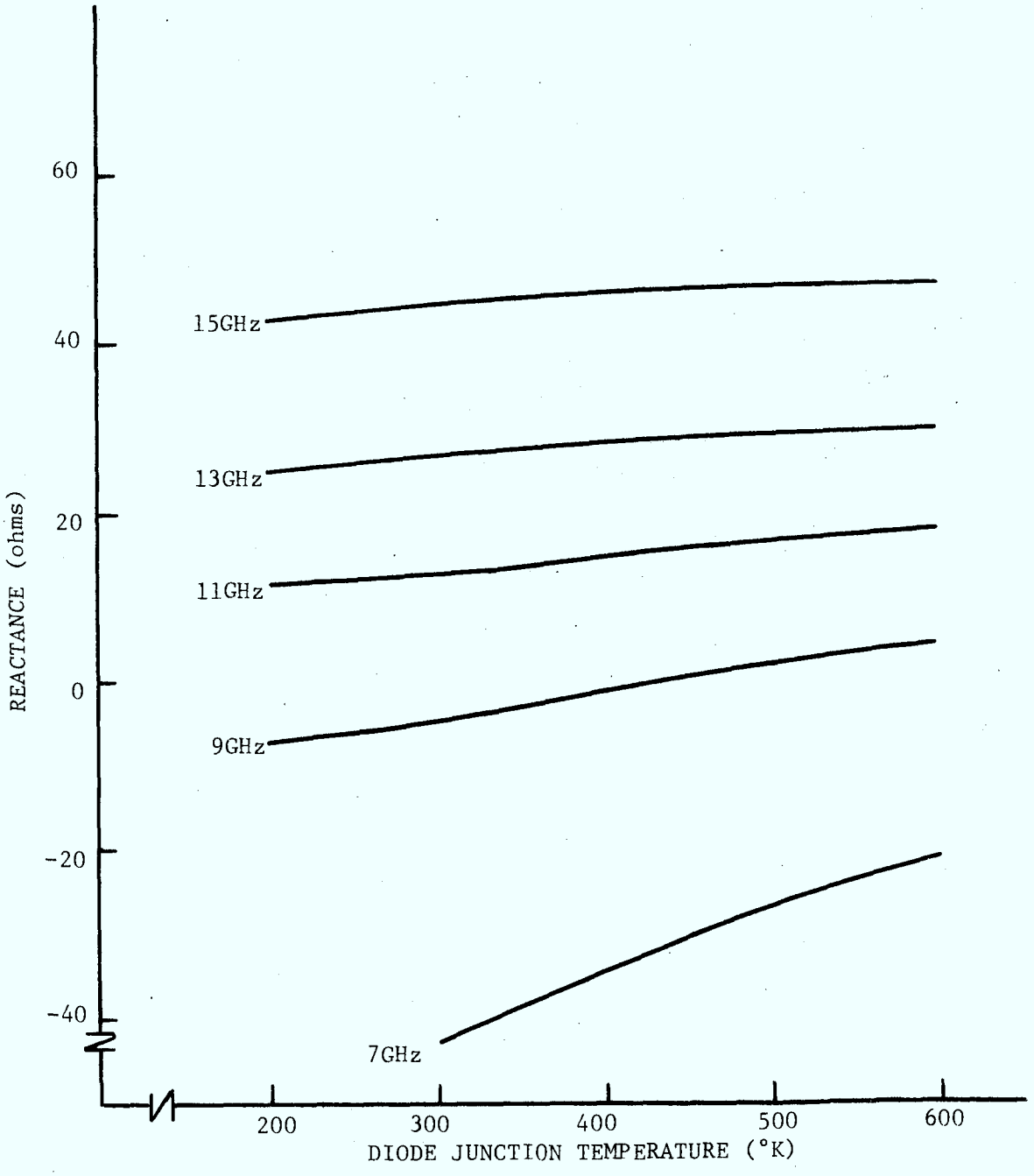

FIG. 11. PACKAGED DIODE REACTANCE VERSUS DIODE-JUNCTION TEMPERATURES FOR DIFFERENT FREQUENCIES: 7, 9, 11, 13 AND 15GHz

2.4 Circuit Effects and Overall Oscillator Performance - Measured and Predicted

The IMPATT oscillators used in this study were constructed on microstrip. Although the characteristics of microstrip transmission lines and circuit elements are not as well behaved as waveguide components, recent advances of theoretical and practical knowledge have been made. This has resulted in a steady rise in the use of microstrip as a circuit element. The experimental results reported here were obtained using a low-Q microstrip oscillator whose design and circuit layout are given in Appendix A.

The relative dielectric constant of the thin plastic substrate† was found to be the predominately temperature-sensitive microstrip parameter. Measurement of the sheet capacitance of the microstrip material for a range of temperatures showed that the relative dielectric constant could be described analytically by the following empirical relationship.

$$\varepsilon_r(T) = \varepsilon_{r_o}\left\{1 + 0.01\left[2\cos\left[\pi\left[\frac{T-225}{130}\right]\right] + 1\right]\right\} \tag{2.35}$$

This variation of the relative dielectric constant with temperature is shown in Figure 12.

---

† ε_r = 2.3 Rogers Teflon - Duroid D5880

In order to demonstrate the effect of temperature and frequency on the microwave circuit, a computer program was developed which calculated the load impedance presented to the diode by the microstrip circuit. It was assumed that the external RF load was constant at 50 ohms for all frequencies and temperatures of interest. The program used the lossless transmission line equations[26] for simplicity; however, the program did account for the high-frequency microstrip parasitic effects (dispersion[27], impedance discontinuities[28]) and for the stray shunt capacitance associated with the diode package flange which overlaps the microstrip substrate. In Appendix A, it is shown that the microstrip IMPATT oscillator may be tuned by adjusting the length of the open-ended stub. For two different stub lengths, and hence two different frequencies (approximately 9GHz and 11GHz), the frequency-temperature characteristic of the oscillator was measured. For these two frequency ranges, the predicted load impedance was computed. Figures 13 and 14 show the impedance plots for the two frequency ranges and it is noted that in both cases the low temperature points tend to move counterclockwise as the microstrip substrate temperature is increased at a constant frequency. The predicted load reactance versus frequency and temperature are shown in Figures 15 (a and b) and 16. As assumed in Section 2.2, it is seen that $\partial X_L/\partial T$ and $\partial X_L/\partial f$ [terms in Equation (2.3] are relatively insensitive to parameter variations of practical interest.

In order to compute the frequency of oscillation of the IMPATT oscillator, a computer program was developed which combined the temperature sensitive packaged diode and microstrip circuit models. For a given ambient temperature and starting frequency, the program calculated

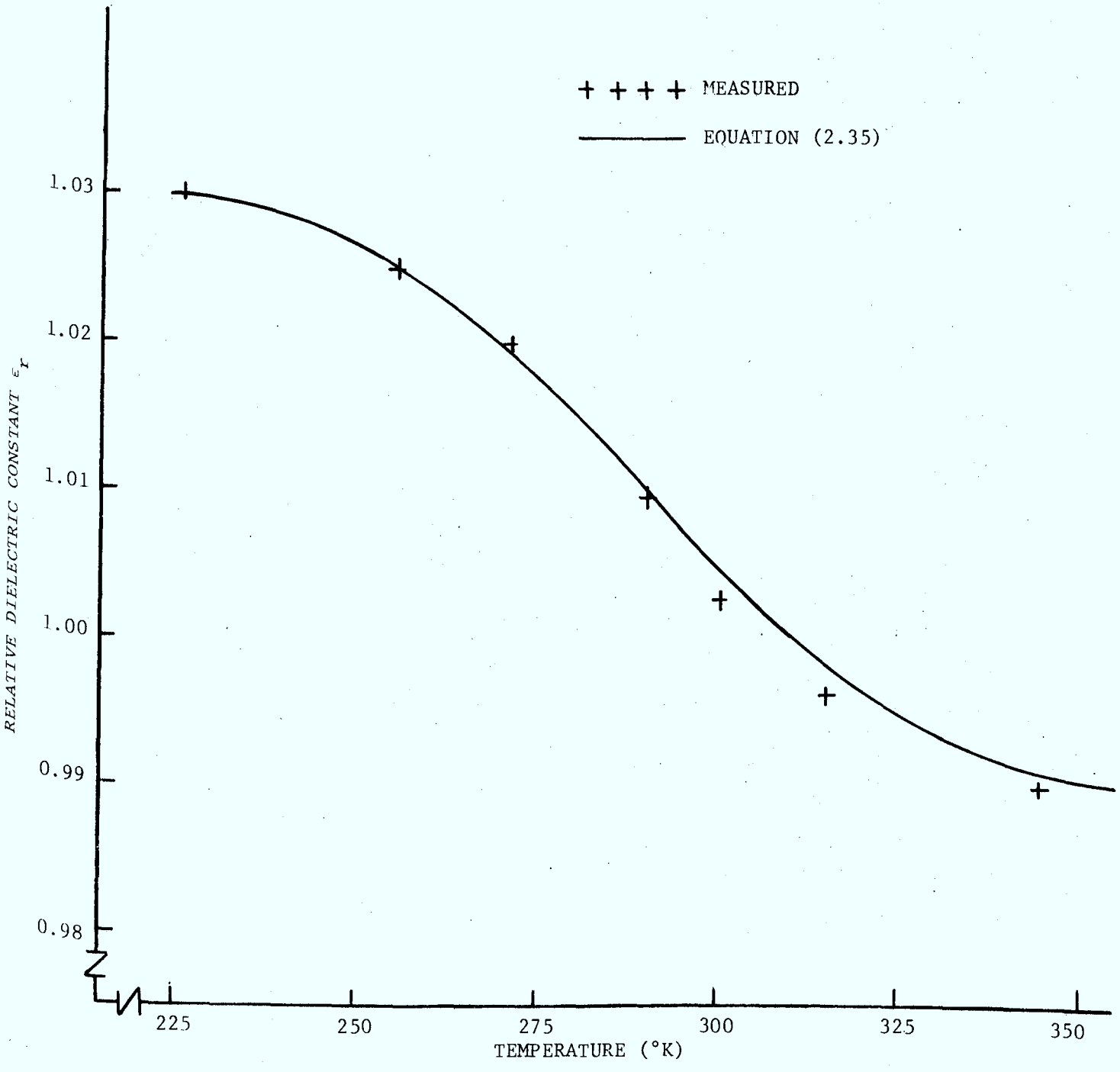

FIG. 12. RELATIVE DIELECTRIC CONSTANT VERSUS TEMPERATURE OF PLASTIC MICROSTRIP SUBSTRATE

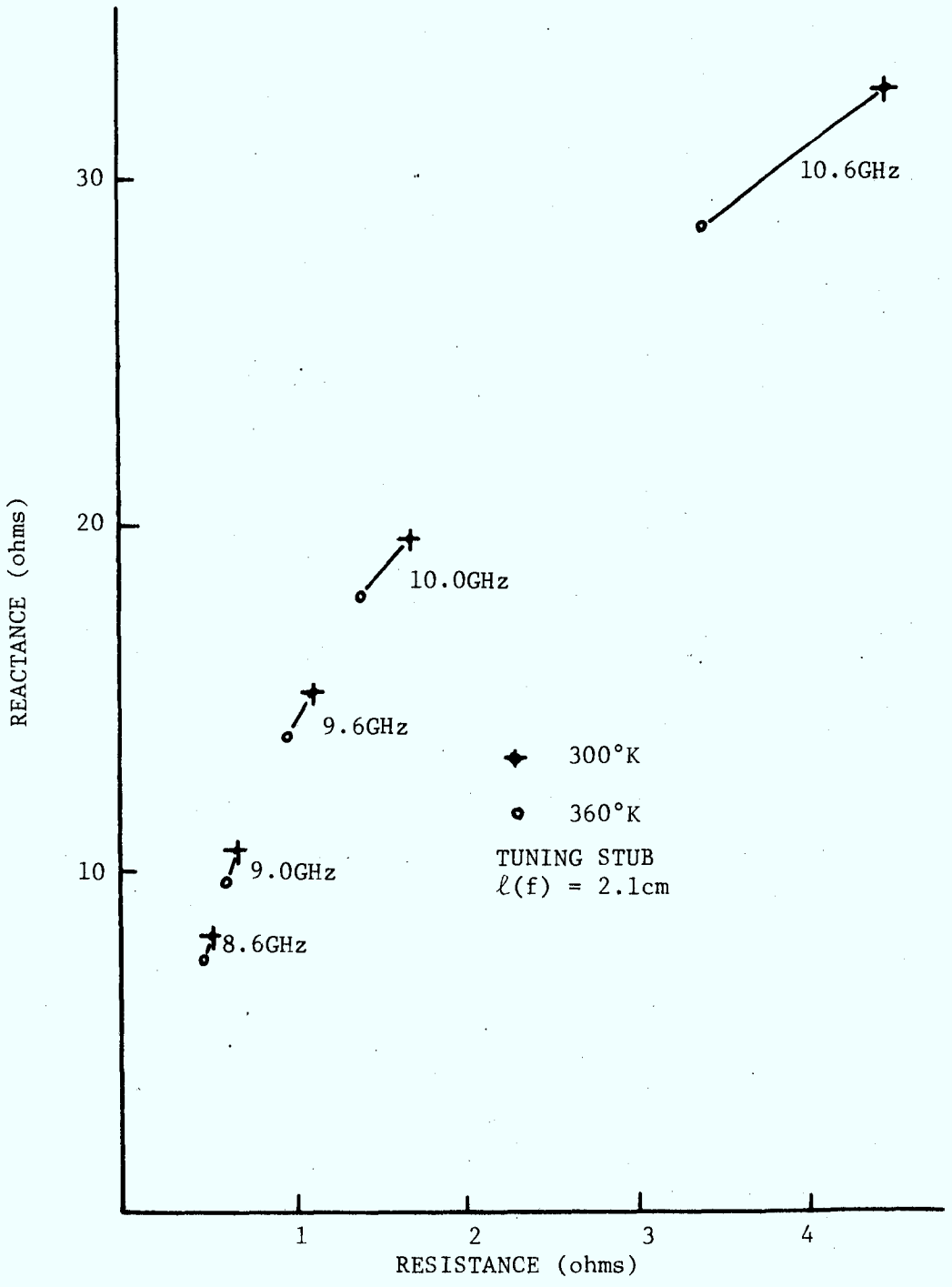

FIG. 13. VARIATION OF CIRCUIT IMPEDANCE AT DIODE TERMINALS WITH TEMPERATURE (300°K AND 360°K). TUNING STUB $\ell(f)$ = 2.1cm

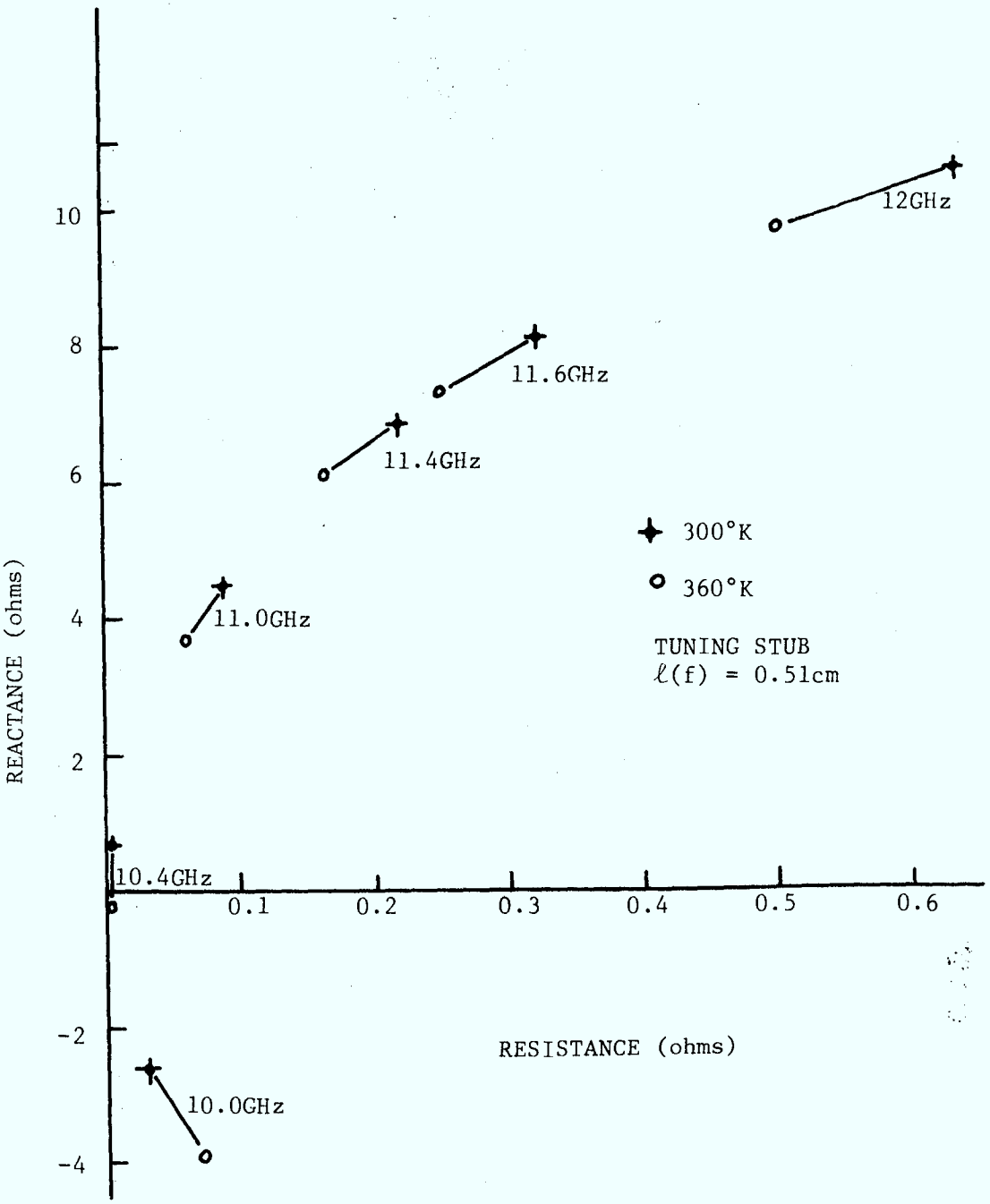

FIG. 14. VARIATION OF CIRCUIT IMPEDANCE AT DIODE TERMINALS WITH TEMPERATURE (300°K AND 360°K). TUNING STUB $\ell(f)$ = 0.51cm

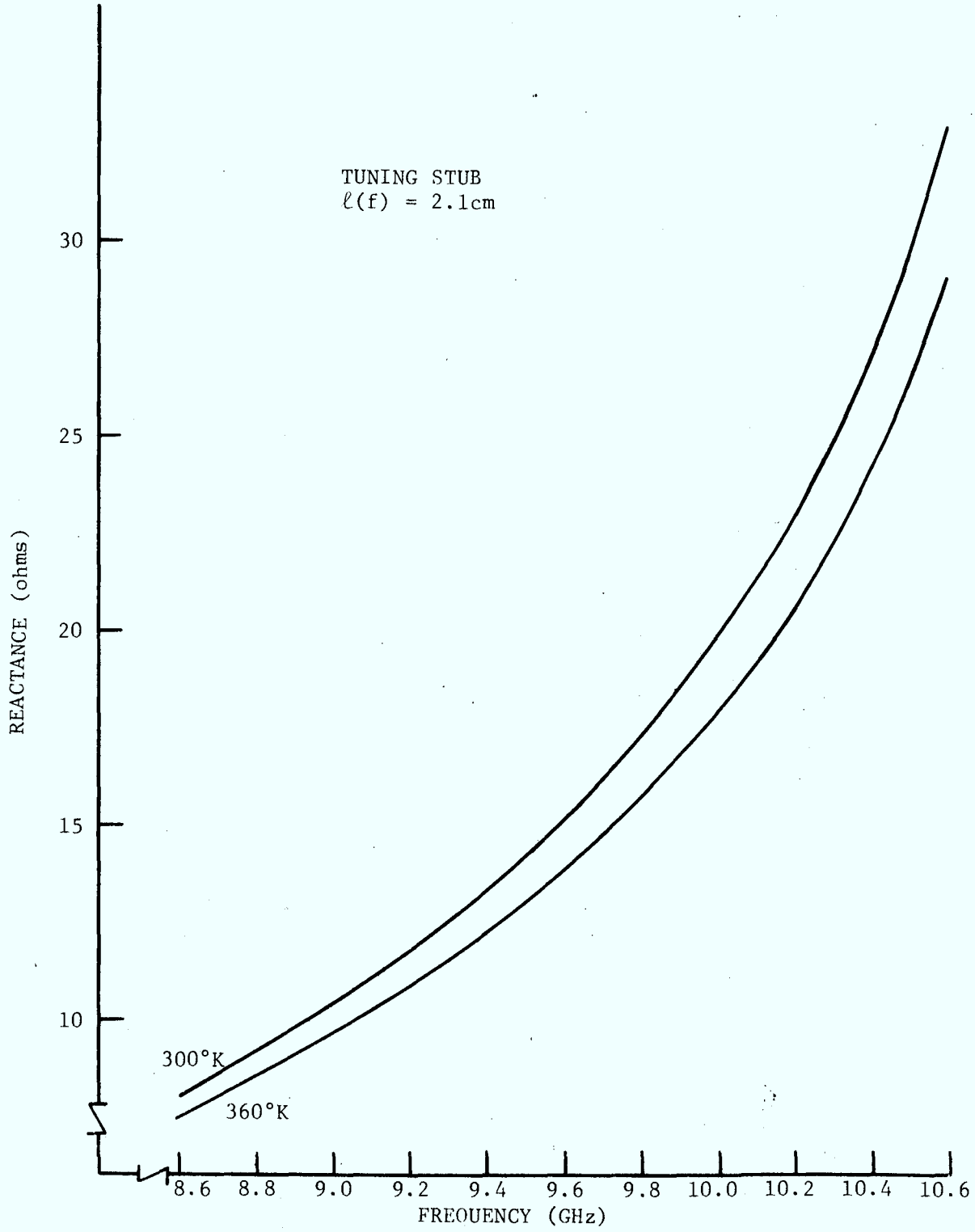

FIG. 15a. CIRCUIT REACTANCE VERSUS FREQUENCY FOR TWO DIFFERENT TEMPERATURES (300°K AND 360°K). TUNING STUB $\ell(f)$ = 2.1cm

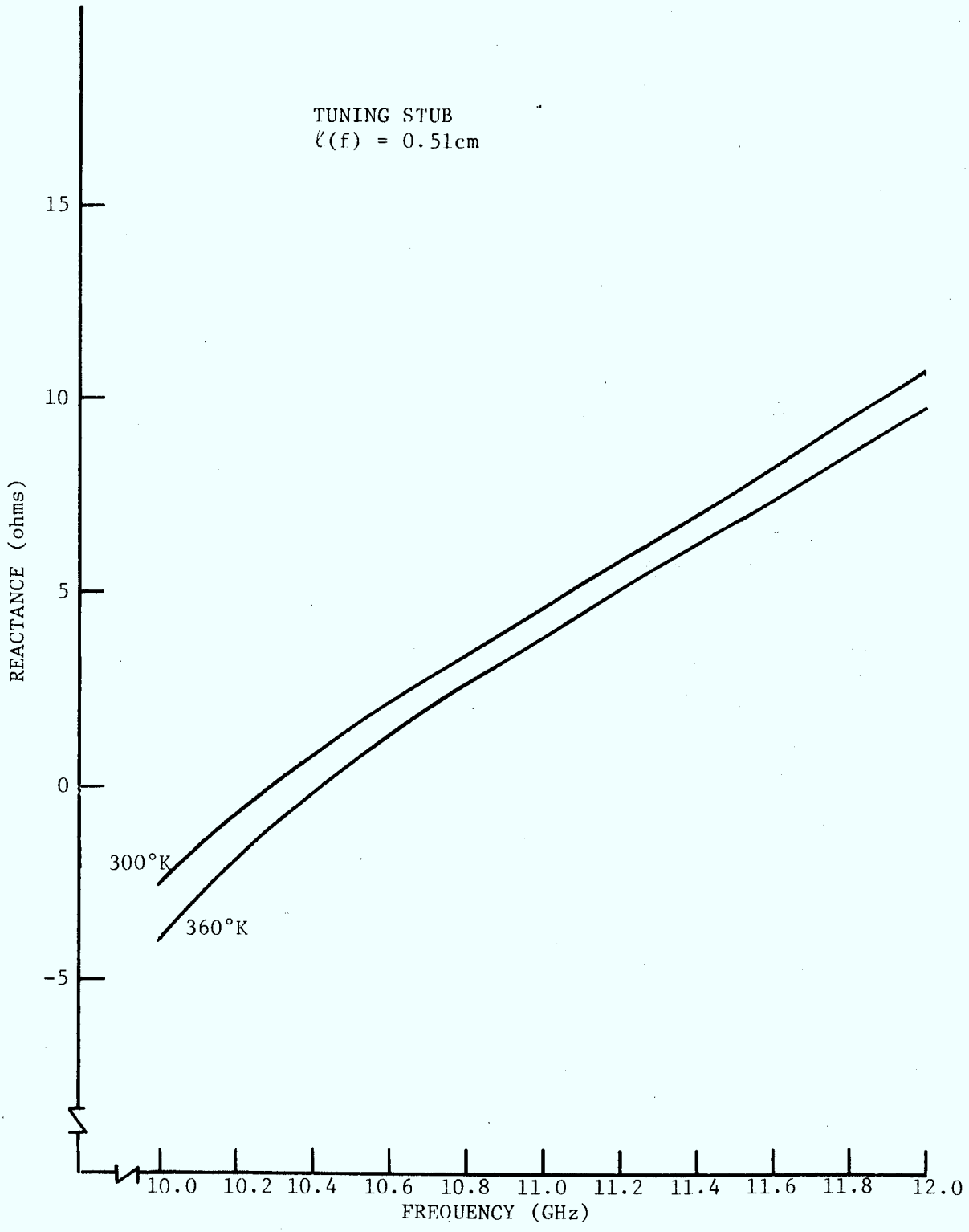

FIG. 15b. CIRCUIT REACTANCE VERSUS FREQUENCY FOR TWO DIFFERENT TEMPERATURES (300°K AND 360°K). TUNING STUB $\ell(f)$ = 0.51cm

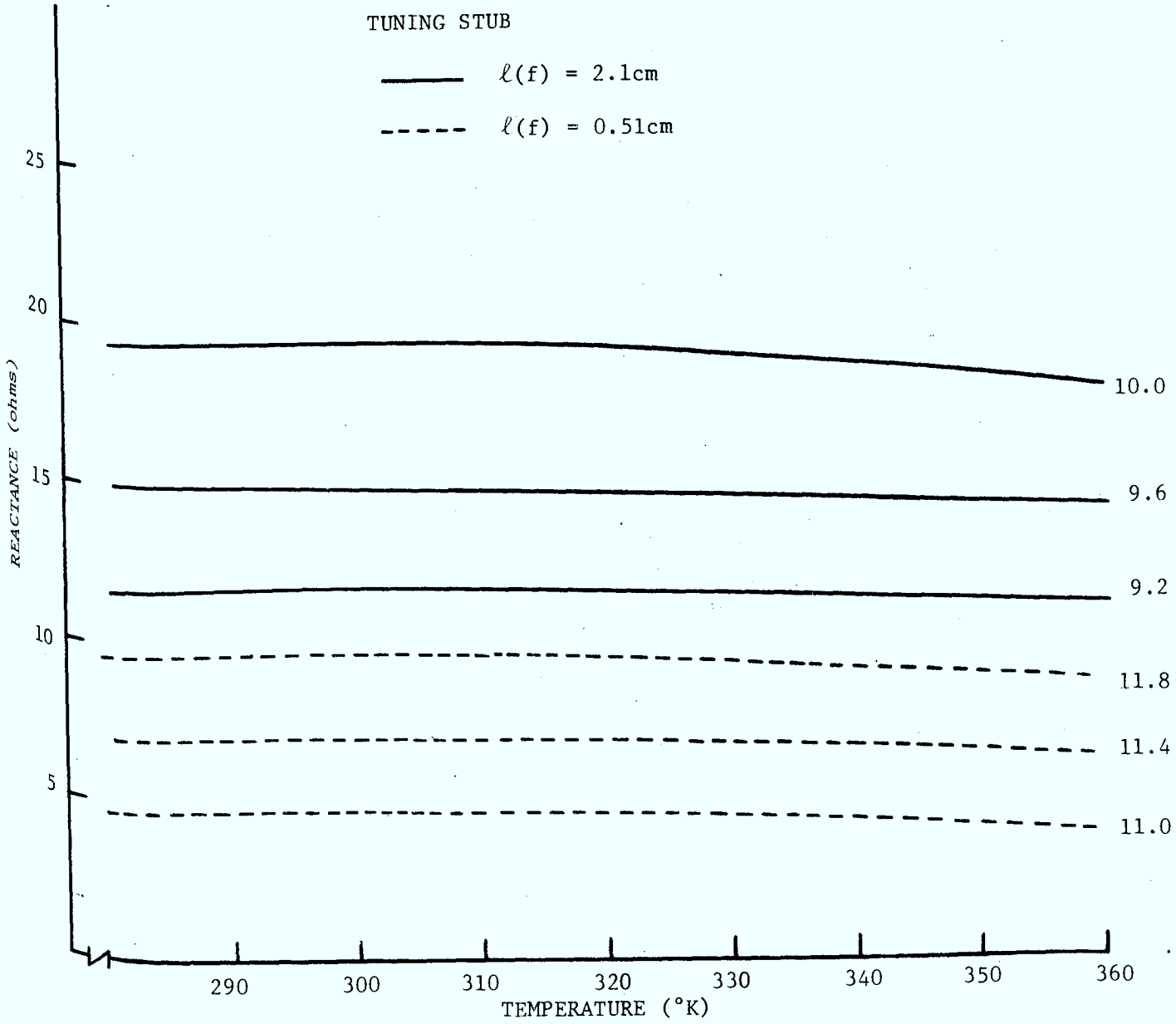

FIG. 16. CIRCUIT REACTANCE VERSUS TEMPERATURE FOR TWO DIFFERENT TUNING STUB LENGTHS:
i) $\ell(f) = 2.1$cm
ii) $\ell(f) = 0.51$cm

the impedance of the packaged diode, and the impedance that the microstrip circuit presented to the diode. The frequency was incremented to find new impedances from which the circuit reactance versus frequency curve and the diode reactance versus frequency curve were solved for that frequency which gave the conjugate circuit and diode reactances. The frequency was iterated and the process continued until a frequency of oscillation accuracy of 10KHz was achieved. This process effectively searched for that frequency which gave a sum reactance of zero ohms and therefore satisfied the basic oscillation condition as given in Equation (2.1). It should be pointed out that the requirement for equal magnitudes of the real parts of the impedances is not considered since this study is concerned with a small-signal analysis only. A large-signal analysis, of course, would account for this fact. Using the last computed oscillation frequency, the ambient temperature was incremented to find the next oscillation point. A large-signal analysis performed by Edridge[29] recently on the frequency stability of GUNN diodes in waveguide circuits considered the requirement mentioned above. Thermal resistance measurements[30] indicated that at the current bias level of interest (a constant current of 40mA was used for the oscillator), the diode-junction temperature rise was approximately 150°K above the heat sink temperature. The temperature of the microstrip circuit was assumed to be constant throughout its entire surface area and to be equal to the heat sink temperature. The calculated frequency of oscillation versus ambient temperature for the two different frequency ranges are shown in Figure 17 (a and b). The measured frequency-temperature results are also shown in Figure 17 and it is seen that the measured and calculated

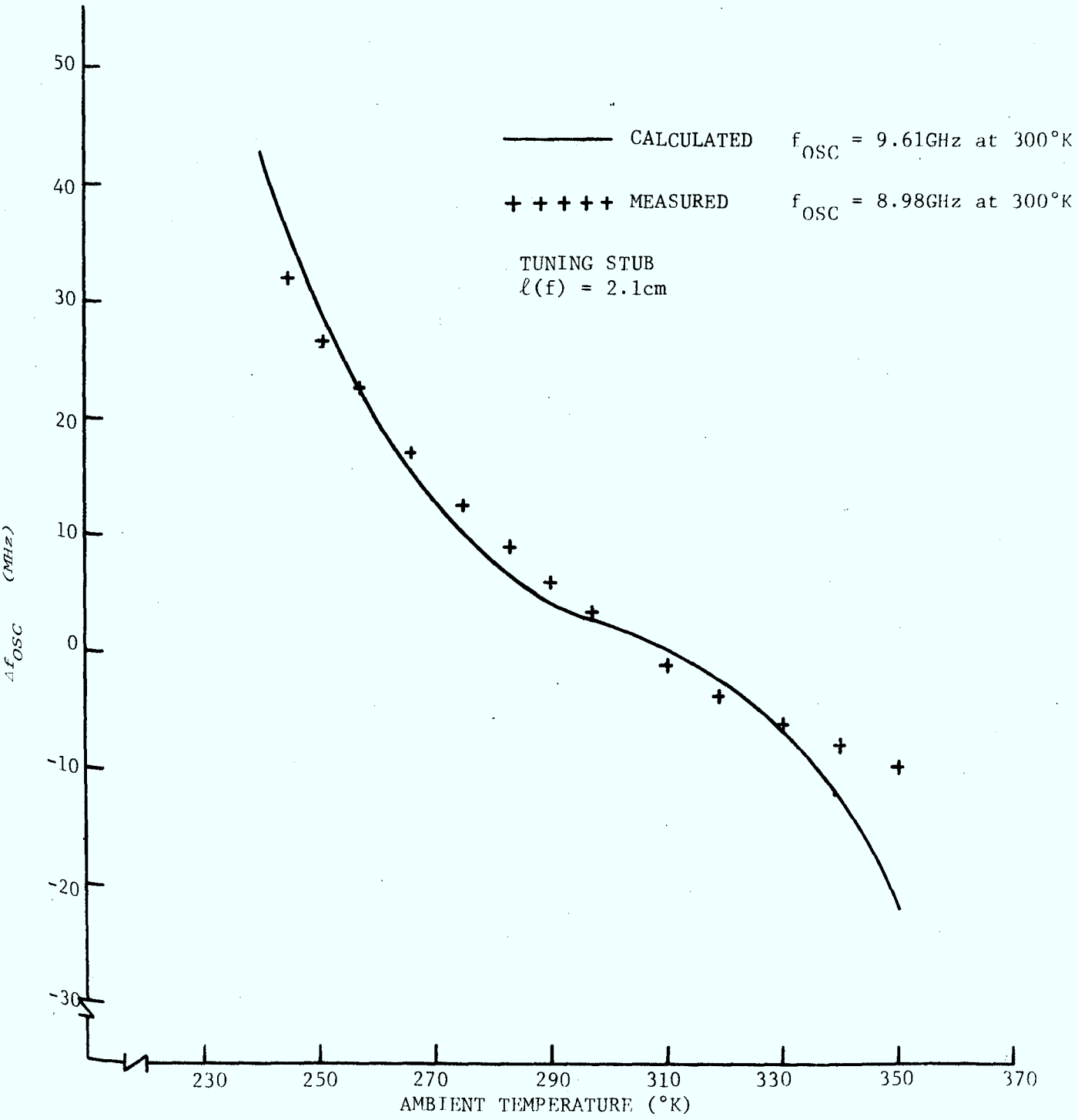

FIG. 17a. FREQUENCY OF OSCILLATION VERSUS AMBIENT TEMPERATURE. TUNING STUB LENGTH = 2.1cm

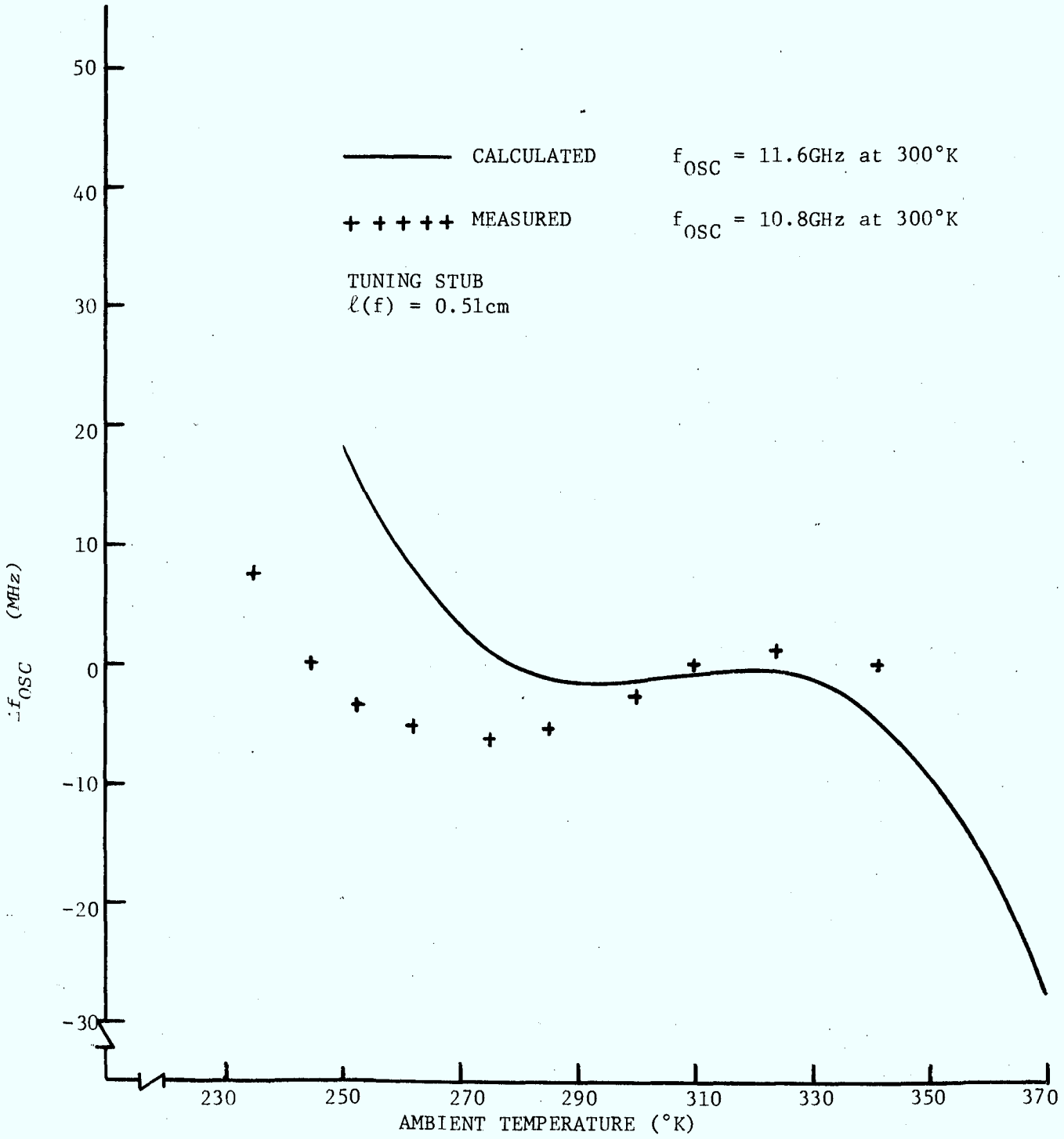

FIG. 17b. FREQUENCY OF OSCILLATION VERSUS AMBIENT TEMPERATURE.
TUNING STUB LENGTH = 0.51cm

results are in general agreement.

It should also be noted that the measured and computed frequency of oscillation differ by a few hundred megahertz. However, this discrepancy is not unrealistic if one considers that the IMPATT diode has been described by a small-signal model which cannot accurately depict the true operating conditions of the diode and circuit. Further, no attempt was made to optimize the parameter values of either the IMPATT diode chip or the microwave package.

Figure 18 shows the experimental test set-up used for measuring the characteristics of the oscillator. In earlier experiments, the coaxial isolator was not used and it was found that the miniature coaxial cable connecting the oscillator to the measuring equipment was temperature sensitive. The temperature sensitivity was manifested in a changing impedance. Reflection measurements on the coaxial isolator indicated that it was impedance stable for all temperatures and its inclusion in the test set-up ensured that the characteristic frequency-temperature signature of the oscillator was independent of external VSWR variations with temperature.

With reference to the oscillator frequency-temperature curves (Figure 17a and b), it is observed that the low frequency curve ($\approx$9GHz) is monotonic in nature while the high frequency curve ($\approx$11GHz) exhibits a hump. The reason for the difference in form of the two curves is apparent from an examination of Figure 11 (X_D versus T) and Figure 16 (X_L versus T). The slope of the X_D versus T curve at 11GHz is approximately 55% less in magnitude than at 9GHz while the slopes of the X_L versus T curves are relatively equal at the same two frequencies. At

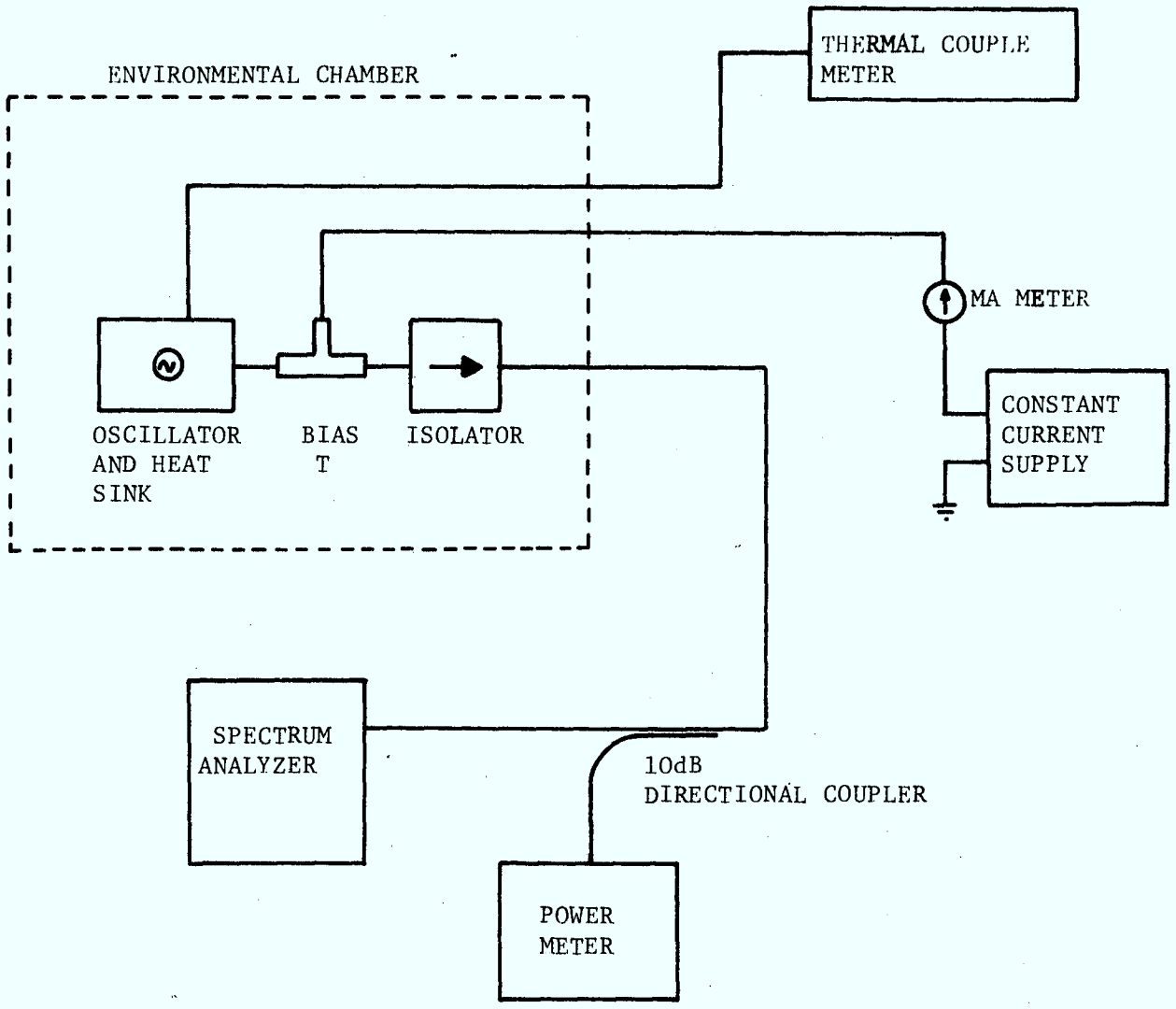

FREQUENCY-TEMPERATURE TEST SET-UP

FIG. 18. EXPERIMENTAL TEST SET-UP FOR MEASURING THE OSCILLATOR TEMPERATURE CHARACTERISTICS

11GHz, the diode predominates at the extremes of ambient temperature (negative f_{OSC} versus T coefficient) while the circuit predominates in the vicinity of room temperature (positive f_{OSC} versus T coefficient). At 9GHz, however, the oscillator frequency-temperature coefficient is determined primarily by the diode effects over the whole temperature range.

It is worth noting the significant difference between the microstrip oscillator and a waveguide oscillator. It has been demonstrated above that the microstrip circuit used in this study exhibits a non-constant rate of change of reactance with temperature. Re-examination of Figure 12 showing the variation of the relative dielectric constant with temperature clearly demonstrates this fact. Waveguide circuits, on the other hand, do not suffer from this characteristic but rather they have a constant rate of change of reactance with temperature as determined by the thermal coefficient of expansion. Sigmon[31], in his study of temperature stabilization of avalanche transit-time oscillators in waveguide circuits, shows that the frequency-temperature coefficient of the oscillator is constant for wide differences in ambient temperature. Schroeder and Haddad[6] have conducted similar experiments and have also shown the constant dependence of oscillator frequency on-diode junction temperature.

The theoretical and experimental results discussed above indicate that the frequency-temperature coefficient depends largely on the frequency of operation. For microstrip circuits at least, it has been shown that the change in circuit reactance at the diode terminals due to temperature variations is relatively constant for different fre-

quencies. For the packaged diode, however, the change in output reactance varies considerably at constant frequency for changes in diode-junction temperature. The impedance plot of the packaged diode for different diode-junction temperatures, plotted in Figure 9, clearly illustrates this point. The relative insensitivity of diode reactance to temperature at high frequencies (see for example, Figure 11, 15GHz) suggests that the frequency-temperature coefficient of an IMPATT oscillator operating at high frequency (greater than 13GHz) would be significantly lower than for lower operating frequencies. It is, of course, implied that the microwave circuit is temperature insensitive. It is interesting to note that the diodes used in this study were manufactured for use in the 8-12GHz frequency range which appears to be the worst range for temperature stable oscillators.

Although this study is mainly concerned with the frequency-temperature characteristics of microstrip IMPATT oscillators, it is appropriate to discuss briefly the effect of temperature on the power output of the oscillator. Figure 19 shows the power output plots for the two different operating frequencies (9GHz and 11GHz) when the ambient temperature is varied. The low frequency curve (9GHz) increases in power for increasing ambient temperatures to a maximum at room temperature. The high frequency curve (11GHz) first increases in power to a maximum at room temperature, then decreases. A qualitative theoretical understanding for this observed effect may be obtained by considering the effect of temperature on the packaged diode output impedance and the impedance that the microstrip circuit presents to it. The impedance plots of the circuit impedance are shown in Figures 13 and

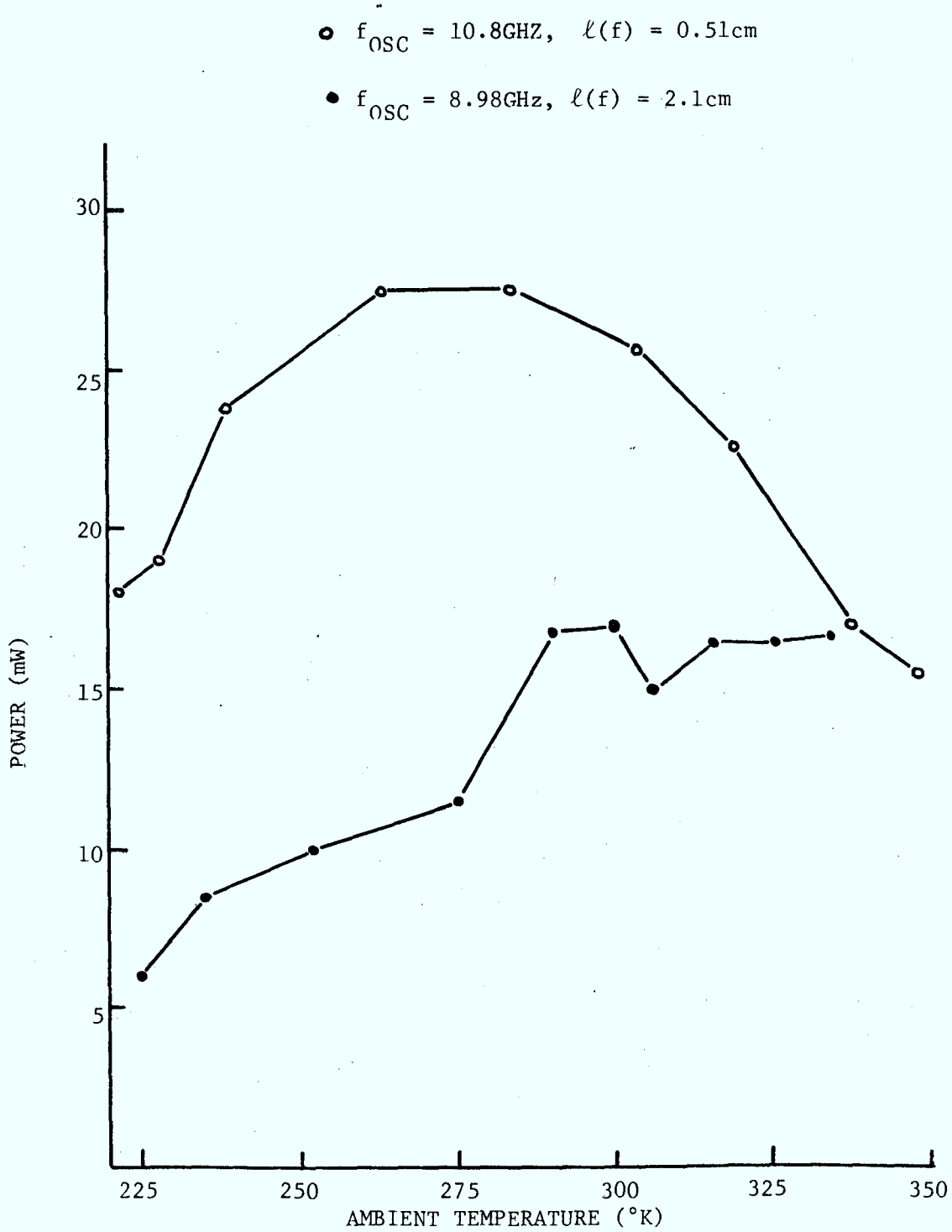

FIG. 19. POWER OUTPUT VERSUS AMBIENT TEMPERATURE FOR TWO DIFFERENT FREQUENCIES: 8.98GHz AND 10.8GHz

14. Both curves indicate a reduction in the real part of the impedance for increasing temperature. In contrast, the real part of the packaged diode output impedance increases with junction temperature at 9GHz and decreases with junction temperature at 11GHz. From an impedance standpoint, the low frequency oscillator power curve may be interpreted to mean that the diode and circuit resistances are approaching each other giving a maximum power condition at high temperature. In the high frequency case, the diode and circuit resistances may move together at lower temperatures, pass through the optimum resistance point in the vicinity of room temperature, then separate at higher temperatures for a reduction in power output. This would explain the hump in the power-temperature curve of the high frequency oscillator. The above discussion is based solely on small-signal theory and therefore must not be considered typical.

Another effect which has not been considered concerns the rise of the input DC power as the ambient temperature increases. The bias current for the oscillators is constant; however, the reduction in the ionization coefficients with temperature causes the diode breakdown voltage to increase, thus increasing the input power. Assuming that the oscillator DC to RF conversion efficiency remains relatively constant with temperature, we would expect the power output to increase with diode temperature. The steady increase in output power with temperature for the low frequency oscillator tends to agree with this hypothesis; however, the high frequency oscillator power-temperature results disqualify this argument. It is, of course, impossible to be quantitative about this from a small-signal analysis.

2.5 Conclusions

The frequency-temperature coefficient of a microstrip silicon IMPATT oscillator is a function of the temperature characteristics of the diode and of the circuit. The correspondence between the measured and predicted frequency-temperature results indicate that Fisher's[15] small-signal model may be adequately modified to include the effect of temperature on the various parameters of the diode. The difference between the low frequency (≈9GHz) and high frequency (≈11GHz) oscillators is due to the smaller change in diode reactance with temperature at higher frequencies and it is concluded that this fact may be used to advantage in designing frequency stable IMPATT oscillators.

CHAPTER 3

TEMPERATURE AND CURRENT EFFECTS OF PULSE MODE IMPATT OSCILLATORS

3.1 Introduction

In this Chapter, the effects of temperature and current on the frequency of a pulsed IMPATT oscillator is discussed. Experiments have shown that for increasing pulse width, the frequency decreases. A number of arguments are presented in order to explain this phenomena and it is shown that the combined effect of the temperature rise of the diode junction and the current density redistribution may account for the observed frequency shift.

3.2 Variation of Oscillator Frequency in Pulse Mode Operation

In some applications, such as pulse code modulated communication systems, there is a need for a pulsed RF signal. Ideally, the frequency spectrum of such a signal should display the theoretical sin X/X shape. For pulsed IMPATT diodes in low-Q circuits, experiments have shown that for narrow pulse widths (<1μsec) the oscillator will display a reasonable sin X/X frequency spectrum. However, for wider pulse widths (>1μsec), the ideal spectrum deteriorates. The experiments have also indicated that the centre frequency of oscillation decreases with increasing pulse width.

The possible reasons for the frequency shifting and frequency spectrum degradation with increasing pulse width may be stated as follows:

i) The thermal resistance and capacitance of the IMPATT diode cause the junction temperature of the diode to increase during the "on" time and decrease during the "off" time. For short pulse widths, the thermal capacitance effectively clamps the diode-junction temperature to its "off" value, while for wider pulse widths, the junction temperature begins to rise to the CW value. In Chapter 2, it was demonstrated that for increasing diode-junction temperatures the frequency of oscillation tends to decrease. This would account for the frequency shifting for increasing pulse widths. Frequency shifting is equivalent to "FM"-ing (frequency-modulating) and so the frequency spectrum would be expected to deteriorate from a sin X/X shape. Further, the temperature variation of the oscillator output power was shown to increase with temperature for the low frequency oscillator and to exhibit a maximum in the high frequency case. Since the pulsed oscillators are driven by constant current, then we would expect some degree of "AM"-ing (amplitude-modulating) due to temperature rise in the diode for increasing pulse widths. This effect will further degrade the frequency spectrum.

ii) The avalanche frequency, ω_o, is dependent on the current and will increase during the finite rise time of applied current pulse and decrease during the falling edge. In Section 2.2 of the previous chapter, Equation (2.4) shows that the diode chip impedance is a relatively strong function

of the avalanche frequency and therefore the frequency of oscillation will depend on the bias current. Thus, the oscillator frequency will shift upwards during the leading edge of the current pulse and shift downwards on the trailing edge producing frequency modulation. Of course, a power variation will accompany the rise and fall of current imparting AM to the signal. Again, the frequency spectrum is affected.

iii) The distribution of the current density in the diode cross-sectional area varies with time in pulse mode operation due to internal heating. It will be shown later that in CW operation, the majority of the current flows at the circumference of the diode's cross-sectional area, whereas in pulse mode operation, the current density varies with the pulse width. If we assume that the avalanche frequency is determined by the location of the maximum current density, then the diode impedance varies as the maximum current density varies with time.

In the following sections, each of the above arguments will be explored further.

3.2.1 Variation of Oscillator Frequency in Pulse Mode Operation Due to Diode-Junction Temperature Rise

The packaged IMPATT diode has a thermal impedance which affects the temperature rise of the diode junction. In pulse mode operation, a step of power is applied to the device and, because of the thermal resistance

and capacitance, the temperature in the diode chip will rise in an exponential manner. The heat sink temperature will remain at the ambient temperature since the thermal time constant of the large metal surface is orders of magnitude larger than the thermal time constant of the diode.

To determine the effect of temperature on the oscillator frequency in pulse mode operation, an approximate analysis is performed which considers only the temperature rise of the diode junction. The frequency-temperature coefficient of an IMPATT oscillator, in terms of the diode and circuit reactance derivatives, was developed in Chapter 2 and is repeated here for convenience.

$$\frac{\Delta f}{\Delta T} = - \frac{\frac{\partial X_D}{\partial T} + \frac{\partial X_L}{\partial T}}{\frac{\partial X_D}{\partial f} + \frac{\partial X_L}{\partial f}} \qquad (2.3) \qquad (3.1)$$

If we assume that only the diode experiences a temperature change in pulse mode operation (this is approximately correct for a low duty cycle) then Equation (3.1) becomes:

$$\frac{\Delta f}{\Delta T} = - \frac{\frac{\partial X_D}{\partial T}}{\frac{\partial X_D}{\partial f} + \frac{\partial X_L}{\partial f}} \qquad (3.2)$$

In Chapter 2, the diode reactance versus frequency curve (Figure 10) and the circuit reactance versus frequency curves (Figures 15a and b) show that, for small changes in frequency of a few hundred megahertz, the

slopes may be linearized. Also, the diode reactance curve versus junction temperature (Figure 11) suggests that the slopes of the constant frequency curves may be approximated by a straight line over at least a 200°K temperature range. With these straight line approximations in mind, Equation (3.2) can be reduced to:

$$\frac{\Delta f}{\Delta T} = - KU \tag{3.3}$$

where

$$K = \frac{1}{\frac{\partial X_D}{\partial f} + \frac{\partial X_L}{\partial f}}$$

and

$$U = \frac{\partial X_D}{\partial T}$$

Thus, for a change in the diode-junction temperature, the oscillator will experience a change in frequency given by:

$$\Delta f = - KU\Delta T \tag{3.4}$$

The term ΔT in the above equation represents the rise in the temperature of the IMPATT diode chip during the "on" time of the applied power pulse.

It was mentioned above that the temperature of the diode junction rises in an exponential manner. This fact can be visualized by referring to Figure 20a[30] which shows an idealized diode on a semi-infinite heat sink in which heat flows only in one direction. This representation is reasonable since the top-cap bonding wire of the diode is incapable of

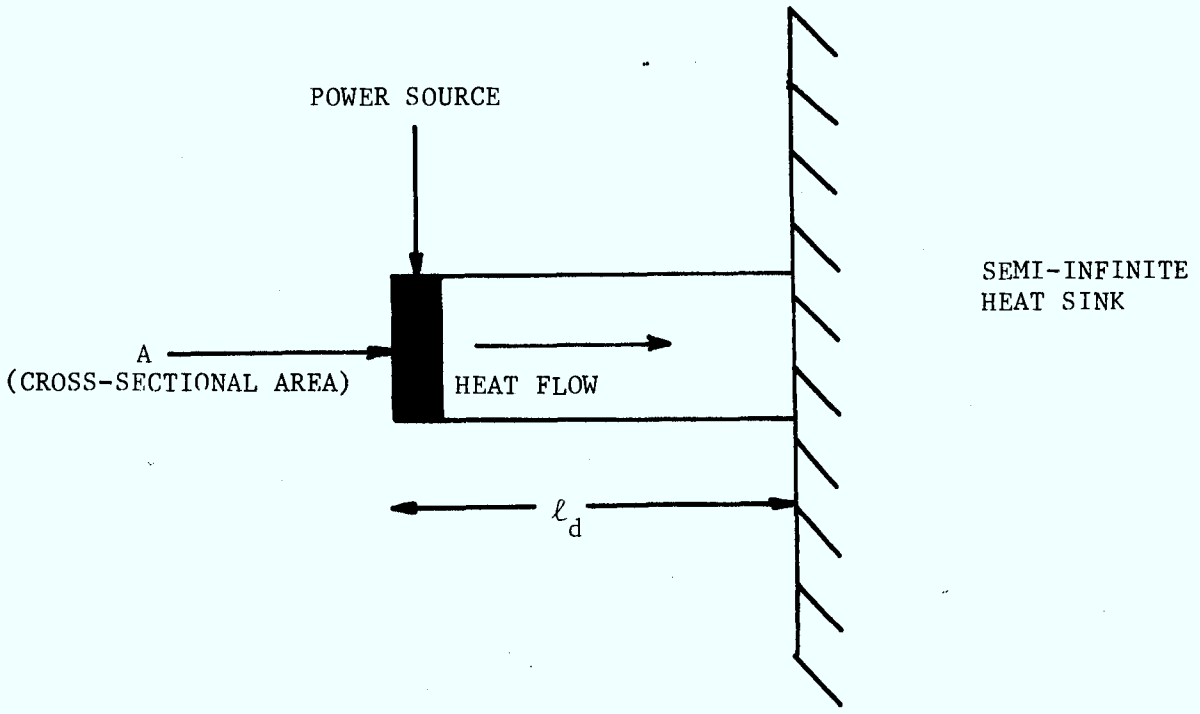

FIG. 20a. IDEALIZED DIODE ON A SEMI-INFINITE HEAT SINK

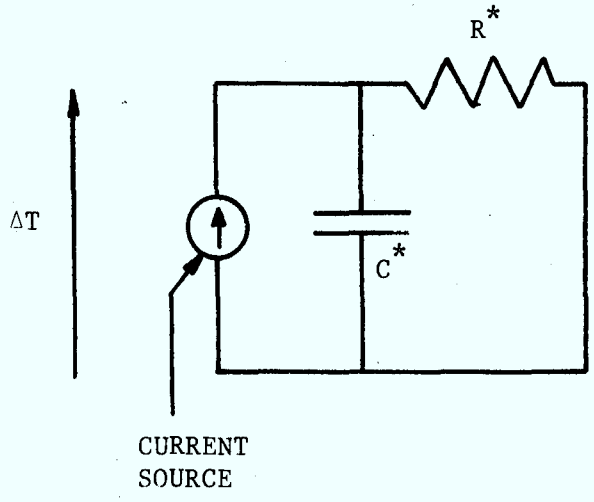

FIG. 20b. ELECTRICAL ANALOG FOR HEAT FLOW CIRCUIT

removing heat efficiently. An electrical analog for the heat flow circuit is shown in Figure 20b.[30]. Assuming that the semi-infinite heat sink temperature remains constant for low duty cycles, the increase in temperature across the thermal resistance R^* represents the diode junction heat rise ΔT. For this simple circuit, a thermal time constant "a" can be stated as:

$$\text{Time Constant} = a = R^*C^* = \left(\frac{1}{kA}\right)\left(\rho c \ell_d A\right) \qquad (32)$$

$$= \frac{\rho\ c\ \ell_d}{k} \qquad (3.5)$$

where

ρ = density of silicon substrate

c = specific heat of silicon

ℓ_d = length of diode

k = thermal conductivity

A = diode area

Utilizing this time constant, we can obtain an expression for the temperature rise in the diode which is:

$$\Delta T(t) = \Delta T_{max}\ (1 - e^{-t/a}) \qquad (3.6)$$

where

t = time

ΔT_{max} = maximum temperature rise of the diode junction

The time dependence of the oscillator frequency in pulse mode operation is obtained by substituting Equation (3.6) into Equation (3.4) which

gives:

$$\Delta f(t) = - KU\Delta T_{max}(1 - e^{-t/a}) \tag{3.7}$$

Experimental measurements were obtained using the low frequency microstrip oscillator (≈9GHz) discussed previously (Figure 17a). A constant current bias pulse of 40mA was used and the shift in centre frequency for various pulse widths was observed on a spectrum analyzer. The measured centre frequency is an average frequency, therefore in order to compare the measured results with the effect of junction temperature rise, we should compute an average frequency over the pulse width.

The instantaneous frequency at any time "t" during the pulse width can be written as:

$$f(t) = f_o - KU\Delta T_{max}(1 - e^{-t/a}) \tag{3.8}$$

where

f_o = oscillator frequency at time 0^+ (≈9GHz for this discussion)

The average frequency of a pulse is obtained by integration of Equation (3.8) over the pulse width. That is:

$$f_{av} = \frac{1}{PW} \int_0^{PW} \left[f_o - KU\Delta T_{max}(1 - e^{-t/a}) \right] dt$$

$$= f_o - KU\Delta T_{max} \left[1 + \frac{a}{PW} (e^{-PW/a} - 1) \right] \tag{3.9}$$

where

PW = pulse width

In evaluating Equation (3.9), all of the variables can be determined from the work in Chapter 2 except the value of the time constant "a". In the next chapter, a method will be described to determine the time constant "a" and it will be shown that for the diode used in the pulse mode experiments, the value of "a" is:

$$a \approx 50\mu sec$$

K and U can be evaluated from Figures 10 and 15a respectively as:

$$K = \frac{1}{\left.\frac{\partial X_D}{\partial f}\right|_{\substack{9GHz \\ 300°K}} + \left.\frac{\partial X_L}{\partial f}\right|_{\substack{9GHz \\ 300°K}}}$$

$$= \frac{1}{11.5 + 6.8}$$

$$= 0.0546 \frac{GHz}{ohm}$$

$$U = \left.\frac{\partial X_D}{\partial T}\right|_{\substack{9GHz \\ 300°K}}$$

$$= 0.045 \frac{ohm}{°K}$$

The maximum diode temperature rise is:

$$\Delta T_{max} = 150°K$$

The exact value of the frequency is relatively unimportant since it represents the frequency of the oscillator for an infinitely small pulse width. In fact, it cannot be measured since a narrow pulse width generates a wide frequency spectrum of almost constant amplitude.

The results of the measured variation of the oscillator frequency for various pulse widths are shown in Figure 21. The exponential behaviour predicted by Equation (3.9) is evident. Equation (3.9) was evaluated using the parameter values as discussed above and is also plotted in Figure 21. The computed curve in Figure 21 corresponds closely to the measured result for pulse widths up to 10μsec; however, for wider pulse widths, the predicted curve departs from the observed behaviour. It should be remembered that this section discusses one of the three reasons for the frequency shift and is not intended to fully explain the observed effect.

A number of comments concerning this analysis should be mentioned.

i) The thermal time constant, a, was assumed to be the time constant of a first order thermal circuit while in reality the true solution would be obtained from the heat flow equation[33].

ii) It was assumed that the effect of temperature on the microwave circuit is negligible. However, the circuit immediately surrounding the diode will undergo a temperature change although it will be significantly less than the diode junction. It has already been demonstrated that the circuit tends to reduce the frequency-temperature coefficient of the oscillator (see Figure 17a). This may be

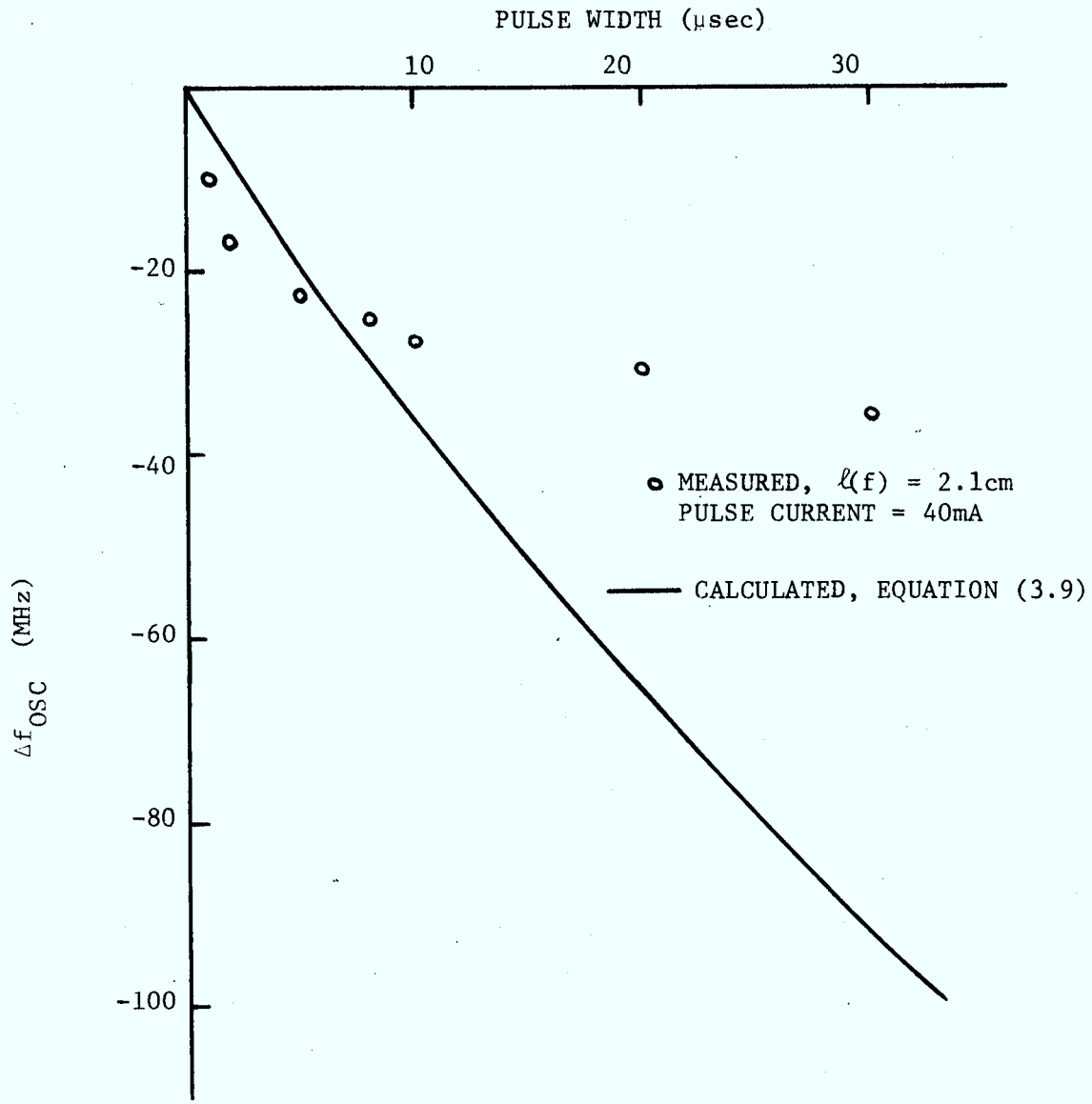

FIG. 21. VARIATION OF OSCILLATOR FREQUENCY WITH PULSE WIDTH IN PULSE MODE OPERATION

partially responsible for the lower frequency shift in the measured results compared to the predicted frequency shift of Equation (3.9).

iii) The factors K and U in Equation (3.9) were determined from the small-signal analysis of Chapter 2 and as such are only qualitative.

3.2.2 Variation of Oscillator Frequency in Pulse Mode Operation Due to the Rise Time of the Current Pulse

In pulse mode operation, the finite rise and fall times of the current pulse leading and trailing edge can account for a frequency shift of the oscillator since the diode impedance is a function of bias current.

The diode impedance is affected by the avalanche frequency, ω_o, which is a function of the bias current as defined in Equation (2.25), repeated here for convenience.

$$\omega_o = \sqrt{\frac{J_o \Phi}{\epsilon_s \tau}} \qquad (2.25) \qquad (15) \qquad (3.10)$$

where

J_o = current density

Gilden and Hines[7] have considered the electronic tuning effect of the bias current in IMPATT diodes and have shown that the oscillator frequency is a strong function of the bias current.

Equation (3.10) predicts the variation of the avalanche frequency with current. In Section 2.3.6 of Chapter 2, it was mentioned that the

avalanche frequency was measured by a reflection measurement. In Figure 22, the results of that measurement indicate that the predicted variation of avalanche frequency is correct. Figure 22 is plotted on log-log co-ordinates in order to negate the curve effect of the square root in Equation (3.10). Plotted also in Figure 22 is a line with a slope of 1/2, the theoretical slope predicted by Equation (3.10) and it is noted that the measured slope is identical to the predicted value.

At a bias current of 40mA, the measured avalanche frequency is 6.0GHz. In Chapter 2, the avalanche frequency at a constant current of 40mA was computed for a range of diode-junction temperatures (see Figure 5) and for a diode temperature 450°K (150°K temperature rise above ambient) the calculated frequency is 6.35GHz. This is in close agreement with the measured value.

To demonstrate the effect of pulse rise and fall times on the pulsed oscillator frequency, an average frequency will be computed in a similar fashion as in the previous section.

For purposes of discussion, assume that the rise and fall times of the current pulse are equal, and further, that the current variation with time is linear. Figure 23 shows a typical current pulse waveform which may be described as follows.

$$I(t) = \begin{cases} D\,t & 0 \leq t \leq t_1 \\ I_o & t_1 \leq t \leq t_2 \\ I_o - D\,t & t_2 \leq t \leq t_3 \end{cases} \qquad (3.11)$$

where

D = current slew rate, ma/second

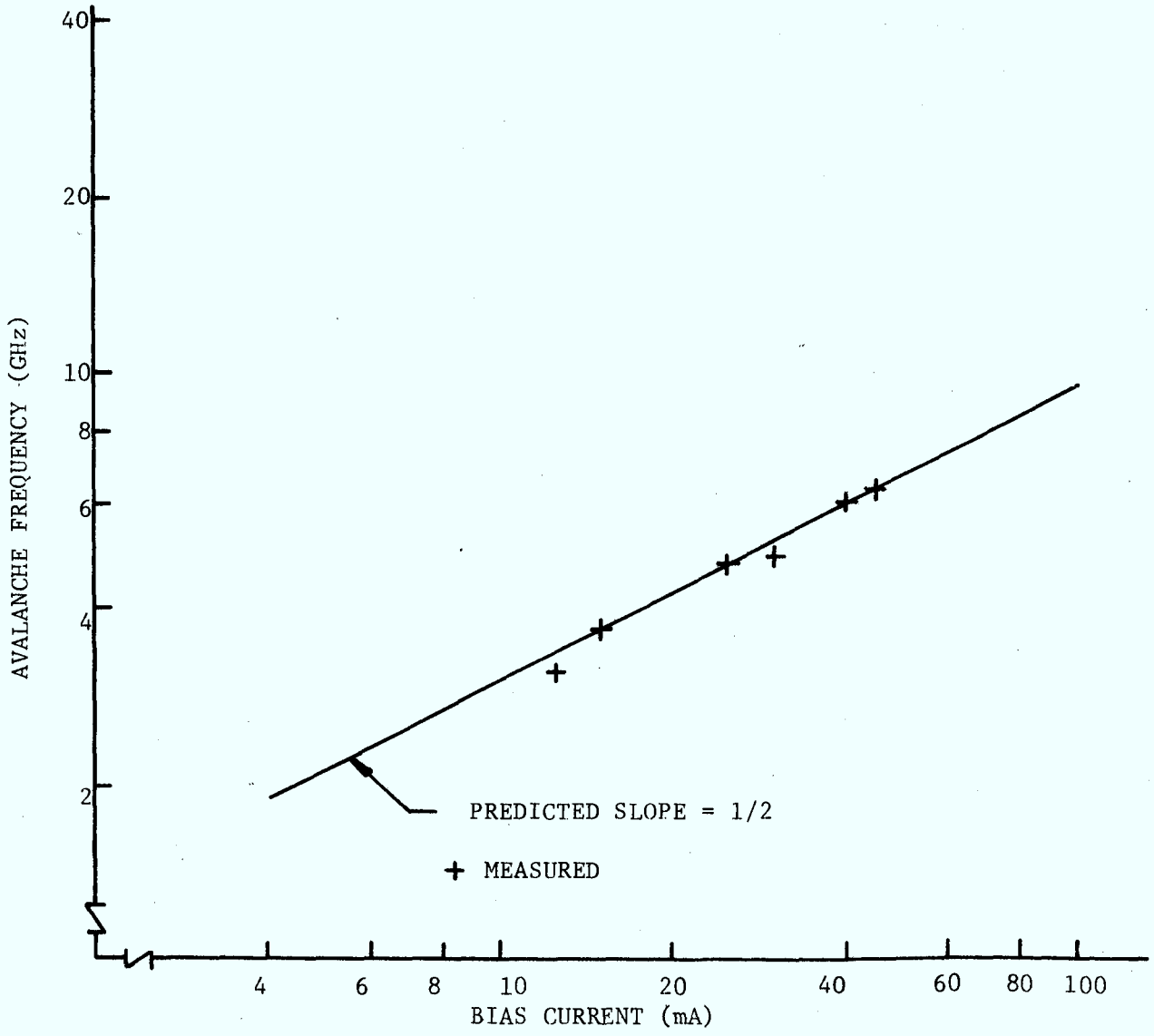

FIG. 22. AVALANCHE FREQUENCY VERSUS BIAS CURRENT

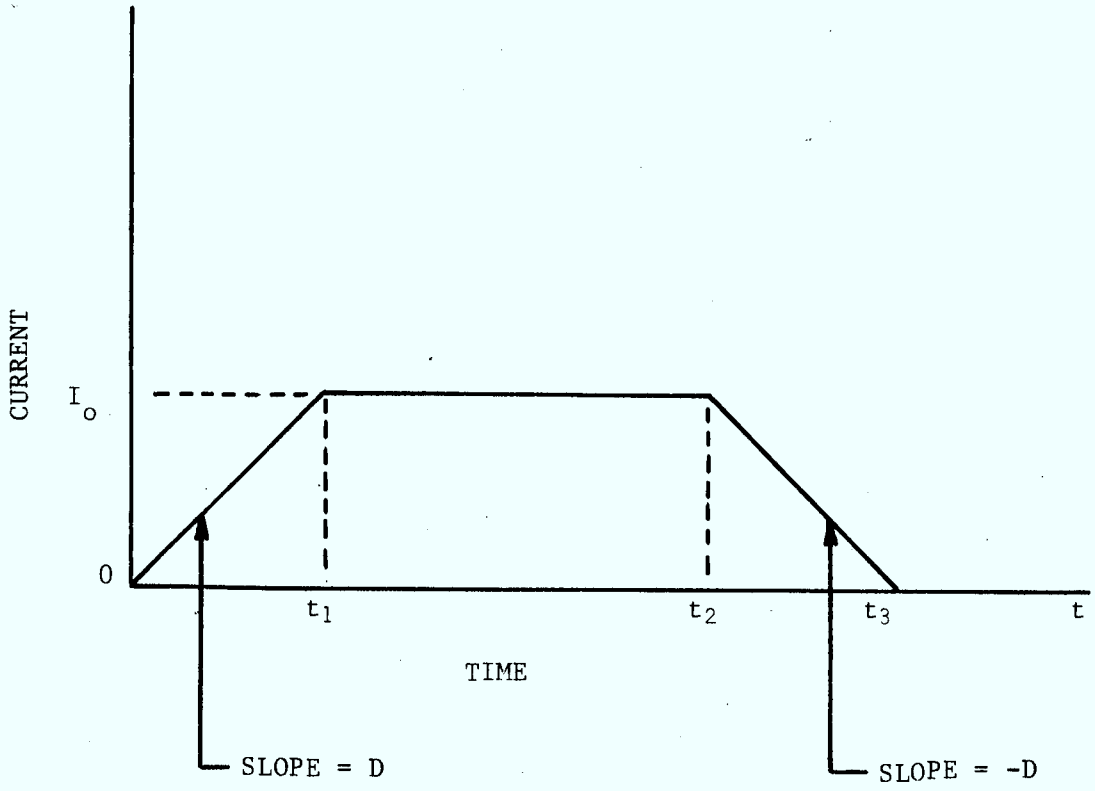

FIG. 23. BIAS CURRENT PULSE WAVEFORM

I_o = maximum steady state current, ma

t = time, seconds

t_1, t_2, t_3 = current shape definition times, seconds

The effect of bias current on the oscillator can be determined from Chapter 2 using the small-signal model. For the low frequency circuit (9GHz), the current can be varied at a constant temperature and the oscillator frequency computed. Figure 24 shows a plot of the oscillator frequency versus bias current. The slope of the curve in Figure 24 is larger than the value observed by experiment; however, it must be realized that in measuring the current tuning effect of an oscillator the diode-junction temperature increases with current. This reduces the oscillator frequency and thus reduces the slope of the current tuning curve. A linear approximation for the curve in Figure 24 was found to be:

$$f(I) = 9.2 + 0.0243I \text{ GHz}$$

$$= a_o + b_o I \tag{3.12}$$

where

I = bias current, mA

Equation (3.12) shows that during the leading edge of the current pulse, the frequency increases and at the trailing edge, the frequency decreases. Therefore, the average frequency over the pulse width should be computed as in the previous section. The average frequency will be:

$$f_{av} = \frac{1}{t_3} \int_0^{t_3} f[I(t)]dt \tag{3.13}$$

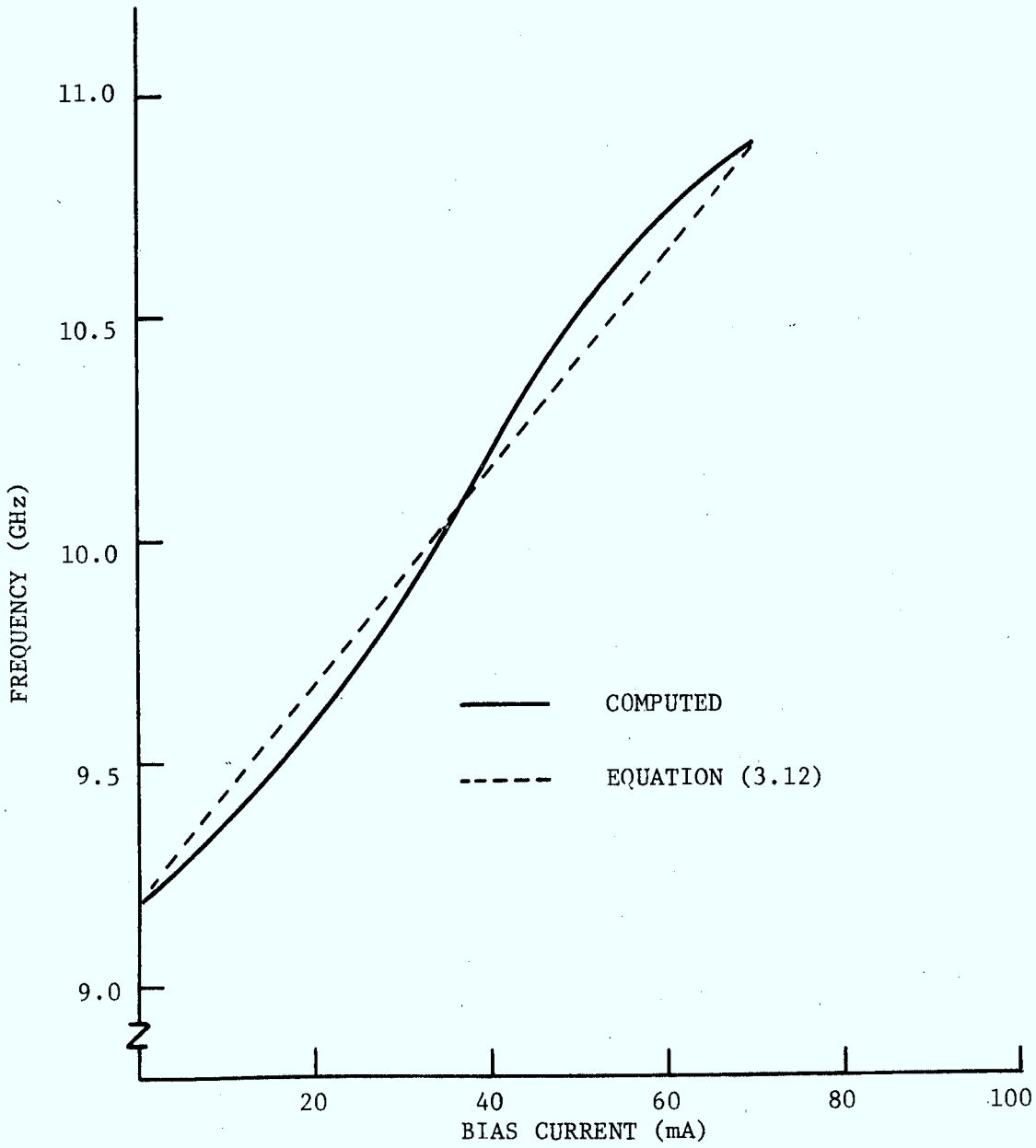

FIG. 24. COMPUTED OSCILLATOR FREQUENCY VERSUS BIAS CURRENT AT A CONSTANT TEMPERATURE (300°K) FOR LOW FREQUENCY OSCILLATOR [$\ell(f) = 2.1$cm]

Using the relationships expressed above in Equations (3.11) and (3.12), we obtain:

$$f_{av} = \frac{(a_o+b_oI_o)(t_3-t_1) + a_ot_1 + b_oD(t_1^2+t_2^2-t_3^2)/2}{t_3} \qquad (3.14)$$

Equation (3.14) is plotted in Figure 25 where the variable is the pulse-top width, t_2-t_1, and the running parameter is current slew rate, D. The current slew rate of 1mA/ns was used in the experimental measurements. For large pulse widths, the average frequency asymtotes to the 50mA CW frequency as computed in the current tuning curve, Figure 24. The curves of Figure 25 indicate clearly the effect of the rise and fall time of the current pulse. It is noted that for current pulses having slow rise and fall times the apparent frequency shifting continues throughout a 1μsec pulse, whereas in a faster pulse the frequency shifting occurs mainly at the beginning of the pulse. While the curves of Figure 25 give some indication of the effect of the current pulse rise and fall times on the frequency of a pulsed oscillator, they must be taken as quantitative. It was assumed that the oscillator began oscillating when the current was applied. It is well known, however,[7,34] that the current must reach a threshold value before the circuit begins oscillating. The reasons for this threshold phenomenon are not fully understood but experiments indicate that the microwave circuit is instrumental in defining the threshold. Microwave circuits which produce high power tend to begin oscillating at lower current levels than circuits which produce only moderate amounts of power. This suggests that the matching of the diode negative resistance to the circuit

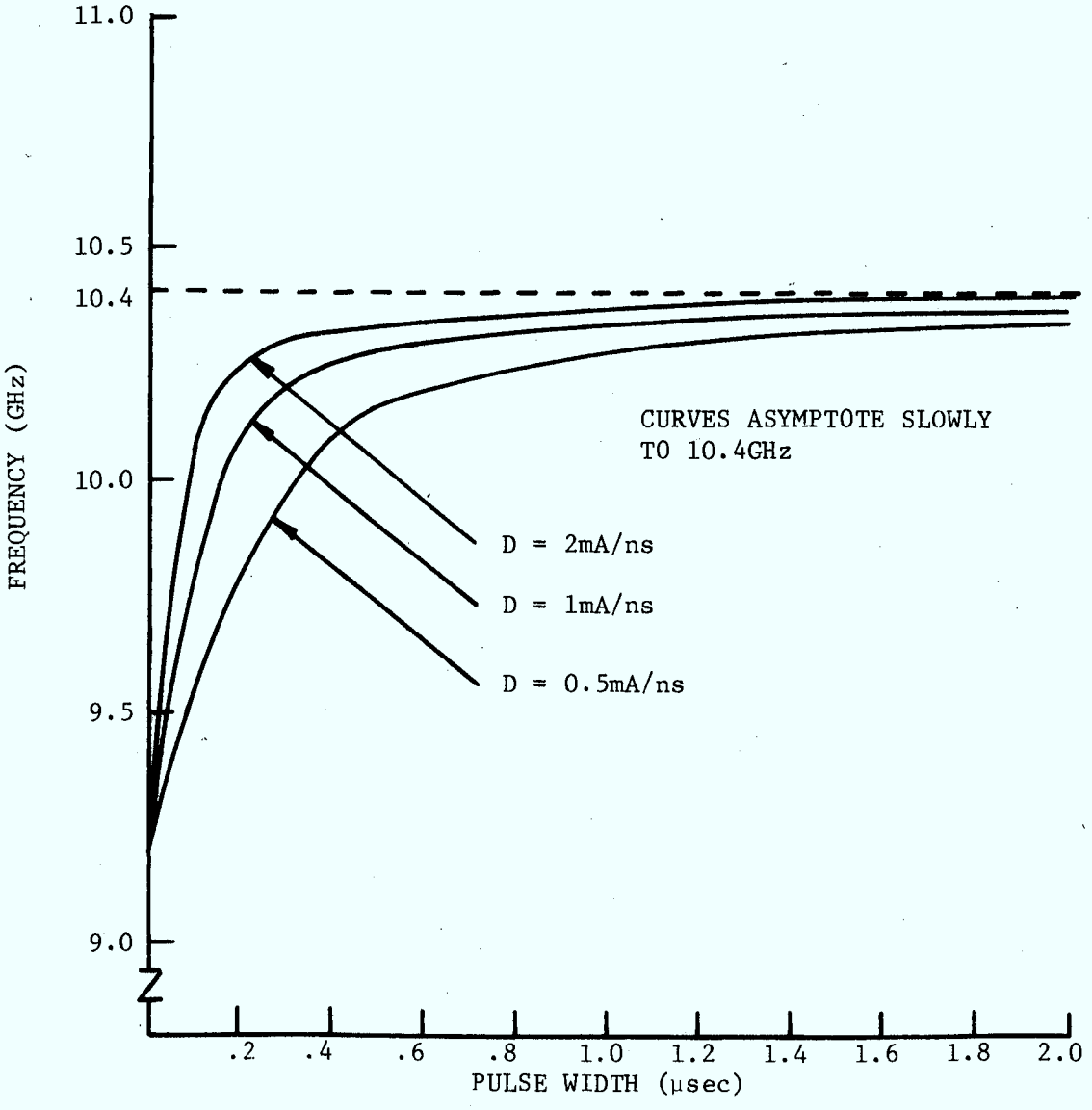

FIG. 25. OSCILLATOR FREQUENCY VERSUS PULSE WIDTH FOR VARIATIONS IN PULSE RISE AND FALL TIMES. CURRENT SLEW RATES ARE 2mA/ns, 1mA/ns AND 0.5mA/ns.

positive resistance is critical for oscillation start-up.

Although the results presented in this section are not exact, they do show the effect of the current pulse rise and fall times on the average frequency in pulse mode operation. The general upward swing of frequency predicted here, along with the downward swing predicted by the previous section, accounts partially for the shape of the measured curve as shown in Figure 21.

In the next section, the effect of current density distribution on the average frequency will be discussed.

3.2.3 Variation of Oscillator Frequency in Pulse Mode Operation Due to the Current Density Distribution

In previous discussions, it has been assumed that the diode is a well behaved junction carrying a uniform current density in all parts of the junction. In practice, however, the current density may vary significantly throughout the junction producing a non-uniform current density. In this section, the variation of the current density with time will be discussed and the effect of this variation on the oscillator frequency examined.

The IMPATT diode chip is mounted on a heat sink which may be considered as semi-infinite since the size of the heat sink is orders of magnitude larger than the diode chip. As power is applied to the diode, a heat source is created and the temperature at the diode heat sink interface rises, with the highest temperature existing at the centre of the diode. The local current density in the diode is a function of the local breakdown voltage which in turn depends on the local temperature.

The diode-heat sink temperature distribution has been calculated by Yu and Glover[35]; however, they assumed that the diode acted as a constant density power source. Earlier, Haitz[34] computed the temperature and current distribution at the diode-heat sink interface for an avalanche diode. In his study, he considered the effect of the local breakdown voltage which produces a non-uniform power density in the diode. These studies, however, have not indicated the manner in which the current density varies with time.

To investigate the current redistribution with time, a computer model was developed. The model consisted of five concentric annular diodes on a large circular heat sink. The individual diodes were modelled as a space-charge resistance in series with a temperature-sensitive voltage source which represents the local breakdown voltage. Figure 26a illustrates the model used. Since the diodes are equally spaced across the heat sink diameter, the areas of the annular rings progressively increase from the centre to the edge; therefore, the space-charge resistances were adjusted so that the current flowing in each diode was equal when the voltage sources were equal. From this figure, the chain of events is clear. Before the constant current is applied, the temperature across the diameter is constant. Upon application of current, power is generated in the diodes and the temperature begins to rise with the centre having the highest temperature. Since the breakdown voltage increases with temperature, the current is reduced in the centre diode and increased in the outside diodes.

The numerical solution for the temperatures and currents was obtained using the general heat flow equation[33] written in cylindrical

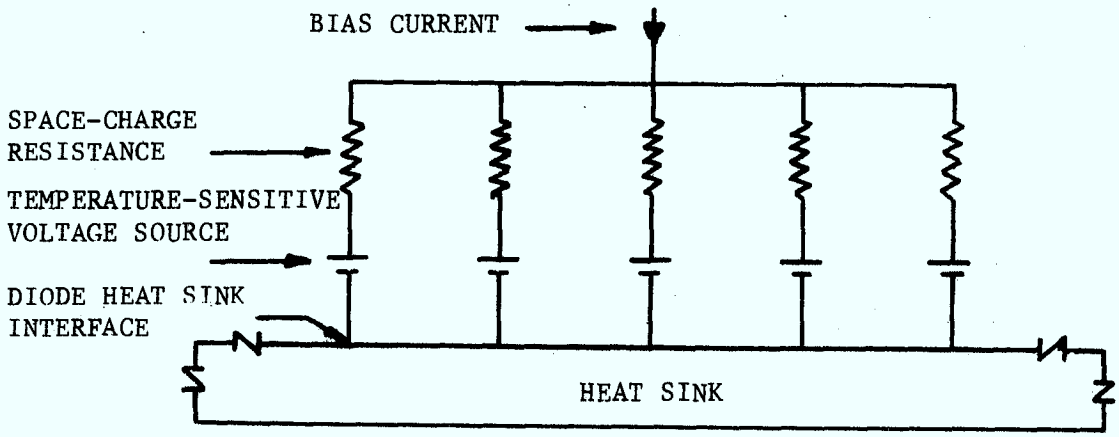

FIG. 26a. COMPUTER MODEL OF DIODE AND HEAT SINK

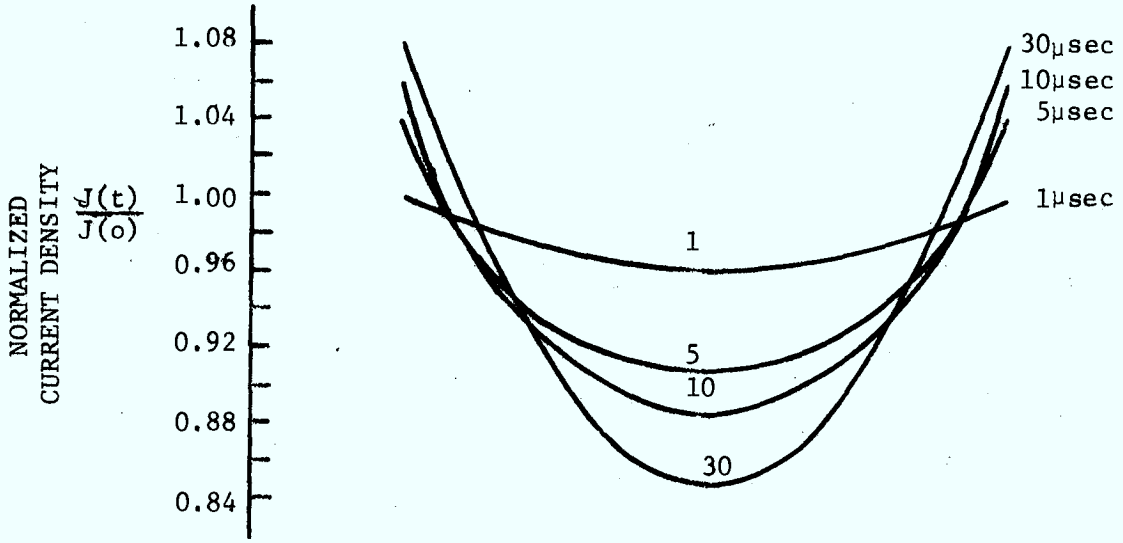

FIG. 26b. CURRENT DENSITY DISTRIBUTION

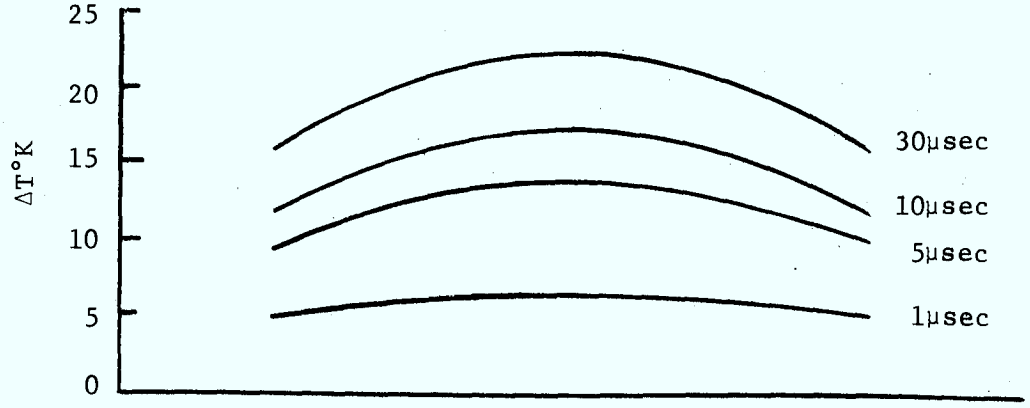

FIG. 26c. TEMPERATURE DISTRIBUTION

co-ordinates. It was assumed that the heat flowed downward in Figure 26a by conduction only and that all surfaces were insulated except the bottom of the heat sink which remained at a constant temperature. Initially, the heat sink was of uniform temperature, and as time progressed, the rise in temperature at the diode-heat sink interface modified the temperature sensitive voltage sources, which in turn varied the currents in the diodes. The computation produced temperature and current data for the diode heat sink interface as a function of time and is shown in Figure 26 b and c. The values for the breakdown voltage, space-charge resistance, supply current and areas were representative of the diodes used in this study. It should be emphasized that no attempt was made to model the diode-heat sink exactly. Rather, approximate values were used to obtain a qualitative result. This simple analysis did not account for the temperature variation of the thermal conductivity of the copper heat sink[55] nor for the heat flow within the diode from the centre to the edge.

The results shown in Figures 26 b and c illustrate the variation of the current density and the temperature distribution at the diode-heat sink interface for various times. The program computed values until steady state conditions were reached and these are indicated in Figures 26 b and c. The low temperature rise is due primarily to the somewhat thin heat sink. The heat sink was thin by necessity since the finite difference formulae require a large number of storage spaces in the computer and further, the computation time increases as the size of the heat sink increases. The lower edge of the heat sink was held at constant temperature whereas in reality this temperature would increase slowly.

In Figure 27, the currents (normalized to the current at start of pulse) in the centre and outside diodes of Figure 26a are plotted and it is noted that the current in the outside diode may be almost twice as great as the current in the centre diode. In other words, the current density at the outer edge of the diode is significantly greater than at the centre. Haitz[34], in his study on the effect of temperature in avalanche diodes, has computed similar results.

In pulse mode operation, the local current density varies with time and the above analysis shows that this variation is significant. In Section 3.2.2, the effect of current on the frequency of the oscillator was investigated and it was shown that the frequency increases with current. If we consider the IMPATT diode to consist of a large number of sub-diodes, each one operating at a frequency defined by the local current density, the power output frequency spectrum would consist of a large number of frequencies. In practice, however, this is not observed and it is felt that all of the individual oscillators are "injection locked" together to form a single frequency source[37,38,39]. If the individual sub-diodes are frequency locked, then it seems reasonable to assume that they will lock to the sub-diode producing the maximum power. Most likely, this would be the diode carrying the largest current density. That is, the maximum local current density will control the oscillator frequency. Therefore, in pulse mode operation, the frequency of the oscillator will increase with time and for increasing pulse width the average frequency will also increase.

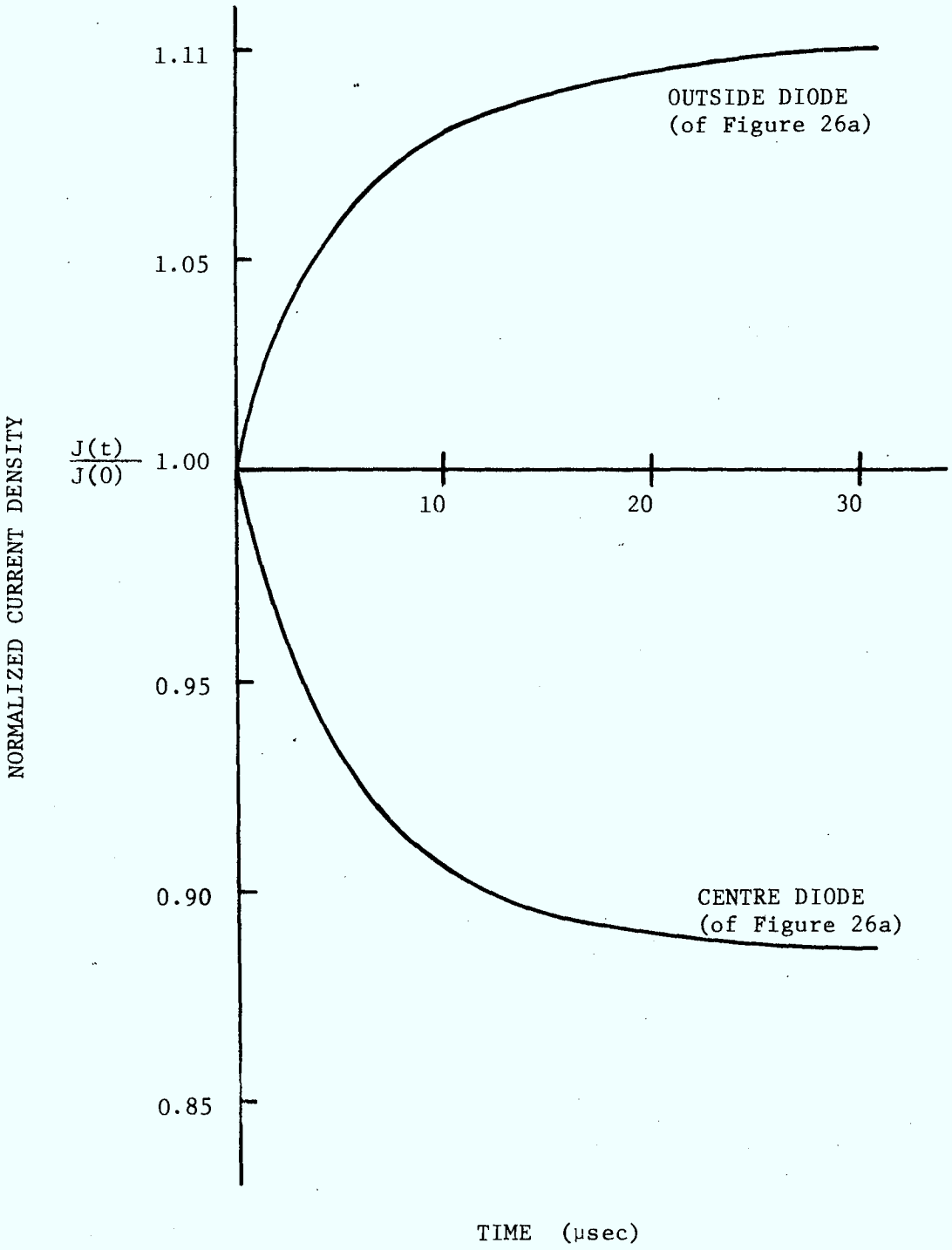

FIG. 27. VARIATION OF CURRENT DENSITY WITH TIME AT THE EDGE AND THE CENTRE OF THE DIODE

3.2.4 Summary

In the three sections above, the causes of frequency shifting in pulse mode operation for increasing pulse width were discussed. In Section 3.2.1, the effect of temperature on diode impedance predicted a decreasing average frequency with increasing pulse width; however, the measured results (see Figure 21) exhibited a smaller frequency shift. Section 3.2.2 predicted an increasing average frequency with pulse width caused by the finite rise and fall times of the current pulse generator. However, this effect is minor since the rise-fall times are significantly smaller than the pulse widths. In Section 3.2.3, it was shown that the local current density increased on the outer edges of the diode with time in pulse mode operation. In conjunction with the current tuning effects demonstrated in Section 3.2.2, the average frequency of the oscillator is forced upwards and therefore the overall frequency shift with pulse width is a combination of the temperature effect in Section 3.2.1 and the electronic tuning effect on Section 3.2.3.

In conclusion, it should be emphasized that the results presented in this Chapter are of a preliminary nature. For instance, in Section 3.2.1, it was assumed that the duty cycle was sufficiently small so that the diode junction temperature returned to the ambient temperature in the interpulse period. In fact, for high duty cycles, the average temperature of the diode will increase which implies that the treatment of Section 3.2.1 should be expanded.

CHAPTER 4

MEASUREMENT OF HEAT FLOW RESISTANCE

4.1 Introduction

The IMPATT diodes considered in this study may operate at power densities as high as 10^5watts/cm^2. This high power density represents a severe problem to the user of these diodes since the efficiency of DC to RF power conversion is typically 1-5%. Therefore, the majority of the input power must be dissipated in a suitable heat sink to prevent the diode junction from reaching a destructive temperature. A knowledge of the diode heat sink - heat flow resistance allows the user of these diodes to estimate a maximum safe input power.

This Chapter will consider the measurement of the heat flow resistance with application to two typical commercially available diodes.

4.2 Direct Method of Heat Flow Resistance Measurement

The temperature dependence of the reverse breakdown voltage $V_b(T)$ characteristic of avalanche diodes is in the order of 50-100mV/°C. In Figure 28, the I-V characteristic of an avalanche diode is shown where $V_b(T_o)$ represents the room temperature breakdown voltage and (I,V) is the point of operation. The slope of the curve is determined, to a large extent, by the increase in breakdown voltage with increasing temperature or applied power. Since there will exist a heat flow resistance between the diode junction and the heat sink, the temperature rise of the junction will be given by the following equation[30]:

$$T_j - T_o = \theta_j \, IV \approx \theta_j \, IV(T_j) \qquad (4.1)$$

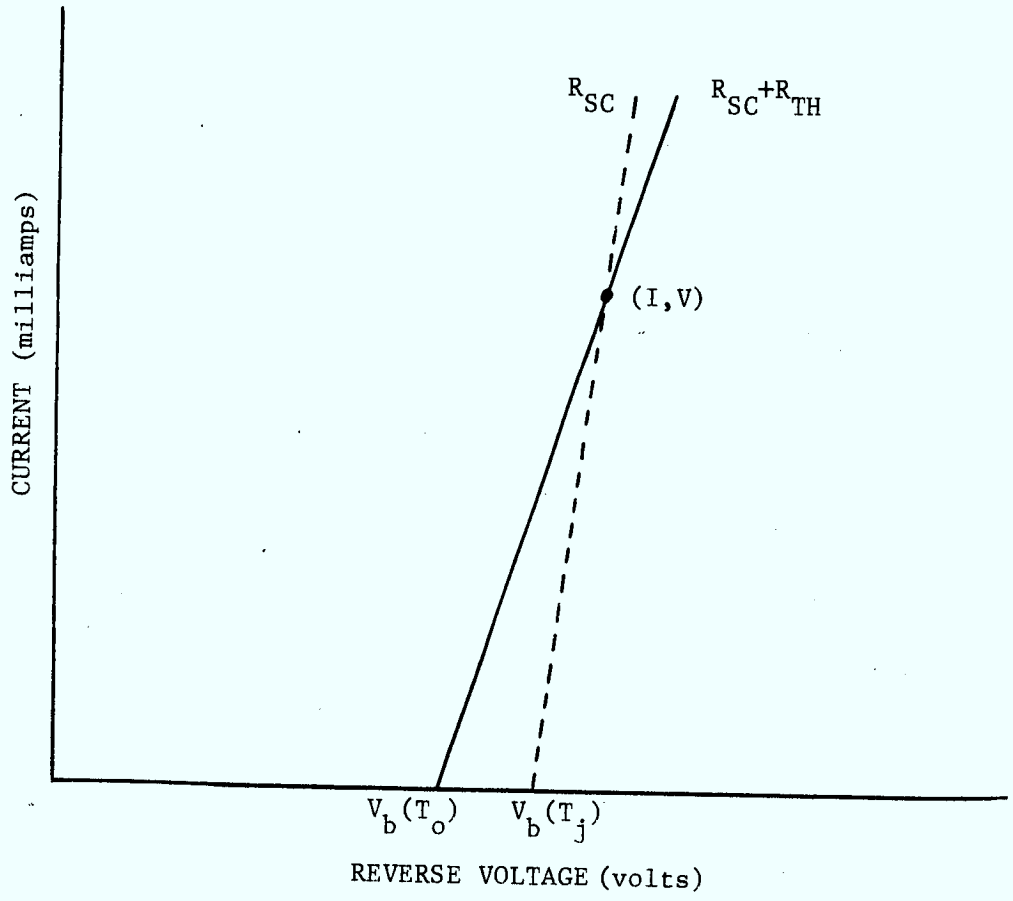

FIG. 28. I-V CHARACTERISTIC OF AN AVALANCHE DIODE

where

θ_j = heat flow resistance, °C/watt

$V \approx V(T_j)$

The temperature difference can be determined from:

$$V_b(T_j) = V_b(T_o) + \frac{dV_b}{dT}(T_j - T_o)$$

$$= V_b(T_o)\left[1 + B(T_j - T_o)\right] \qquad (4.2)$$

where

$$B = \frac{1}{V_b(T_o)} \cdot \frac{dV_b}{dT}$$

the temperature coefficient.

Equation (4.1) and Equation (4.2) can be solved for the heat flow resistance θ_j:

$$\theta_j \approx \frac{V_b(T_j) - V_b(T_o)}{B\, V_b(T_o) V_b(T_j) I} \qquad (4.3)$$

Equation (4.3) can be simplified in manner suggested by Haitz et al[30] to give:

$$\theta_j \approx \frac{V_b(T_j) - V_b(T_o)}{B\, I\, V_b^2} \qquad (4.4)$$

where

$$V_b(T_j) \approx V_b(T_o) = V_b$$

is assumed for terms which do not contain the difference $V_b(T_j) - V_b(T_o)$.

The effect of this simplification can be demonstrated by an example. Suppose:

$$V_b(T_o) = 80V$$

$$V_b(T_j) = 90V$$

$$B = 10^{-3}°C^{-1}$$

$$I = 40ma$$

Equation (4.3) then gives

$$\theta_j = 34.7°C/watt$$

while Equation (4.4) gives

$$\theta_j = 39°C/watt$$

Assuming that Equation (4.3) is more accurate, then Equation (4.4) gives an error, for this example, of 12.4%.

In using either Equation (4.3) or (4.4), the temperature coefficient, B, and the operating current and voltage levels may be determined with a minimum of four measurements and thus provide a relatively fast method for determining the heat flow resistance.

4.3 Small-Signal Method of Heat Flow Resistance Measurement

A more exact formulation for the heat flow resistance can be obtained by utilizing the fact that the temperature dependence of the breakdown voltage, V_b, contributes an electrical resistance to the small-signal AC resistance of the avalanching diode. Haitz et al[30]

in their paper concerning thermal resistance measurements have shown that:

$$R_{TH} = \theta_j \, B \, V_b^{\,2}(1 + 2\theta_j B \, V_b I + 2 \, R_{SC} \, I/V_b) \tag{4.5}$$

where

R_{TH} = thermal resistance

R_{SC} = space-charge resistance

In most cases, the last two factors within the bracket of Equation (4.5) are much less than unity and Haitz et al[30] reduce Equation (4.5) to:

$$R_{TH} \simeq \theta_j \, B \, V_b^{\,2} \tag{4.6}$$

The total small-signal AC resistance is composed of the thermal resistance, the space-charge resistance and the heat sink spreading resistance[40]; however, the spreading resistance is usually negligible. For frequencies less than the avalanche frequency, the space-charge resistance is given by:

$$R_{SC} = \frac{1}{2 \, \varepsilon_s \, V_n} \left(\frac{\ell_o^{\,2}}{A}\right) \quad (30) \tag{4.7}$$

where

V_n = saturation drift velocity

ℓ_o = drift length

A = diode junction area

Therefore, the total small-signal AC resistance is given by:

$$R_{TOT} = R_{TH} + R_{SC} \quad (30) \tag{4.8}$$

for $\omega << \omega_o$.

By using a lumped element thermal circuit, Haitz et al[30] have shown that the thermal resistance is frequency sensitive and that for frequencies above one megahertz, R_{TH} becomes negligible. Therefore, by measuring the DC resistance of the avalanching diode (in a heat sink) and the AC resistance at a frequency in excess of 1MHz, R_{TH} may be determined, and hence the heat flow resistance calculated.

In Figure 29, a schematic representation is shown of the circuit employed to measure the AC and DC resistance of an IMPATT diode. For various DC currents, the DC resistance of the diode can be measured by two digital meters to a high degree of accuracy. The resistor in series with the diode provided the most convenient means to measure the AC current in the diode.

In Figures 30 and 31, the results of the measurements on two typical X-band commercially available diodes are shown. The frequency dependence of R_{TOT} is clearly evident in both figures as predicted by Haitz et al[30]. The DC resistance values are also shown in the figures and it is noted that $R_{DC} > R_{TOT}$ indicating that some heat flow exists between the diode and the environment. The analysis of Haitz et al assumes that heat flow occurs only between the diode and the heat sink. Therefore, we shall compute the thermal resistance to be:

$$R_{TH} = R_{DC} - R_{SC} \tag{4.9}$$

In Figures 30 and 31, the frequency at which the total resistance reached a minimum is in the order of 10MHz. By employing a pulse generator having a rise time of less than the quarter period of 10MHz,

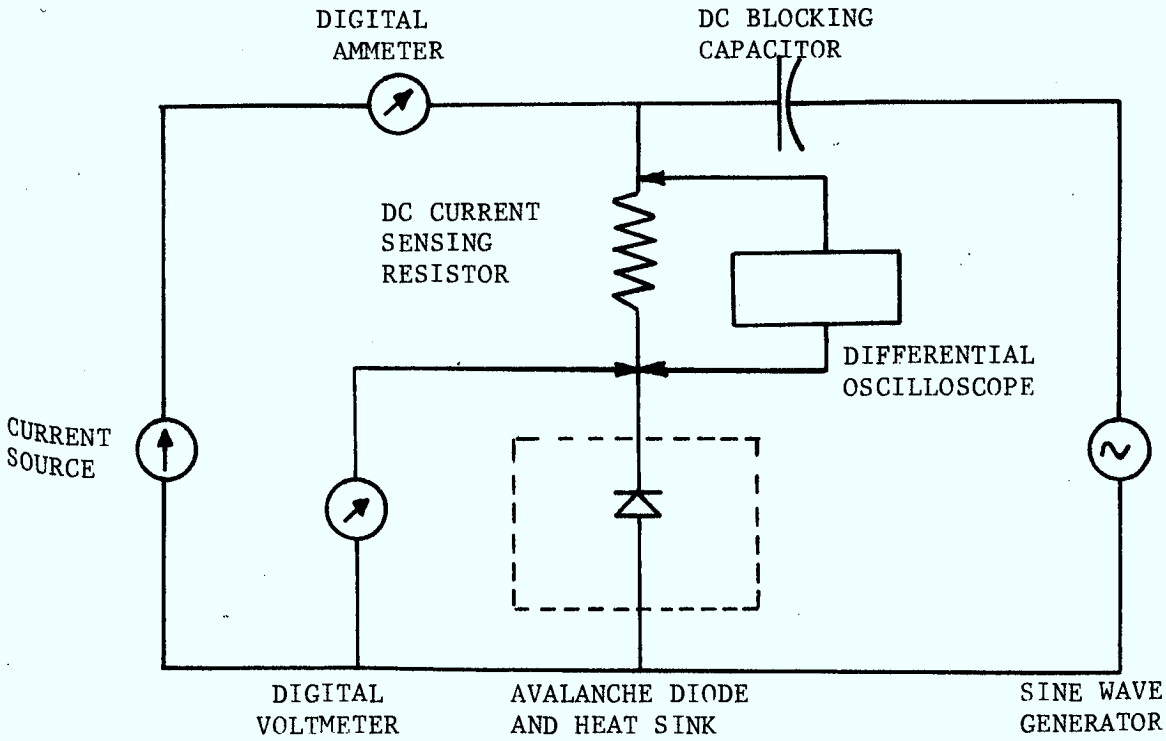

FIG. 29. TEST SET-UP FOR MEASURING DC AND AC RESISTANCES OF AVALANCHE DIODE

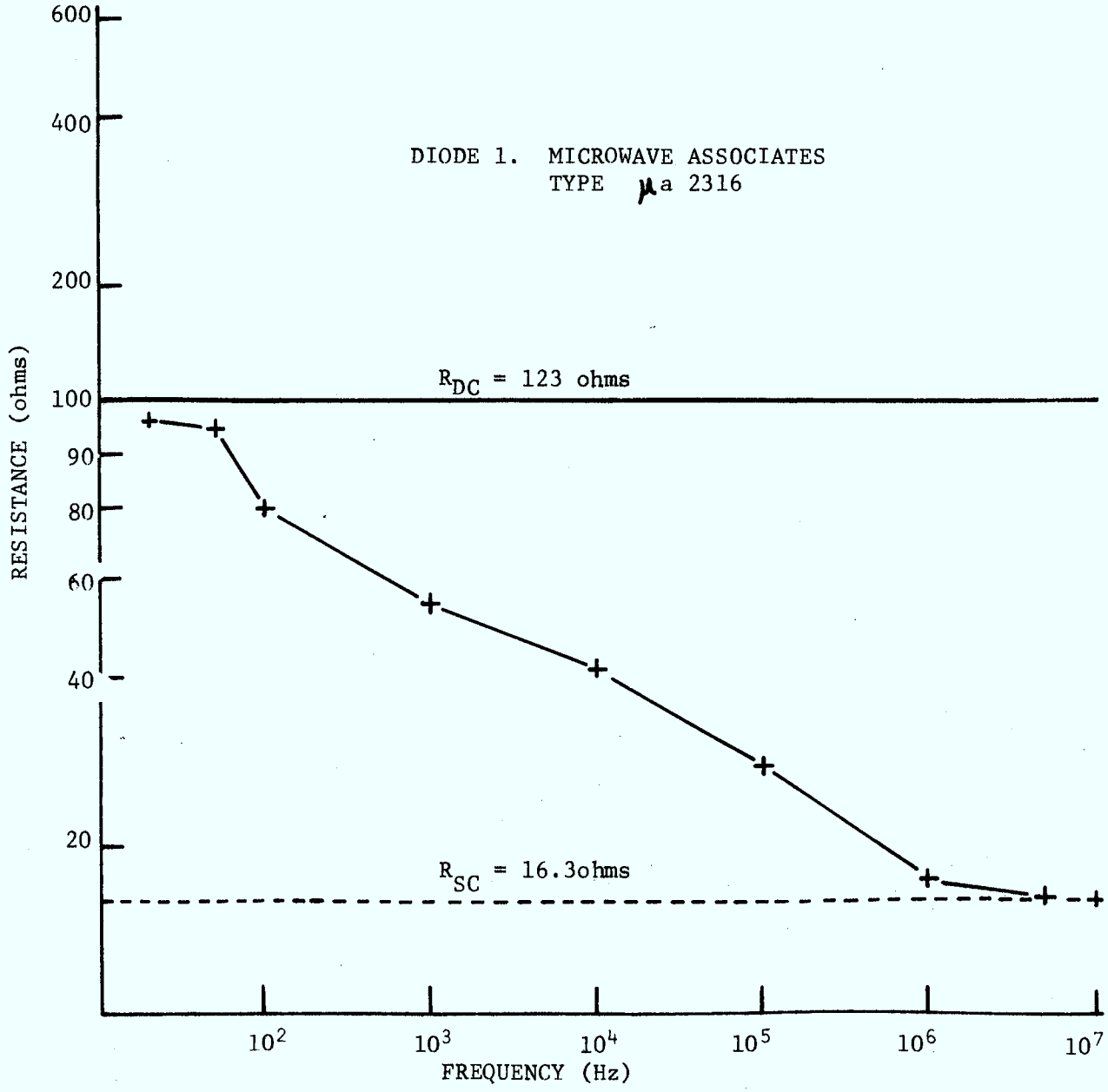

FIG. 30. SMALL-SIGNAL AVALANCHE DIODE RESISTANCE VERSUS FREQUENCY FOR FREQUENCIES LESS THAN THE AVALANCHE FREQUENCY. DIODE 1.

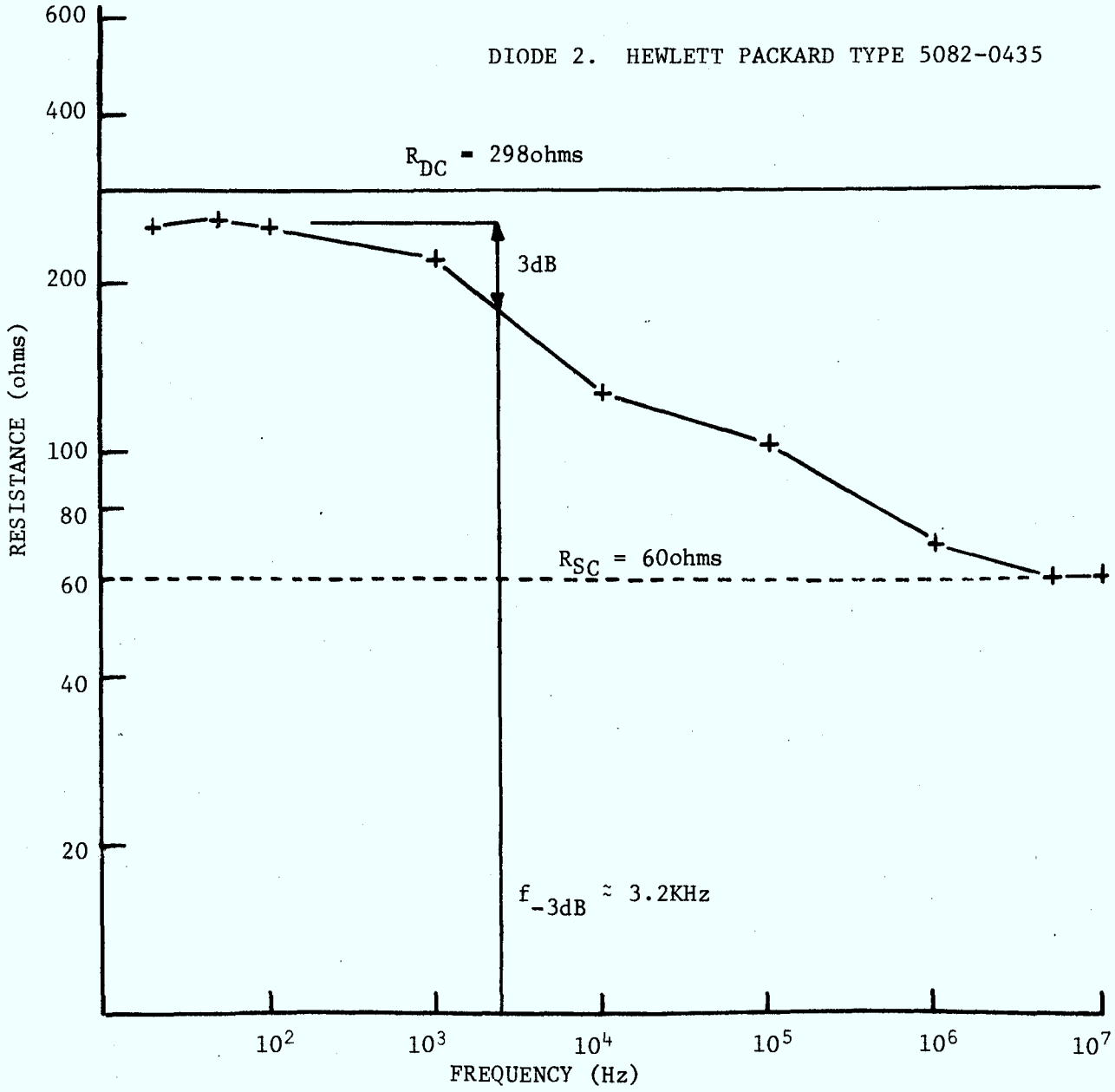

FIG. 31. SMALL-SIGNAL AVALANCHE DIODE RESISTANCE VERSUS FREQUENCY FOR FREQUENCIES LESS THAN THE AVALANCHE FREQUENCY. DIODE 2.

the incremental current and voltage in the diode may be measured, and thus the space-charge resistance, R_{SC}, is obtained. Nigrin[41] has used this method and has obtained good results in the measurement of junction temperature. Pulse measurements were performed on the two diodes. As expected, the pulse method and the small signal method gave the same results for the space-charge resistance.

The heat flow resistance was computed for both diodes using Equation (4.6). From Equation (4.6),

$$\theta_j \approx \frac{R_{TH}}{B\ V_b^2} \tag{4.10}$$

The temperature coefficients, B, for the diodes were measured with a reverse current of 100μa.

In Table 4.1, the relevant data for both diodes are listed and the heat flow resistance for the diodes in a heat sink shown. In computing the heat flow resistance, the two methods were employed as expressed by Equations (4.4) and (4.10).

A direct comparison of the results of the heat flow measurements with the manufacturer's quoted values is not applicable here since no mention is given of the heat sinking method. A comparison of the methods discussed here, however, show that the more exact method of Haitz et al[30] result in a lower value for the heat flow resistance than the approximate method.

A useful result of the small-signal method is that a thermal time constant may be obtained from the curves of resistance versus frequency. In Chapter 3, Section 3.2.1, the thermal time constant was used in computing the rate of temperature rise in the diode junction. Diode 2,

TABLE 4.1

	Diode 1	Diode 2
$V_b(T_o)$	53.5V	81.4V
$V_b(T_j)$	58.75V	89.7V
I	30ma	30ma
B	$0.00116°C^{-1}$	$0.00117°C^{-1}$
R_{DC}	123 ohms	298 ohms
R_{TOT}	107 ohms	252 ohms
R_{SC}	16.3 ohms	60 ohms
R_{TH}	106.7 ohms	238 ohms
θ_j (Eqn. 4.4)	52.6°C/watt	35.8°C/watt
θ_j (Eqn. 4.10)	32.2°C/watt	30.8°C/watt

considered in this section, is similar to the diode used in the experiments of Chapters 2 and 3. From Figure 31, the time constant is obtained from the -3dB resistance point. For diode 2, this results in:

$$\text{Time Constant} = \frac{1}{2\pi f_{-3dB}} \approx 50\mu\text{sec}$$

The usefulness of the heat flow resistance can be easily shown. For IMPATT diodes, the maximum safe temperature rise of the junction is in the order of 200°C above ambient. Thus, the power which may be dissipated in the diode, P_{DIS}, is given as:

$$P_{DIS} = \frac{\Delta T_j}{\theta_j} \tag{4.11}$$

The efficiency of DC to RF power conversion can be defined by:

$$\eta = \frac{P_o}{P_{IN}} = \frac{P_o}{P_o + P_{DIS}} \tag{4.12}$$

where

η = efficiency

P_o = RF power output

P_{IN} = total input power

Combining Equations (4.11) and (4.12), the power output is given by:

$$P_o = \frac{\eta}{1-\eta} \cdot P_{DIS} = \frac{\eta}{1-\eta} \cdot \frac{\Delta T_j}{\theta_j} \tag{4.13}$$

For a maximum temperature of 200°C and an efficiency of 2% (typical for

low power IMPATT's) the RF power output of an oscillator can be estimated to be:

For Diode 1

$$P_o = \frac{2}{98} \cdot \frac{200}{32.2} = 127mW$$

For Diode 2

$$P_o = 133mW$$

The diode junction temperature rise, ΔT_j, may be obtained by rearrangement of these equations to give:

$$\Delta T_j = \theta_j (P_{IN} - P_o) \qquad (4.14)$$

Equation (4.14) is extremely useful during experiments with IMPATT diodes. The input power, P_{IN}, is easily measured by monitoring the current and voltage. It has been found that the heat flow resistance, θ_j, is relatively constant over large current ranges, and so, the diode junction temperature rise may be monitored continually.

4.4 Conclusions

Two common methods for measuring the heat flow resistance of IMPATT diodes have been examined. The direct method provides a relatively fast answer for the heat flow resistance; however, the more exact small-signal method gives a lower value. The lower value allows the user to apply more power safely to the diode and consequently, more power may be extracted from the device. The small-signal method gives, as a by-

product, the thermal time constant of the heat flow circuit of the diode chip which is useful in estimating the rate of temperature rise of the diode junction.

CHAPTER 5

CONCLUSIONS AND RECOMMENDATIONS

5.1 Summation and Conclusions

An equation for the frequency-temperature coefficient of an IMPATT diode oscillator has been developed and is given by:

$$\frac{\Delta f}{\Delta T} = - \frac{\frac{\partial X_D}{\partial T} + \frac{\partial X_L}{\partial T}}{\frac{\partial X_D}{\partial f} + \frac{\partial X_L}{\partial f}}$$

This equation may be used to compute the frequency-temperature coefficient of an oscillator in terms of the diode and circuit temperature-frequency characteristics.

In Chapter 2, the small-signal model of an IMPATT diode, as described by Fisher[15] is used as a basis in examining the frequency-temperature characteristics of IMPATT microstrip oscillators. The various parameters of the model were modified to reflect the effect of temperature on the immittance (impedance or admittance) of the diode chip. At a constant frequency, the results show that for increasing diode-junction temperatures the magnitude of the negative conductance decreases while the capacitive susceptance increases. The inclusion of the small-signal model in a microwave diode package provided an easy means for examining the diode-terminal characteristics. For constant frequency and various diode-junction temperatures, it was found that the change of reactance with temperature was positive, which immediately suggests a reducing oscillator frequency for increasing temperature.

The microwave microstrip-circuit was modelled for frequency and temperature and coupled with the packaged diode model in order to solve for the frequency of oscillation. The predicted frequency-temperature characteristic was compared to measured results with good agreement. It was found that the microstrip circuit reduced the drift of frequency with temperature because of the change in the relative dielectric constant of the microstrip substrate with temperature. It is thus concluded that "the negative frequency-temperature coefficient of the IMPATT microstrip oscillators considered in this study is primarily due to the diode-junction characteristics".

Further, it was found that the reduction of the oscillator frequency in pulse mode operation was caused by three phenomena. First, the rapid rise of the diode-junction temperature during the pulse causes an increase in the packaged diode capacitance which results in a decreasing frequency. A model incorporating this effect was compared against the measured results and good agreement was achieved for narrow pulse widths. However, the model predicted a larger change in the oscillator frequency than the measurements indicated. Second, the finite rise and fall times of the applied current pulse caused the average oscillator frequency to increase as the rise and fall times reduced. The rise and fall times of the current pulses in this study were fixed, however, and it was found that for very narrow pulse widths the average frequency of the oscillator would increase substantially as the pulse width was increased. Third, the variation of the current density distribution with time during pulse mode operation showed that the oscillator frequency would increase by

virtue of the electronic tuning effect. The current density on the circumference of the diode increased to roughly twice the value at the centre. The frequency of oscillation is strongly dependent on the current density and thus as the current density increases, the frequency also increases. In conclusion, the three phenomena are responsible for the downward shift in the oscillator frequency in pulse mode operation.

In Chapter 4, heat flow resistance measurements were performed by two methods and it is felt that the small-signal method proposed by Haitz et al[30] is more accurate than the direct method. Although the measurement technique is more complex, a thermal time constant may be obtained which is useful for estimating the rate of diode-junction temperature rise during experiments in pulse mode.

5.2 Recommendations for Future Work

The results of Chapter 2 showed that the microstrip circuit was responsible for reducing the temperature coefficient of the oscillator. It is suggested, therefore, that various microstrip substrate materials and various microstrip circuit configurations be further investigated in order to achieve an oscillator with a low frequency-temperature coefficient. The small-signal results for the packaged diode impedance (see Figure 9) suggest that IMPATT's operating at frequencies just above the avalanche frequency or at the maximum frequency exhibit the least change in reactance with temperature. Thus, oscillators operating at either of these two frequency ranges should be investigated to obtain an oscillator with a low frequency-temperature coefficient.

APPENDIX A

DESIGN OF A 10GHz IMPATT MICROSTRIP OSCILLATOR

For the purposes of this study, a simple microstrip oscillator is required.

In the design of oscillators using single-port negative-resistance devices, such as IMPATT diodes, the circuit external to the diode must present the proper conjugate impedance in order to achieve maximum power output. For IMPATT diodes, this restraint can be a major problem since the real part of the diode impedance may be in the order of half an ohm. Experiments have shown that impedance transforming circuits consisting of a single transformer are unacceptable for two reasons. First, small dimensional errors in the fabrication process of the microstrip circuits result in large errors of the load impedance presented to the diode. Second, a single transformer requires a microstrip line width to substrate thickness ratio, w/h, of approximately 100 to achieve a load impedance of half an ohm starting from an impedance of fifty ohms. For low dielectric constant substrates (e.g.: Teflon), a w/h ratio of this magnitude gives a line width in excess of one wavelength at 10GHz, hence the transformer cannot be easily modelled and it is felt that the actual transformed impedance may be incorrect. The results of fabricating an oscillator using a single transformer are that the power output is low and the frequency of oscillation may depart from the design frequency by as much as 1GHz.

A more tractible circuit can be realized by using a double-stage transformer to obtain the required low resistance for the real part of

the RF load. An immediate advantage here is that all line widths are much less than one wavelength while the disadvantage is that a longer microstrip circuit is required which may reduce the available power output due to the extra line loss. However, this disadvantage is not serious and it is more likely that the impedance discontinuity arising from a connector will overshadow the microstrip loss.

The design of the oscillator circuit used in this study did not account for transformer impedance discontinuities or microstrip dispersion. The design procedure follows the steps outlined below.

(a) Load Impedance

For the diodes used in this study, the typical microstrip load impedance was found to be:

$$Z_L = 0.5 + j\ 12.5 \text{ ohms (at 10GHz)}$$

(b) Reactive Tuning

The imaginary part of the load impedance in (a) is obtained by a transmission line of characteristic impedance of 50 ohms. The length of this line is determined with a Smith chart and is 0.037λ long. With the diode in shunt with this line, the impedance at the end of the line consists of a real part only, of magnitude 0.4 ohms.

(c) Low Resistance to 50 Ohm Transforming

To obtain the resistance transformation, a two-stage quarter wave transformer was used. The circuit layout is shown in Figure A1. The characteristic impedance of transformer 2 was chosen as

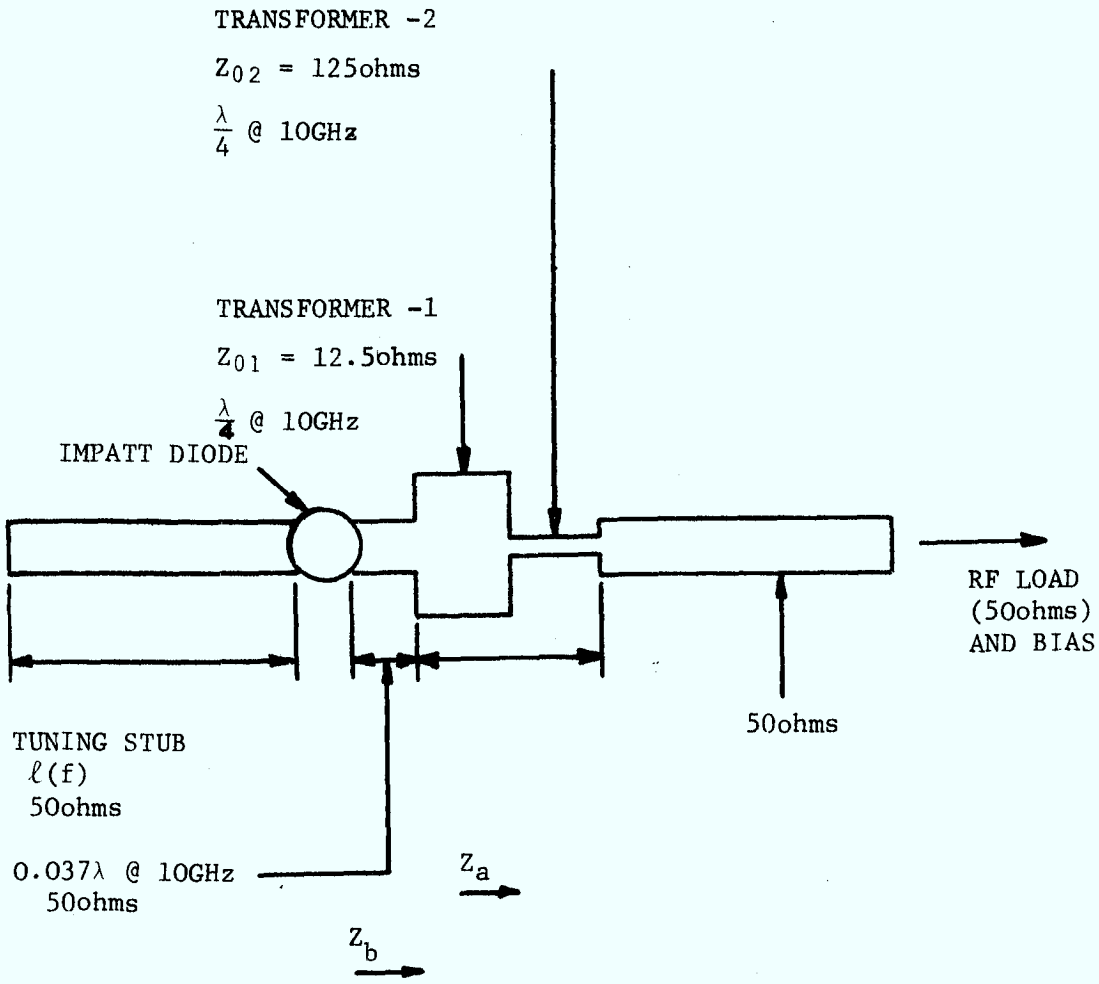

$\varepsilon_r = 2.3$

h = 10mils

$7 < f_{OSC} < 13GHz$

FIG. A1. MICROSTRIP IMPATT OSCILLATOR CIRCUIT CONFIGURATION

Z_{02} = 125 ohms.

The impedance at the transformer-1-transformer-2 interface, looking right is Z_a and is computed from:

$$Z_a = \frac{Z_{02}^2}{Z_o} = \frac{125^2}{50} = 313 \text{ ohms}$$

The impedance at the left of transformer-1- looking right is Z_b and was calculated as 0.4 ohms in Section (b) above. Hence, the characteristic impedance of transformer Z_{01} may be calculated as:

$$Z_{01} = \sqrt{0.5Z_a} = \sqrt{0.5\times313} = 12.5 \text{ ohms}$$

(d) Fine Tuning

Fine tuning may be easily accomplished by the addition of an open-ended stub as shown in Figure A1. The length of this open stub must be one-half wavelength at the design frequency. For a fixed frequency, the alteration of the tuning stub length causes the admittance of the load to move on a constant conductance path.

(e) Circuit Fabrication

Since the microwave circuit is a microstrip circuit with a plastic substrate†, the lengths and widths of the lines were determined according to the work of Wheeler[42].

---

† ε_r=2.3 Rogers Teflon - Duroid D5880

The microstrip circuit and IMPATT diode were mounted on an aluminum heat sink and a miniature microstrip connector was attached to the circuit.

The complete oscillator was tested at room temperature and both operating frequency and power output were monitored. In Figure A2, the measured and computed tuning curve is shown. The computed tuning curve was obtained by a computer program in which the circuit was described by simple transmission line theory and the IMPATT diode reactance versus frequency characteristic was described by a three-point interpolation curve. The frequency of oscillation was solved for in an iterative fashion for a continually reducing stub tuning length. The measured and computed curves show that tuning discontinuities exist and an initial guess on the oscillation frequency had to be used to prevent divergence in the computer calculations. It is noted that for frequencies below 10GHz the measured and computed tuning curves do not agree at all while at higher frequencies the measured tuning curve bears a close resemblance to the computed curve. The discrepancy between measured and computed results was determined to be an excess phase shift of the load impedance. A reflection measurement made at the diode contact point (in Figure A1, the reflection test set measurement point replaced the diode and the impedance as a function of frequency was measured when the output side of the circuit was terminated in 50 ohms) showed that circuit impedance at 10GHz contained an extra 30° phase shift from the design value. A number of reasons for the extra phase shift are available. First, the design method did not account for any excess phase shift resulting from

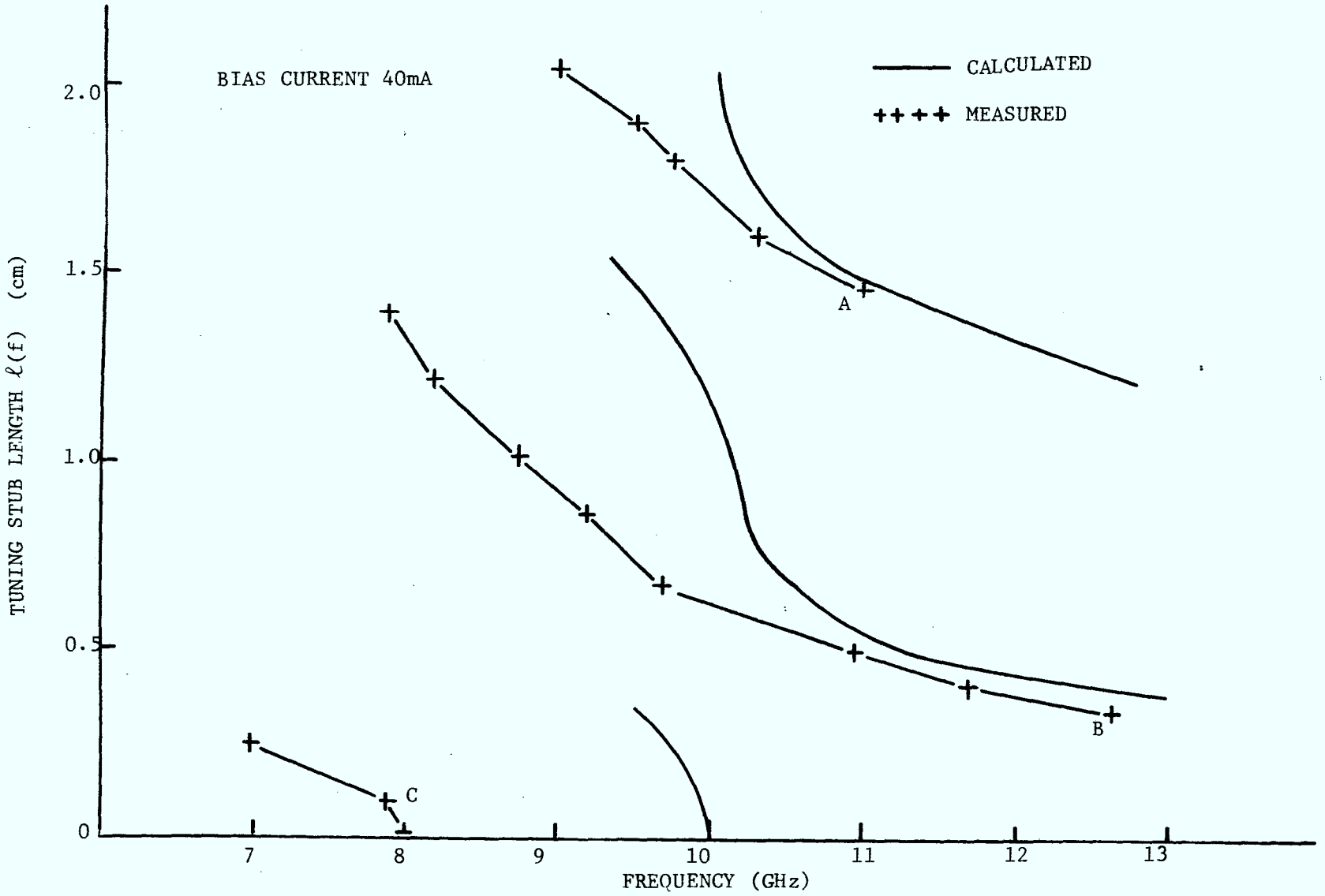

FIG. A2. TUNING STUB LENGTH VERSUS FREQUENCY FOR IMPATT MICROSTRIP OSCILLATOR

the large impedance discontinuities[28] at the quarter wave transformers. Second, microstrip dispersion[27] was not considered. Studies have shown[27] that dispersion need only be considered for frequencies above the dispersive cut-off frequency. For the low characteristic impedance line (12.5 ohms), calculations indicate that dispersion exists for all frequencies considered here. Thus, the low impedance line transformer actually appears electrically longer, adding an excess phase shift. Third, the microstrip connectors are imperfect and usually add an excess phase shift to propagating signals[28].

Figure A3 shows the power curves resulting from the mechanical tuning and indicate that the oscillator may be mechanically tuned from 7 to 13GHz.

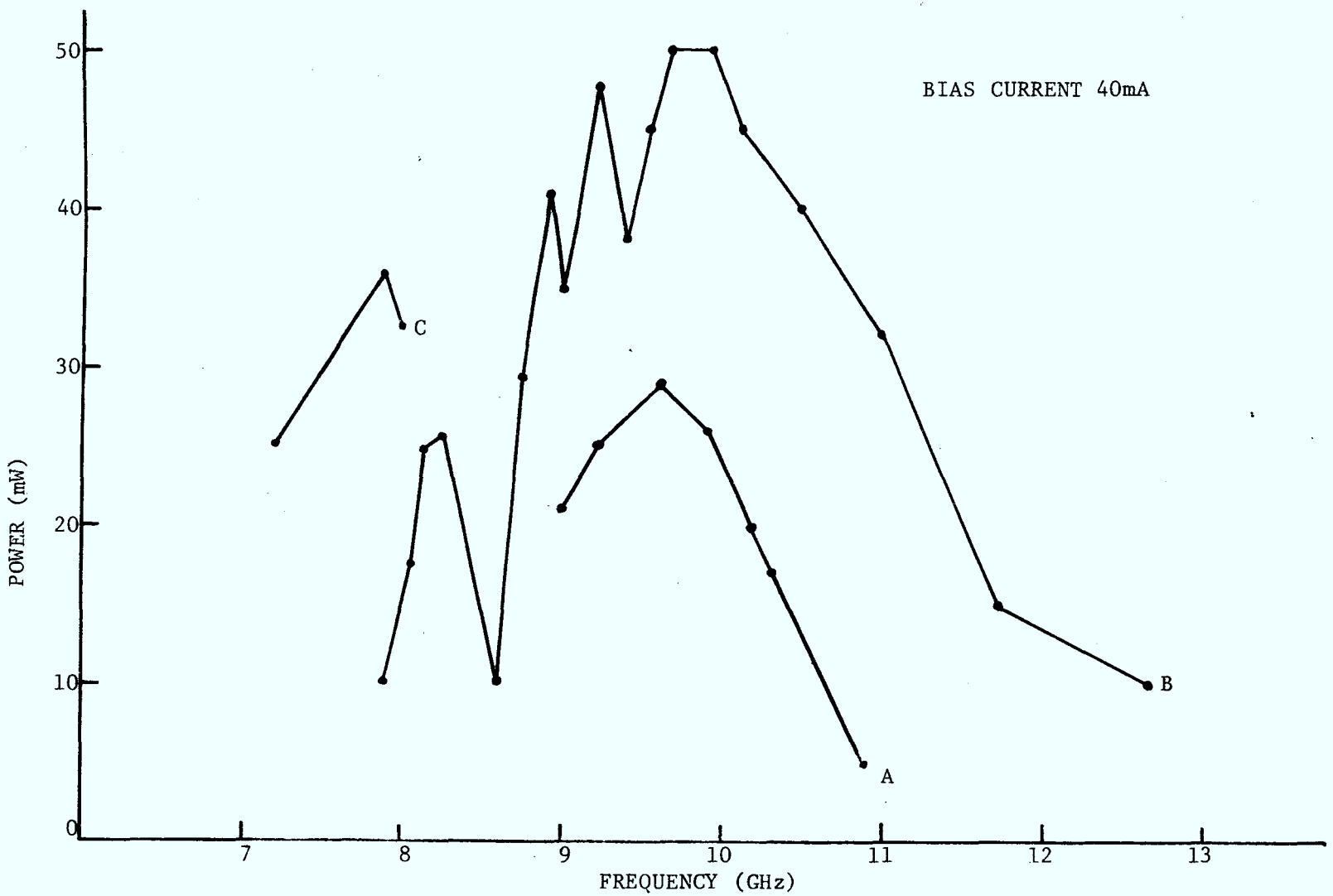

FIG. A3. POWER VERSUS FREQUENCY OF IMPATT MICROSTRIP OSCILLATOR. CURVES A, B AND C CORRESPOND TO CURVES A, B AND C OF FIGURE A2.

BIBLIOGRAPHY

1. W. Schockley, "Negative resistance arising from transit time in semiconductor diodes", Bell Sys. Tech. J., Vol. 33, pp. 799-826, July 1954.

2. W.T. Read, "A proposed high-frequency, negative resistance diode", Bell Sys. Tech. J., Vol. 37, pp. 401-466, March 1958.

3. R.L. Johnson, B.C. De Loach and B.G. Cohen, "A silicon diode microwave oscillator", Bell Sys. Tech. J. Briefs, Vol. 44, pp. 369-372, February 1965.

4. E. Allamando, E. Constant and M. Lefebvre, "Influence de la temperature sur la puissance delivree par un oscillateur A.T.T.", Onde Electrique, Vol. 48, pp. 737-738, July-August 1968.

5. W.J. Chudobiak, "Thermal effects and pulse mode operation of IMPATT diodes", Proc. IEEE (Lett.), Vol. 58, pp. 935-936, June 1970.

6. W.E. Schroeder and G.I. Haddad, "The effect of temperature on the operation of an IMPATT diode", Proc. IEEE (Lett.), Vol. 59, pp. 1242-1244, August 1971.

7. M. Gilden and M.F. Hines, "Electronic tuning effects in the Read microwave avalanche diode", IEEE Trans. Electron Devices, Vol. ED-13, pp. 169-175, January 1968.

8. J.R. Greirson, "Theoretical calculations on the effect of temperature on the operation of an IMPATT diode", Electronic Letters, Vol. 8, pp. 258-260, May 1972.

9. T. Misawa, "Negative resistance in p-n junctions under avalanche breakdown conditions, Part I and II", IEEE Trans. Electron Devices, Vol. ED-13, pp. 137-151, January 1968.

10. S. Nagano and H. Kondo, "Highly stabilized half-watt IMPATT oscillator", IEEE Trans. Microwave Theory and Techniques, Vol. MTT-18, pp. 885-890, November 1970.

11. W.J. Evans and G.I. Haddad, "A large-signal analysis of IMPATT diodes", IEEE Trans. Electron Devices, Vol. ED-15, pp. 708-717, October 1968.

12. D.L. Scharfetter and H.K. Gummel, "Large-signal analysis of a silicon Read diode oscillator", IEEE Trans. Electron Devices, Vol. ED-16, pp. 64-77, January 1969.

13. P.T. Greilling and G.I. Haddad, "Large-signal equivalent circuits of avalanche transit time devices", IEEE Trans. Microwave Theory and Techniques, Vol. MTT-18, pp. 842-876, November 1970.

14. K. Mouthaan, "Nonlinear analysis of the avalanche transit-time oscillator", IEEE Trans. Electron Devices, Vol. ED-16, pp. 935-945, November 1969.

15. S.T. Fisher, "Small-signal impedances of avalanching junctions with unequal electron and hole ionization rates and drift velocities", IEEE Trans. Electron Devices, Vol. ED-14, pp. 313-322, June 1967.

16. K.M. Johnson, "Small-signal analysis of the Read avalanche diode", IEEE Trans. Electron Devices, Vol. ED-15, pp. 141-150, March 1968.

17. C.R. Cromwell and S.M. Sze, "Temperature dependence of avalanche multiplication in semiconductors", Appl. Phys. Letts., Vol. 9, pp. 242-244, September 1966.

18. G.A. Baraff, "Distribution junctions and ionization rates for hot electrons in semiconductors", Phys. Rev., 128, 2507, 1962.

19. S.M. Sze, "Physics of Semiconductor Devices", New York: Wiley, 1969, pp. 57-58.

20. C.Y. Duh and J.L. Moll, "Electron drift velocity in avalanching silicon diodes", IEEE Trans. Electron Devices, Vol. ED-14, pp. 46-49, January 1967.

21. V. Rodriguez, H. Ruegg and M.A. Nicolet, "Measurement of the drift velocity of holes in silicon at high-field strengths", IEEE Trans. Electron Devices, Vol. ED-14, pp. 44-46, January 1967.

22. S.M. Sze, "Physics of Semiconductor Devices", New York: Wiley, 1969, p. 222.

23. Microwave Associates Micronotes, "Cavity controlled avalanche diode oscillators, part one", Vol. 7, October 1969.

24. C.N. Dunn and J.E. Dalley, "Computer-aided small-signal characterization of IMPATT diodes", IEEE Trans. Microwave Theory and Techniques, Vol. MTT-17, pp. 691-695, September 1969.

25. A.E. Winter and R.H. Mitchell, "Characterization of IMPATT diodes", Int. J. Electronics, Vol. 31, pp. 471-483, 1971.

26. E.C. Jordan and K.G. Balmain, "Electromagnetic Waves and Radiating Systems", New Jersey: Prentice-Hall, 1968, p. 219.

27. W.J. Chudobiak, O.P. Jain and V. Makios, "Dispersion in microstrip", IEEE Trans. Microwave Theory and Techniques, Vol. MTT-19, pp. 783-784, September 1971.

28. J.S. Wight, W.J. Chudobiak and V. Makios, "Equivalent circuits of microstrip impedance discontinuities and launchers", to be published.

29. A.L. Edridge, "Frequency stability of GUNN oscillators with variation of ambient temperature", Solid State Electronics, Vol. 15, pp. 1187-1196, November 1972.

30. R.H. Haitz, H.L. Stover and N.J. Tolar, "A method for heat flow resistance measurements in avalanche diodes", IEEE Trans. Electron Devices, Vol. ED-16, pp. 438-444, May 1969.

31. B.E. Sigmon, "Frequency-versus-temperature stabilization in avalanche transit-time oscillators by use of diode parasitic elements", IEEE Trans. Microwave Theory and Techniques, Vol. MTT-18, pp. 971-973, November 1970.

32. J.P. Holman, "Heat Transfer", New York: McGraw-Hill, 1968, p. 75.

33. F. Kreith, "Principles of Heat Transfer", Scanton: International Text Book Company, 1968, pp. 80.

34. R.H. Haitz, "Nonuniform thermal conductance in avalanche microwave oscillators", IEEE Trans. Electron Devices, Vol. ED-15, pp. 350-361, June 1968.

35. S.P. Yu and G.H. Glover, "Heat sink temperature distribution of the annular solid state microwave diode", Electronic Letters, Vol. 7, pp. 182-183, April 1971.

36. S.M. Sze, "Physics of Semiconductor Devices", New York: Wiley, 1969, p. 55.

37. R. Adler, "A study of locking phenomena in oscillators", Proc. IRE, Vol. 34, pp. 351-357, June 1946.

38. Y. Takayama, "Power amplification with IMPATT diodes in stable and injection-locked modes", IEEE Trans. Microwave Theory and Techniques, Vol. MTT-20, pp. 266-272, April 1972.

39. C.H. Chien and G.C. Dalman, "Subharmonically injected phase-locked IMPATT oscillator experiments", Electronic Letters, Vol. 6, pp. 240-241, April 1970.

40. R.L. Bernick, "Temperature profile and thermal spreading resistance for a semi-infinite Type IIa diamond heat sink", Electronic Letters, Vol. 8, pp. 180-181, April 1972.

41. J. Nigrin, "Pulse measurements of transient thermal response and temperature of avalanching p-n junction", Electronic Letters, Vol. 7, pp. 481-482, August 1971.

42. The Microwave Engineers Handbook and Buyers Guide, Brookline, Mass.: Horizon House-Microwave Inc., 1969, pp. 65-66.